2022 Ph.D. Dissertation

Identification of Network Structures in Dynamical Network Systems Using Koopman Operators

Department of Mechanical Systems Engineering
Graduate School of Systems Design
Tokyo Metropolitan University

MEI, Zhuanglin

Supervisor
Professor
OGUCHI, Toshiki

Contents

1 Introduction

1.1 Network identification problems

In recent years, large progress is made in the field of network theory resulting from the developments of hardware and communication technologies. Complex networks form an essential part of modern infrastructure, and as networks become larger in scale and more complex in structures, understanding the structures of networks can no longer be achieved intuitively with simple calculations but requires new methodologies [1]. In many cases, precise mathematical models of given networks are desired, but only time-series data of the nodes of the network can be measured as available information, and this leads to the problem of network structure identification.

Networks play important role in our daily lives, and many real-life problems can be solved by modelling complex systems as network systems and analysing the structures. For example, human brains can be modeled as groups of interconnected neurons whose electrical activities represent the activity of the underlying structures. The specific structure of the brain is then revealed as the patterns of data exchanges between certain groups of neurons, which are identified from temporal measurements by EEG [2] and spatial measurements by fMRI [3]. In [4], the dependence between signals from human cardiovascular systems is studied to reveal the influences on human heart rate variability. In financial markets, stock returns were considered random processes before the correlations of differences in daily stock prices were studied. Mathematical models are constructed using the correlations of measured data and reveal new structures of stock trades in financial markets [5]. A social media platform can be modeled as a communication network, where the activities of the assets are the posted comments, photos or videos, and the data exchanges are the interactions between users. Specific properties of such network, e.g., heterogeneity, allow the providers to fully grasp the platform and help optimize network service in various aspects such as the allocations of server resources, advertisement delivery and targeted content recommendation [6]. In the case of rumors or computer virus spreading, the problem of source tracing can be considered as finding the root of a tree network using measured time series of individuals [7]. Similarly in a pandemic, patient zero, which is the root of the infection network, can be identified from the time order of close contracts between patients to stop the spreading of infection and find infected suspects [8]. Gene regulatory networks reveal the functions of cells from the level of gene expression [9], and

the climate network helps search patterns of global weather [10].

From the viewpoint of system engineering, network identification also plays important rolls. In many cases, failures of network systems can be modeled as sudden disconnections of certain paths of the associated network [11]. As an example, infrastructures such as power grids that are supposed to work under synchronized (or consensus) states may desynchronize under failure situations [12]. Such failure may be located by monitoring the influenced nodes and identifying the change in network topology and dynamics. In communication systems, a server suffering from malicious attacks can be modeled as a network with external input signals, and the attack signals may give false commands and destabilize nodes in the original network. The problem of recovering from the attack can be reduced to the problem of identifying the attack signal and locating the attacked channel, so the attack can be blocked and the communication path can be cut off [13, 14]. In machine learning, studying the structure of Bayesian networks is an important topic, which can be represented by a graph that models the characteristic relationship between the nodes [15].

As mentioned above, identifying the network structures is of great importance in modeling, analyzing and maintening the systems. Nowadays, gathering data becomes easier with the help of the Internet, and the development of network identification methodologies are highly desired. In the next section, a brief review of previous studies concerning the network identification problem is given.

1.2 Background studies

From a historical perspective, the network identification problem can be traced back to the study of whether any dependence exists between signals, processes or subsystems (transfer functions) [16, 17, 18, 19]. The dependence was considered as random processes, and statistical tools were often employed such as entropy analysis [20, 15], Granger causality [21, 22] and other statistic-based methods, e.g., [23]. Also, the viewpoint of control engineering brings controlling methods such as applied synchronization [24, 25], response dynamics [26] and phase/variable resetting [27, 28]. As networks become larger in scale and more complex, the expressions of state-space models are widely adopted, and graphs from graph theory are employed to model network topology. It is found that the topology of networks can be derived from the covariance (correlations) of signals in terms of the adjacency matrix associated with the network topology [29], and correlation becomes an important tool that leads to the methods of delay coordinating [30, 31], noise injection [32], etc. On the other hand, with the developments of computers and data processing techniques [33], solving the identification problem using large amounts of data by direct calculation becomes possible. This leads to the sparsity based methods [34, 35, 36, 37,

38, 39] and other iterative methods [40, 41].

Next, some milestone identification methods are described along with their problem settings.

Granger causality and transfer entropy

Granger causality [42, 43] and transfer entropy [16, 19, 44] are statistical tools that reveal causal relationships between signals or processes from measured data.

Consider two processes $x(t)$ and $y(t)$. In *Granger causality* analysis, process $y(t)$ is considered to be (at least a part of) the 'cause' of the process $x(t)$ if past time series data of $y(t)$ is 'useful' for prediction of future values of $x(t)$. Let $\mathcal{S}_x = \{x_i(k) \mid i = 1, \cdots, m,\ k = t_1, \cdots, t_K\}$ and $\mathcal{S}_y = \{y_j(l) \mid j = 1, \cdots, n,\ l = t_1, \cdots, t_L\}$ denote the sets of measured data of processes x and y, respectively, then y is considered to be independent on x if the following equality holds:

$$p(x(t_{k+1})|\mathcal{S}_x) = p(x(t_{k+1})|\mathcal{S}_x, \mathcal{S}_y),$$

where $p(x(t_{k+1})|\mathcal{S}_x)$ is the conditional probability of $x(t_{k+1})$ being measured. Methods of verifying the equation are omitted here and can be found in, e.g., [42, 21]. Granger causality is widely used in various fields, such as identifying Bayesian networks in machine learning studies [43].

On the other hand, the term *transfer entropy* quantifies the 'incorrectness' of the hypothesis that two processes are independent, and is another measure that describes casual relationships.

Consider a process $x(t)$ and its measurements $x_1, x_2, \cdots, x_m$. Suppose that samples are measured following some probabilistic distribution $p(\cdot)$, i.e., the probability of x_i being measured is $p(x_i)$, such that $\sum_{i=1}^{m} p(x_i) = 1$. The *information*, also known as the *surprise*, of measurement x_i is defined by $-\log p(x_i)$, and the average amount of information $H(x)$ is

$$H(x) = -\sum_{i=1}^{m} p(x_i) \log p(x_i),$$

which is more commonly known as the *Shannon Entropy* of x considered as a random variable. Also, consider another process $y(t)$ and its measurements $y_1, y_2, \cdots, y_n$ which are measured under probability $q(y_j)$, respectively for $j = 1, \cdots, n$ and $\sum_{j=1}^{n} q(y_j) = 1$.

Denote the *joint probability* of measured x_i and y_j by $P(x_i, y_j)$ for $i = 1, \cdots, m$ and $j = 1, \cdots, m$, and define the *joint entropy* $H(x, y)$ by

$$H(x, y) = -\sum_{i=1}^{m} \sum_{j=1}^{n} P(x_i, y_j) \log P(x_i, y_j),$$

which is also known as the *mutual information*. If the two processes $x(t)$ and $y(t)$ are independent, then $P(x_i, y_j) = p(x_i)q(y_j)$ and $H(x, y) = H(x) + H(y)$ hold. The dependence between the two processes is then defined by the error of assuming the two processes are independent, i.e.,

$$M(x, y) = \sum_{i=1}^{m} \sum_{j=1}^{n} P(x_i, y_j) \log \frac{P(x_i, y_j)}{p(x_i)q(y_j)},$$

which is also known as the *Kullback entropy*. By using the conditional entropy $H(x|y) = -\sum_{j=1}^{n} q(y_j) \sum_{i=1}^{n} p(x_i|y_j) \log p(x_i|y_j)$, the following equation holds:

$$M(x, y) = H(x) + H(y) - H(x, y).$$

The concept of *transfer entropy* extends the above measure in the sense that the dynamics of information transportation is taken into account. Suppose that x is a Markov process of order k, and denote the probability of x_{t+1} being measured by $p(x_{t+1}|x_t^{(k)})$, where $x_t^{(k)}$ denotes the multiple $\{x_t, x_{t-1}, \cdots, x_{t-k+1}\}$. Consider another process y with measurements $y_{t+1}, \cdots, y_{t-k+1}$. If the two processes are independent, one has $p(x_{t+1}|x_t^{(k)}) = p(x_{t+1}|x_t^{(k)}, y_t^{(k)})$. Then the transfer entropy from y to x is defined by the difference

$$T_{y \to x} = \sum p(x_{t+1}|x_t^{(k)}, y_t^{(t)}) \log \frac{p(x_{t+1}|x_t^{(k)}, y_t^{(k)})}{p(x_{t+1}|x_t^{(k)})}.$$

The transfer entropy $T_{y \to x}$ is 0 if process x is independent of process y.

Transfer entropy analysis releases the requirement that data have to be measured from regressive processes, which is required by the Granger causality analysis, and therefore can be applied to a wider range of systems. As an example, the transfer entropy between neurons is studied to identify synapses in [45], where simulated spike data from a Hudgkin-Huxley type model are employed.

Applied Synchronization

The applied-synchronization-based methods [24, 25] are successful attempts of applying controlling strategies to the network identification problem. The structure of a network is modeled as the entries of the adjacency matrix associated with the topology, and the key idea is to construct an auxiliary system (also named *estimator*) making use of measured data as input. The dynamics of the auxiliary system is carefully designed such that the state variables converge to the entries of the adjacency matrix.

Consider networks of N autonomous systems (*nodes*) modeled by

$$\dot{x}_i(t) = f_i(x_i) + \sum_{j=1}^{N} a_{ij} g_j(x_j),$$

for $i = 1, \cdots, N$, where $x \in \mathbb{R}^n$ is the state vector of node i, $f_i(x_i) : \mathbb{R}^n \to \mathbb{R}^n$ describes the unforced dynamics, $g_j(x_j) : \mathbb{R}^n \to \mathbb{R}^n$ describes the transported information from node j. Functions f_i, g_i are assumed to be known, and the goal is to identify a_{ij} with measured time series of $x_i(t)$.

In [24], the following estimator is proposed:

$$\begin{aligned}\dot{\hat{x}}_i =& f_i(\hat{x}_i) + \sum_{j=1}^{N} \xi_{ij} g_j(\hat{x}_j) + \Delta_i(\hat{x}, \xi_{ij}, t) + u_i \\ \dot{\xi}_{ij} =& -\gamma_{ij} g_j^\top(\hat{x}_j)(\hat{x}_i - x_i),\end{aligned}$$

where $\gamma_{ij} > 0$, $\hat{x}_i \in \mathbb{R}^n, \xi \in \mathbb{R}$, and $\Delta_i(\hat{x}, \xi_{ij}, t)$ represents the unknown nonlinearity such as modeling errors and noises, which is assumed to be bounded by known nonlinear functions of $\hat{x}_i$ and t. The input can be designed as

$$u_i = -k_1(\hat{x}_i - x_i) - f(\hat{x}_i) + f(x_i) - \frac{1}{4\varepsilon}\delta^2(\hat{x}_i - x_i),$$

where $k_1, \varepsilon, \delta > 0$. The variables ξ_{ij} converge to a_{ij} as $\hat{x}_i - x_i \to 0$, and the entries of the adjacency matrix are estimated. Note that the convergence is not asymptotic, although the estimation error can be arbitrarily small by adjusting k_1 and ε.

In [25], an estimator with a dynamical input is proposed to ensure asymptotic convergence of $\xi_{ij} \to a_{ij}$. The coupling functions are assumed to be identical, i.e., $g(x) := g_1(x) = g_2(x) = \cdots = g_N(x)$, and the estimator is designed by

$$\dot{\hat{x}}_i = f_i(\hat{x})_i + \sum_{j=1}^{N} \xi_{ij} g(\hat{x}_j) + u_i$$

where

$$\begin{aligned}u_i =& -k_i(\hat{x}_i - x_i), \\ \dot{k}_i =& c_i(\hat{x}_i - x_i)^\top(\hat{x}_i - x_i), \\ \dot{\xi}_{ij} =& -(\hat{x}_i - x_i)^\top g(\hat{x}_j).\end{aligned}$$

Asymptotic stability of tracking error $\hat{x}_i - x_i$ is ensured by Lyapunov's direct method, and $\xi_{ij} \to a_{ij}$ is ensured by applying the invariance principle [46]. It is also remarked that when the nodes in the network synchronize, the estimator-based approach fails, because data exchange, i.e., $\sum_{j=1}^{N} a_{ij} g(x_j)$, would vanish in such a case. If the network allows state resetting or external inputs, then identification can be achieved by introducing manual desynchronization to the network, which can be found in [47].

Data correlation

In statistics, data correlation [29, 48, 49, 50, 51, 32] also describes the dependence between data sets.

It is found in [29] that noise helps reveal the topology of networks. Consider a network of N dynamical systems described by

$$\dot{x}_i(t) = f_i(x_i) + \sum_{j=1}^{N} a_{ij} g(x_j) + \eta_i,$$

for $i = 1, \cdots, N$, where $x \in \mathbb{R}^n$ is the state of node i, $f_i(x_i) : \mathbb{R}^n \to \mathbb{R}^n$, $g_j(x_j) : \mathbb{R}^n \to \mathbb{R}^n$, and η_i is the noise signal. Here f_i and g are considered to be known. Suppose that x_i differs a small perturbation δ_i from y_i, the situation with no noises, i.e., $x_i = y_i + \delta_i$ and $\dot{y}_i = f_i(y_i) + \sum_{j=1}^{N} a_{ij} g(y_j)$. Then the following equations hold:

$$\begin{aligned}\dot{\delta}_i =& f_i(y_i + \delta_i) - f(y_i) + \sum_{j=1}^{N} a_{ij}(g(y_j + \delta_j) - g(y_j)) + \eta_i \\ =& (F_i(y_i) + \sum_{j=1}^{N} a_{ij} G(y_j))\delta_i + \eta_i,\end{aligned}$$

where $F_i(y)$ and $G_i(y)$ are the Jacobian matrices of $f(y)$ and $g(y)$, respectively. By left multiplying $\delta_j^\top$ and defining a time-averaging operator $\langle \cdot \rangle$ by $\langle r \rangle = \frac{1}{m} \sum_{k=1}^{m} r(t_k)$, the following equations hold:

$$0 = \langle \frac{\mathrm{d}\delta_i^\top \delta_j}{\mathrm{d}t} \rangle = \langle \delta_j^\top B_i(y_i)\delta_i \rangle + \langle \delta_i^\top B_i(y_j)\delta_j \rangle + \langle \delta_j^\top \eta_i \rangle + \langle \delta_i^\top \eta_j \rangle,$$

where $B_i(y_i) := F_i(y_i) + \sum_{j=1}^{N} a_{ij} G(y_j)$. The first equality holds since the perturbations are considered independent and 0-mean signals. Define correlation matrices

$$\begin{aligned} B = \mathrm{diag}(F_1(y_1), \cdots, F_N(y_N)) + H, \quad & \text{where } [H]_{ij} = a_{ij} G(y_j), \\ [C]_{ij} =& \langle \delta_i^\top \delta_j \rangle, \\ [N]_{ij} =& \langle \delta_i^\top \eta_j \rangle, \end{aligned}$$

where $[C]_{ij}$ denotes the (i, j) entry of matrix C, and it follows that

$$0 = BC + CB^\top + N + N^\top.$$

Also, $N + N^\top = D$ holds where D is the covariance matrix of the noises η_i. Entries of the adjacency matrix associated with the network are then identified by solving the above equation. Refer to [29] for computational details. Specifically in the case that the network is undirected, and the perturbation $F(y_i)$ can be considered small, the Laplacian matrix L associated with an undirected network is given by

$$C = \frac{1}{2} D L^\dagger,$$

where $L^\dagger$ denotes the pseudo-inverse of L, and C is estimated from measured data.

In [48], the correlation between variables and their derivatives is employed to reveal the topology of the associated network. Consider a network of N dynamical systems described by

$$\dot{x}_i(t) = f_i(x_i) + \sum_{j=1}^{N} a_{ij} g_j(x_j),$$

for $i = 1, \cdots, N$, where $x \in \mathbb{R}^n$, $f_i(x_i) : \mathbb{R}^n \to \mathbb{R}^n$ and $g_j(x_j) : \mathbb{R}^n \to \mathbb{R}^n$. Define correlation matrices $B, C, F \in \mathbb{R}^n$ by

$$\begin{aligned}
[B]_{ij} =& \langle \psi^\top(x_i)\dot{x}_j \rangle, \\
[F]_{ij} =& \langle \psi^\top(x_i) f_j(x_j) \rangle, \\
[C]_{ij} =& \langle \psi^\top(x_i) g_j(x_j) \rangle,
\end{aligned}$$

where $\psi(x) : \mathbb{R}^n \to \mathbb{R}^n$ is a specially designed observable function. By left-multiplying $\psi(x_i)$ to the dynamical model and applying time-averaging, $B = F + AC$ is obtained, which leads to

$$A = C^{-1}(B - F),$$

where A is the adjacency matrix associated with the network topology.

The data correlation-based methods are also employed in the cases where time delays occur in data transmission paths, see, e.g., [31, 52].

Compressive Sensing

Sparse identification (compressive sensing) [53] is a method that recovers sparse signals from the measurements making use of sparsity, and the method is applied to the network identification problem [34, 35, 36, 37, 38, 39].

In [34], the network identification problem is transformed into the form of

$$\text{finding } x, \quad \text{such that} \quad y = Ax.$$

Networks with nodes modeled in discrete-time by

$$x_i[k+1] = F_i(x_i^*[k]) + AF_i(x_i^*[k])(x_i[k] - x_i^*[k]) + \mathcal{O}(\|x_i[k] - x_i^*[k]\|^2),$$

are considered, where $x_i^*[k]$ is a chosen expansion point of the first order Taylor series. $F_i(x_i^*[k])$ is a constant matrix and is considered known. The adjacency matrix corresponding to the network topology is then calculated by augmenting vectors and performing ℓ_1-minimization with thresholding.

In [38], sparse identification is employed to identify nonlinear networks with the help of basis functions. Networks with nodes modeled by *nonlinear structural equation models*

are considered:

$$y_{im} = \sum_{j \neq i}^{N} a_{ij} \psi^{\top}(y_{jm}) \boldsymbol{c}_{ji} + b_{ii} x_{im} + e_{im},$$

where y_{im} denotes the mth observation, and x_{im} denotes the mth input of node i. $\psi^{\top}(y_{jm})\boldsymbol{c}_{ji}$ is a nonlinear function, where ψ is the vector of known basis functions, and $\boldsymbol{c}_{ij}$ is an unknown coefficient. Data matrices X, Y and coefficient matrices W, B are constructed with measured data, and it follows the above equation that

$$Y = \Psi W + XB,$$

where the entries of W Matrix X is then solved by minimizing the ℓ_1-norms of its columns with the alternating direction method of multipliers (ADMM). Finally, the entries a_{ij} of the adjacency matrix associated with the network topology are extracted from matrix X.

1.3 Purposes and outline of this dissertation

Although the network structure identification problem has been widely studied, there are still open problems remaining and an identification method is desired which has the following properties:

1) the method only gives connectivity results,

2) the method does not apply to networks with topology changes,

3) the method requires the full states of the nodes to be measurable.

The data-correlation-based methods are model-free and are only able to recover the adjacency matrices in terms of casual relationships, which makes the methods hardly applicable to networks with nonlinear data exchanges, i.e., the Kuramoto model [54]. The sparsity-based methods make use of the dynamical models of the nodes to construct equations of the form $y = Ax$ and require all the states to be measured, which is a strict and unpractical requirement in most cases. On the other hand, both the correlation-based methods and the sparse identification-based methods are intended for post-processing uses, which does not apply to networks with time-varying topology. The applied synchronization-based methods perform identification in real-time, although it requires both the unforced dynamics and the coupling function to be known.

In this work, identification problems of networks consisting of possibly nonlinear systems with possibly nonlinear data exchanges are addressed. In detail, interconnected N nodes

modeled in discrete time are considered, i.e.,

$$x_i[k+1] = f(x_i[k]) + Bu_i[k], \tag{1.1a}$$

$$u_i[k] = \sum_{j \neq i}^{N} a_{ij} g_{ij}(y_i[k], y_j[k]), \tag{1.1b}$$

$$y_i[k] = Cx_i[k], \tag{1.1c}$$

for $i = 1, \cdots, N$, where $x_i \in \mathbb{R}^n$ is the state of node i, $u_i \in \mathbb{R}^m$ is the coupling input, $y_i \in \mathbb{R}^m$ is the output, $B \in \mathbb{R}^{n \times m}, C \in \mathbb{R}^{m \times n}$, $f : \mathbb{R}^n \to \mathbb{R}^n$ describes the unforced dynamics, and $g : \mathbb{R}^m \times \mathbb{R}^m \to \mathbb{R}^m$ describes the transmitted information from node j to node i. a_{ij} is the (i, j) entry of the adjacency matrix associated with the network topology. **The purpose of this work is to develop a method that identifies the data transmission $u_i = \sum_{j \neq i}^{N} a_{ij} g_{ij}(x_i, x_j)$ from measured output data series $y_i[1], \cdots, y_i[M]$, which is capable of detecting changes in network structures**. For simplicity, the case where the outputs of the nodes are the full states is first considered, i.e., networks consisting of nodes modeled by

$$x_i[k+1] = f(x_i[k]) + u_i[k], \tag{1.2a}$$

$$u_i[k] = \sum_{j \neq i}^{N} a_{ij} g_{ij}(x_i[k], x_j[k]), \tag{1.2b}$$

where $u_i \in \mathbb{R}^n$, and $g_{ij} : \mathbb{R}^n \times \mathbb{R}^n \to \mathbb{R}^n$.

Chapters 2 and 3 consider the case where all the states of the nodes can be measured as data. Throughout Chapters 2 and 3, networks modeled by (1.2) are considered.

Chapter 2 assumes that at least one node can be isolated from the network, and the full-state data series of all the nodes in the network system can be measured. The identification method proposed in the chapter gives the core idea of the proposed identification method using Koopman operators and a sparse identification technique. First, define two Koopman operators K_1 and K_2 corresponding to the dynamics of the original network and a fully unconnected network where all the nodes in the network are isolated, respectively. The coupling function describing the data exchange among nodes is then extracted from the operator K_g, defined by $K_g = K_1 - K_2$, acting on the state variables. Numerically, finite-dimensional approximations of infinite-dimensional operators K_1 and K_2 are calculated from measured data, and an approximation of K_g can be obtained as the difference between K_1 and K_2. Sparse identification techniques are employed to reduce the required amount of measured data and construct an identification algorithm. It is also shown theoretically that the obtained coupling function is a projection of the original coupling function into the space spanned by the observable functions, which are designed for identifications of nonlinearity.

Chapter 3 modifies the method proposed in Chapter 2 to achieve the identification of structure changes in networks. The assumption on the existence of an isolated node is relaxed by assuming instead that the network topology is undirected and data transmissions in both directions between any two nodes are symmetric. The modified method allows to detect changes in network structures by performing the method proposed in Chapter 2 with streaming data sets, i.e., using time-varying data matrices which are updated with newly measured data at every time step. A Koopman operator associated with the dynamics of the original network is defined and approximated with measured data, and the unforced dynamical models of all the nodes are then extracted from the Koopman operator under the relaxed assumption. It is also shown that the modified method applies to networks with topology changes. On the other side, the case where the restrictions on the network structure do not hold is also addressed.

Chapters 4 and 5 consider the case where only the output signals of the nodes are available as measured data. Specifically, Chapter 4 considers a special case of the identification problem where the dynamics of isolated nodes are known. In these two chapters, networks modeled by (1.1) are considered.

Chapter 4 considers the case where both B, C and the unforced dynamics $f_i(\cdot)$ are known. It is assumed that each node can be decomposed into the input-output dynamics and the internal dynamics and that the internal dynamics is convergent, i.e., the difference between two trajectories of the nodes converge to 0 if they have the same outputs. A drive-response system is designed by imitating the known models of the nodes and tracking past data of the original network system. The coupling function is formulated as a linear combination of the observables, and the coefficient matrix is considered a variable in the response system. The dynamics of the response system is then designed such that the error between the coefficient matrix as a variable and the true expansion matrix of the coupling function converges to 0 asymptotically. On the other side, although the response system tracks past data of the original, the states of the original network system at the current step are obtained by iterating the identified dynamical model of the response system.

Chapter 5 also considers the identification problem using output signals, and it is assumed that the dynamical models of the nodes are unknown. The dynamical model of the network is reformulated such that the outputs of each node are considered as the full states and the dynamics of the output signals as the dynamics of the node. Then the unmeasurable hidden states are modeled as unknown dynamical inputs. Defining such dynamical inputs as new variables, time series data of the new variables are calculated and the dynamics of such variables can be identified with the help of Koopman operators. The network dynamics is then identified in terms of the outputs and the new variables using measured data, and the network structure is extracted as the data transmission in the network. If the dimension of the output is so low that the dynamics of the network

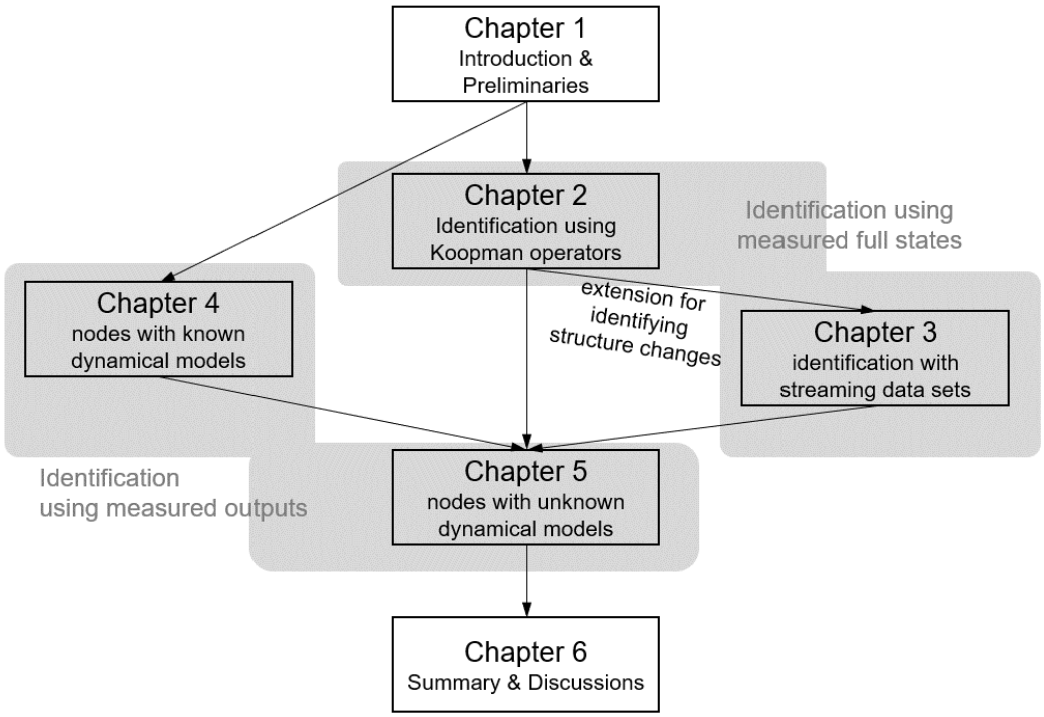

Fig. 1.1: The outline of this dissertation.

cannot be embedded into the space spanned by the outputs and the new variables, then additional variables are introduced based on past data. In this case, it may be impossible to identify the coupling function in its original form, so the goal here is to identify what is equivalent to the hidden nodes in the sense that the identified network system admits the same dynamical behaviors as the original. The method proposed in this chapter also applies to the problem considered in Chapter 4.

Chapter 6 concludes this dissertation and gives some remarks. The chapter also discusses problems that remain in this study and provides future directions to which this study can be extended.

An outline of this dissertation is given as follows and shown in Fig.1.1. Chapters 2 and 3 consider identifications using measured full states, where Chapter 3 describes an extension of the method proposed in Chapter 2 for identifying network topology changes. Chapters 4 and 5 consider identifications using measured output data, assuming the dynamical models of the nodes are known or not, respectively. Chapter 4 considers the case where the dynamical models of the nodes without inputs are known, and Chapter 5 considers the more general case where the dynamics of the nodes is unknown. Specifically, the method proposed in chapter 5 can be considered as an extension of the methods described in Chapters 2 and 3. Finally, Chapter 6 summarizes the dissertation and gives some remarks and discussions.

1.4 Mathematical preliminaries

1.4.1 Notations

Throughout this dissertation, $\mathbb{R}$ and $\mathbb{C}$ denote the space of all the real numbers and all the complex numbers, receptively. x^* denotes the complex conjugate of x, where x is a complex scalar number, a vector, or a matrix. Let $\mathbb{K}$ be either $\mathbb{R}$ or $\mathbb{C}$. $\mathbb{K}^n$ denotes the n-dimensional vector space:

$$\mathbb{K}^n = \left\{ x = \begin{pmatrix} x_1 \\ \vdots \\ x_n \end{pmatrix} \;\middle|\; x_i \in \mathbb{K}, i = 1, \cdots, n \right\},$$

where x is a vector in $\mathbb{K}^n$, which is an ordered n-tuples of numbers in $\mathbb{K}$. $\|x\|_p$ denotes the p-norm of vector x defined by $\|x\|_p = (\sum_{i=1}^n |x_i|^p)^{1/p}$ where $p = 1, 2, \cdots, \infty$. $\boldsymbol{e}_i$ denotes the ith basis vector of vector space $\mathbb{K}^n$, i.e.,

$$\boldsymbol{e}_i = \begin{pmatrix} \vdots \\ e_j \\ \vdots \end{pmatrix}, \quad j = 1, \cdots, n, \quad e_j = \begin{cases} 1, & j = i, \\ 0, & j \neq i. \end{cases}$$

$f(x) : X \to Y$ denotes a function f that maps elements x in a set X to elements in set Y. $\mathbb{K}^{n\times m}$ denotes the space of matrices, which are linear maps, that maps (subspaces of) $\mathbb{K}^m$ to (subspaces of) $\mathbb{K}^n$:

$$\mathbb{K}^{n\times m} = \left\{ A = \begin{bmatrix} a_{11} & \cdots & a_{1m} \\ \vdots & \ddots & \vdots \\ a_{n1} & \cdots & a_{nm} \end{bmatrix} \;\middle|\; \begin{array}{l} Ax = y,\ a_{ij} \in \mathbb{K},\ i = 1, \cdots, n,\ y = 1, \cdots, m, \\ x \in X \subseteq \mathbb{K}^m,\ y \in Y \subseteq \mathbb{K}^n \end{array} \right\}.$$

$A = [a_{ij}]$ denotes a matrix A whose (i, j) entry is a_{ij}, and $[A]_{ij}$ returns the (i, j) entry of matrix A. $A^\top$ denotes the transpose of matrix (or vector) A, and A^* denotes the conjugate transpose of A, i.e., $[A^\top]_{ij} = a_{ji}$ and $[A^*]_{ij} = a^*_{ji}$. $\|f\|_{L_2(X)}$ denotes the L_2-norm of function f calculated over set X. $\|A\|_2$ and $\|A\|_F$ denote the induced 2-norm and the Frobenius norm of matrix A defined by $\|A\|_2 = \max_{\|x\|_2=1} \|Ax\|_2$ and $\|A\|_F = \sqrt{\sum_{i=1}^n \sum_{j=1}^m |a_{ij}|^2}$, respectively. $\mathcal{F}$ denotes the space of complex-valued scalar functions, i.e., $\mathcal{F} = \{f \mid f : X \to \mathbb{C}, X \subseteq \mathbb{K}^n\}$, and $\mathcal{F}_k$ denotes the k-dimensional space of functions in the sense that

$$\mathcal{F}_k = \{f \in \mathcal{F} \mid \exists c_i \in \mathbb{C} : f = \sum_{i=1}^k c_i \psi_i,\ \psi_i \in \mathcal{F}\}.$$

$\psi_1, \cdots, \psi_k$ are called the basis of space $\mathcal{F}_k$, and $\mathcal{F}_k$ is said to be spanned by basis $\psi_1, \cdots, \psi_k$, or $\mathcal{F}_k = \text{span}\{\psi_1, \cdots, \psi_k\}$. $\mathcal{F}^n$ denote the space of ordered n-tuple of functions in $\mathcal{F}$, i.e.,

$$\mathcal{F}^n = \left\{ f = \begin{pmatrix} f_1 \\ \vdots \\ f_n \end{pmatrix} \;\middle|\; f_i \in \mathcal{F}, \quad i = 1, \cdots, n \right\}.$$

$\text{col}_i^n(x_i)$ denotes the column composing operator by

$$\text{col}_i^n(x_i) = \text{col}(x_1, \cdots, x_n) = \begin{pmatrix} x_1 \\ \vdots \\ x_n \end{pmatrix},$$

where x_i can be scalar numbers, vectors, matrices, or functions. For a function f in $\mathcal{F}$ defined over some subset of $\mathbb{K}^n$, $\mathbb{P}_{\text{span}\{\Psi\}} : \mathcal{F} \to \mathcal{F}_k$ denotes the projection operator defined by

$$\mathbb{P}_{\text{span}\{\Psi\}} f = (\underset{c \in \mathbb{C}^{1\times k}}{\text{argmin}} \|f - c\Psi\|_{L_2}^2)^* \Psi,$$

where $\Psi : \mathbb{K}^n \to \mathbb{K}^q$ is a set of q basis functions. x^{i+} denotes the time evolution of discrete-time variable x such that $x^{i+}[k] = x[k+i]$. Specifically, $x^{0+} = x$ and $x^+ = x^{1+}$.

1.4.2 Linear algebra, functional analysis and measure basics

This section gives brief introductions to fundamental concepts of linear algebra and functional analysis. Vectors and spaces are introduced, and then inner products and norms. Functions (maps) and operators are then introduced, and linear functions are studied in detail in terms of eigendecomposition. Specifically, basic measure theory is included to introduce L_p spaces. Here $\mathbb{K}$ denotes a scalar field, which can be $\mathbb{C}$, $\mathbb{R}$ or the set of all rational numbers, etc.

Vector spaces [55, 56]

Definition 1.1. A *vector space* (or linear space) X is a set of vectors over field $\mathbb{K}$, on which two operations, *addition* and *scalar multiplication*, are defined with the following properties:

a) For any $x, y, z \in X$, $x + y \in X$. Also, $x + y = y + x$ and $(x + y) + z = x + (y + z)$ hold.

b) X contains a unique vector 0 such that $x + 0 = x$ for every $x \in X$. Also, there exists a $-x \in X$ corresponding to x such that $x + (-x) = 0$ for every $x \in X$.

c) For any $x \in X$ and $\alpha, \beta \in \mathbb{K}$, there exists an αx contained in X in such a way that $1x = x$ and $\alpha(\beta x) = (\alpha\beta)x$.

Definition 1.2. Let S be a subset of vector space X over $\mathbb{K}$. The *span* of S, denoted by $\text{span}\{S\}$, is the intersection of all subspaces of X that contains S.

If S is nonempty, then $\text{span}\{S\} = \{a_1v_1 + \cdots + a_kv_k \mid a_i \in \mathbb{K}, v_i \in S, k = 1, 2\cdots\}$. Set S is said to span X if $\text{span}\{S\} = X$.

Definition 1.3. A *linear combination* of vectors in a vector space X over field $\mathbb{K}$ is an expression of the form $a_1v_1 + \cdots + a_kv_k$, where $a_i \in \mathbb{K}$ and $v_i \in X$ for $k = 1, 2, \cdots$. A list of vectors is said to be *linearly dependent* if there exists $a_i \in \mathbb{K}$, which are not all zeros, such that $a_1v_1 + \cdots + a_kv_k = 0$.

Note that a linear combination is a sum of finitely many elements in the vector space, i.e., $k < \infty$. A list of vectors is said to be *linearly independent* if it is not linearly dependent. Note that it is often convenient to say, 'the vectors are linearly dependent' instead of using the statement 'the list'. A set S of vectors is linearly independent if every finite list of distinct vectors in S is linearly dependent.

Definition 1.4. Let X be a vector space over $\mathbb{K}$. The *basis* of X is a list of linearly independent vectors whose span is X. The basis of an empty space is an empty list.

Example 1.1.

- Let $S = \{(1, 0, 0)^\top, (0, 1, 0)^\top\}$. Then $\text{span}\{S\} = \{[a, b, 0]^\top \mid a, b \in \mathbb{R}\}$.
- Let $S = \{e^{\mathrm{i}k\omega t} \mid k = 0, 1, 2, \cdots\}$ where $\mathrm{i}=\sqrt{-1}$. Then $\text{span}\{S\}$ is the space of all bounded ω^{-1}-periodic functions.
- The polynomials $1, t, t^2, t^3, \cdots$ are linearly independent.
- The list of vectors $\boldsymbol{e}_1 = (1, 0, 0)^\top, \boldsymbol{e}_2 = (0, 1, 0)^\top, \boldsymbol{e}_3 = (0, 0, 1)^\top$ is a basis of $\mathbb{R}^3$.

Definition 1.5. The *dimension* of a vector space X is a positive integer n, such that every basis of X consists of exactly n vectors.

The dimension of a vector can also be defined in other equivalent ways, e.g., the minimum number of vectors in S such that $\text{span}\{S\} = X$. A vector space can be infinite-dimensional or finite-dimensional.

Definition 1.6. Let X be a vector space over $\mathbb{K}$. A *norm* is a real-valued nonnegative scalar function $\|\cdot\| : X \to \mathbb{R}$ with the following properties: for any $x \in X$ and $\alpha \in \mathbb{K}$,

a) $\|x\| \geq 0$, and the equality holds only $x = 0$.

b) $\|\alpha x\| = |\alpha|\|x\|$, where $|a|$ denotes the absolute value of α.

c) $\|x+y\| \leq \|x\| + \|y\|$.

Example 1.2.

- $\langle x, y\rangle = \sum_{i=1}^{n} x_i y_i$ is an inner product, where $x, y \in \mathbb{R}^n$.
- $\langle f, g\rangle = \int_a^b f(t)g^*(t)\mathrm{d}t$ is an inner product, where $f, g : [a, b] \to \mathbb{C}$.
- $\|x\|_p = (\sum_{i=1}^{N} |x_i|^p)^{1/p}$ and $\|x\|_\infty = \max |x_i|$ are norms, where $x \in \mathbb{R}^n$.
- every inner product induces a norm $\|x\| = \langle x, x\rangle$ (Cauchy-Schwarz).

A vector space equipped with an inner product is called a *Hilbert space*, and a vector space equipped with a norm is called a *Banach space*.

Functions and bounded linear operators [55, 57]

Definition 1.7. A *function* (or a map) $f : X \to Y$ is a binary relation defined on a set X that associates elements in X with an exact element in another set Y. The notation $y = f(x)$ means that f associates $x \in X$ with $y \in Y$.

Here X and Y are called the *domain* and the *image* of f, respectively. The notation of $Y = f(X)$ is also adopted in this dissertation.

Definition 1.8. Consider $f : X \to Y$. If $B \subset Y$, then the inverse image $f^{-1}(B)$ of B is defined by $A = \{x \in X \mid f(x) \in B\}$.

Definition 1.9. A function $f : X \to Y$ is said to be *linear* if $f(\alpha x + \beta y) = \alpha f(x) + \beta f(y)$ holds for any $x, y \in X$ and $\alpha, \beta \in \mathbb{K}$.

Definition 1.10. Let X and Y be Banach spaces equipped with the same norm $\|\cdot\|$. An *operator* $A : X \to Y$ is a map that maps X to Y. If the map is linear, then A is called a linear operator (or a linear transformation). If further there exists a constant $c > 0$ such that $\|Ax\| \leq c\|x\|$ for any $x \in X$ and A is linear, then A is called a *bounded linear operator*.

Let $A : H \to H$ be a bounded operator defined on H, which is a Hilbert space. Then the adjoint operator A^* of A is such that $\langle Ax, y\rangle = \langle x, A^*y\rangle$ and $\|A\| = \|A^*\|$, where the operator norm is defined by $\|A\| = \sup_{x\in H} \frac{\|Ax\|}{\|x\|}$. It is often convenient to say that A is an operator on H if $A : H \to H$.

Definition 1.11. An operator A defined on a Hilbert space H is said to be

a) *normal* if $AA^* = A^*A$.

b) *self-adjoint* or *Hermitian* if $A^* = A$.

c) *unitary* if $AA^* = A^*A = I$, where I is the identity operator on H.

Example 1.3.

- The ceiling function $f(x) = \lceil x \rceil, x \in [0, 2)$ is a function whose domain is $[0, 2)$ and image is $\{0, 1, 2\}$.
- A matrix $A \in \mathbb{R}^{n\times m}$ is a bounded linear operator that maps $\mathbb{R}^m$ to $\mathbb{R}^n$. If $\mathbb{R}^n$ and $\mathbb{R}^m$ are considered as Banach spaces equipped with 2-norms, then $\|A\| = \max_{x\in\mathbb{R}^m} \frac{\|Ax\|_2}{\|x\|_2}$ or $\|A\| = \max_{x\in\mathbb{R}^m, \|x\|_2=1} \|Ax\|_2$, which is known as the *induced 2-norm* of matrix A.
- The adjoint operator A^* of matrix $A \in \mathbb{R}^{n\times m}$ is its conjugate transpose $[A^*]_{ij} = \overline{[A]_{ji}}$.
- $A(z) = e^{\mathrm{i}\theta} z$ is a linear unitary operator over $\mathbb{C}$, where $z \in \mathbb{C}$.

1.4.3 The Koopman operator theory

Koopman operators [58, 59, 60]

The *Koopman operator*, named after mathematician Bernard O. Koopman (1900-1981), was first proposed in [58] in 1931. In [58], energy transformation in Hamiltonian systems was described with a linear unitary operator, which is known as the Koopman operator. The operator, together with its dual, the *Perron-Frobenius operator* [61], mainly describes measure-preserving dynamics, and is then extended to non-conservative systems (e.g., [62]). Together with the success of powerful data processing tools (POD [63], DMD [64], EDMD [65], etc.), a great amount of interest has been focused on the Koopman operator framework. Originating from [66], Koopman operators play important roles in fluid analysis [67, 68], stability analysis [69], control design [70, 71, 72], thermal analysis [73] and identification [74].

Definition 1.12. Consider a (Banach) space $\mathcal{F}$ of *observable (functions)* $\psi : X \to \mathbb{C}$. The *Koopman operator* K associated with a map $f : X \to X$ is defined through the composition

$$K\psi = \psi \circ f.$$

In this dissertation, X usually stands for $\mathbb{R}^n$, and $f : \mathbb{R}^n \to \mathbb{R}^n$, $\psi : \mathbb{R}^n \to \mathbb{C}$. Specifically, if f describes the dynamics of a discrete-time time-invariant system, i.e.,

$$x[k+1] = f(x[k]), \tag{1.3}$$

where $k = 1, 2, \cdots,$, then Koopman operator K describes the evolution of the states in terms of the evolution of the observables, i.e.,

$$K\psi(x[k]) = \psi(x[k+1]) = \psi(f(x[k])),$$

where $\psi \in \mathcal{F}$. Koopman operators are also defined for continuous-time systems and time-varying systems, refer to [59, 60] for more details.

Koopman operators are linear operators in the sense that

$$K(a\psi_1 + b\psi_2) = aK\psi_1 + bK\psi_2,$$

for $\psi_1, \psi_2 \in \mathcal{F}$ and $a, b \in \mathbb{C}$, and the linearity allows eigenvalues and eigenfunctions to be defined (these are also known as the *spectral properties*).

Definition 1.13. An eigenvalue $\lambda \in \mathbb{C}$ of Koopman operator K associated with map $f : \mathbb{R}^n \to \mathbb{R}^n$ is such that

$$K\phi = \phi \circ f = \lambda\phi,$$

where $\phi(x) \in \mathcal{F}$ is the *eigenfunction* associated with λ.

Example 1.4.

- Let X be the space of ordered triplets of real numbers, i.e., $X = \{(a, b, c) \mid a, b, c \in \mathbb{R}\}$, and $f : X \to X$ be a permutation map such that $f((a, b, c)) = (c, a, b)$. Define an observable by $\psi((a, b, c)) = 2b + c$, then $K\psi = \psi(f((a, b, c))) = \psi((c, a, b)) = 2a + b$. Further, $\phi((a, b, c)) = \frac{1}{\sqrt{3}}a + (-\frac{1}{\sqrt{12}} + \frac{1}{2}\mathrm{i})b + (-\frac{1}{\sqrt{12}} - \frac{1}{2}\mathrm{i})c$ is an eigenfunction associated with eigenvalue $\frac{1}{2} + \frac{\sqrt{3}}{2}\mathrm{i}$.
- Consider the linear system $x[k + 1] = Ax[k]$ where $x \in \mathbb{R}^n$. If A is diagonalizable by $A = P^{-1}\Lambda P$ where $\Lambda = \mathrm{diag}\{\lambda_1, \cdots, \lambda_n\}$, then $Px[k + 1] = \Lambda Px[k]$ holds. As a result, $(\lambda_1, p_1x), \cdots, (\lambda_n, p_nx)$ are eigenpairs of Koopman operator K associated with $x[k + 1] = Ax[k]$, where p_i is the ith row of P, and λ_i is the ith eigenvalue of matrix A.

In this dissertation, Koopman operators act on vectors in entry-wise manners, i.e., $Kv = \mathrm{col}(Kv_1, \cdots, Kv_n)$ for $v = \mathrm{col}(v_1, \cdots, v_n)$.

Koopman mode decomposition [59, 75]

Unless the state space is a finite set, the Koopman operator is infinite-dimensional in the sense that $\mathcal{F}$ has an infinite amount of basis [60]. Suppose that $\phi_1, \phi_2, \cdots$, the eigenfunctions of K, span the observable space $\mathcal{F}$. Then for any $f \in \mathcal{F}$, there exists c_i for $i = 1, 2, \cdots$ such that $f = \sum_{i=1}^{\infty} c_i\phi_i$, and the action of Koopman operator K on f can be decomposed into

$$Kf = K\sum_{i=1}^{\infty} c_i\phi_i = K\sum_{i=1}^{\infty} c_i\lambda_i\phi_i, \tag{1.4}$$

where λ_i is the eigenvalue associated with eigenfunction ϕ_i. Decomposition (1.4) is called the *Koopman Mode Decomposition (KMD)* of Kf, and c_i are called the eigenmodes.

It is usually convenient to consider finite-dimensional dimensional approximations of Koopman operators using the first k dominant eigenpairs:

$$Kf \approx K\sum_{i=1}^{k} c_i\phi_i = K\sum_{i=1}^{k} c_i\lambda_i\phi_i,$$

where k is chosen such that the first k linearly independent dominant eigenfunctions approximately span the observable space, i.e., $\mathcal{F}_k := \text{span}\{\phi_1, \cdots, \phi_k\} \approx \mathcal{F}$. Here c_i is such that the linear combination $\sum_{i=1}^{k} c_i\phi_i$ minimizes the projection error of f from $\mathcal{F}$ to $\mathcal{F}_k$, i.e.,

$$c_1, \cdots, c_n = \underset{v_1,\cdots,v_n}{\text{argmin}} \ \|f - \sum_{i=1}^{k} v_i\phi_i\|_{L_2(\mu)},$$

where μ is a positive measure defined on $\mathbb{R}^n$. In a vector form, define $\Phi = \text{col}(\phi_1, \cdots, \phi_N)$ and $\Lambda = \text{diag}\{\lambda_1, \cdots, \lambda_n\}$. For any $f \in \mathcal{F}$, the following equation holds:

$$Kf = c^*\Lambda\Phi, \tag{1.5}$$

where $c \in \mathbb{C}^n$ is such that $c\Phi \approx f$. Decomposition (1.5) is said to be a finite-dimensional approximation of Kf on space $\mathcal{F}_k$.

Numerically, it is usually hard to find the eigenfunctions explicitly, however, KMD can also be obtained with other appropriately defined basis functions. Let $\Psi = \text{col}(\psi_1, \cdots, \psi_k)$ be a set of observables such that $\text{span}\{\Psi\} \approx \mathcal{F}$. If the basis functions ψ_i's are linearly independent, then there exists an invertible map T such that $\Psi = T\Phi$. Then,

$$K\Psi = KT\Phi = T\Lambda\Phi = (T\Lambda T^{-1})\Psi.$$

Specifically, for some $b \in \mathbb{C}^n$ such that $b\Psi \approx f$, the following equations hold:

$$Kf = bK\Psi = b(T\Lambda T^{-1})\Psi. \tag{1.6}$$

Compared to (1.5), decomposition (1.6) allows us to obtain an approximation of Kf using basis functions (observables) designed manually. Kf is then obtained by designing Ψ such that $f = b\Psi$, and finding the matrix $T\Lambda T^{-1}$ such that $\Psi(f(x)) = T\Lambda T^{-1}\Psi(x)$.

The problem of finding approximations of Koopman operators is often related to the Dynamic Mode Decomposition (DMD) method [64] and the Extend DMD (EDMD) method [65], which are data-driven identification methods of dynamical models. The DMD method can be related to the Koopman operator theory by considering the states as observables: consider the relationship between data matrices

$$\begin{bmatrix} v_2 & v_3 & \cdots & v_{n+1} \end{bmatrix} = \begin{bmatrix} v_1 & v_2 & \cdots & v_n \end{bmatrix} S + r_n,$$

where $v_i \in \mathbb{R}^N$ consists of N snapshots measured at time step i, r_n is the residual and S is a transition matrix of the form

$$S = \begin{bmatrix} 0 & & & & a_1 \\ 1 & 0 & & & a_2 \\ & \ddots & \ddots & & \vdots \\ & & 1 & 0 & a_{n-1} \\ & & & 1 & a_n \end{bmatrix},$$

where $a_1, \cdots, a_n$ are unknown. S is then obtained from data by minimizing the residual r_n, and spectral information of the underlying dynamics can be extracted. On the other hand, the EDMD method makes use of observables and does not assume the data to be measured from the same trajectory. Define data matrices X, Y by

$$X = \begin{bmatrix} \Psi(x_1) & \Psi(x_2) & \cdots & \Psi(x_m) \end{bmatrix},$$
$$Y = \begin{bmatrix} \Psi(y_1) & \Psi(y_2) & \cdots & \Psi(y_m) \end{bmatrix},$$

where Ψ are usually polynomials or radius-basis functions, and x_i, y_i are such that $y_i = f(x_i)$. Then the underlying dynamics f can be approximated by $f(x) \approx CYX^\dagger x$, where C is such that $C\Psi(x) = x$ and † denotes the Moore-Penrose pseudo-inverse.

The DMD and the EDMD methods have been studied widely, and various extensions have been proposed, e.g., DMD with noisy data [76], DMD with streaming data set [77], DMD for compressive systems [78], controlled system analysis [79, 80], etc. The methods are also employed in various fields, e.g., model predictive control design [71], perturbation estimation [81], fluid analysis [77], etc. However, note that these numerical methods can only recover eigenvalues of Koopman operators, which are the point spectra of the operator. The spectrum $\sigma(K)$ of Koopman operators is defined by

$$\sigma(K) = \{\lambda \mid K - \lambda \mathbf{1} \text{ is not invertible}\}.$$

This happens in three cases where a) $(K-\lambda\mathbf{1})\psi = 0$, b) $(K-\lambda\mathbf{1})$ is not closed over $\mathcal{F}$ and c) the image of $(K-\lambda\mathbf{1})$ is not dense over $\mathcal{F}$, respectively. The corresponding spectra are named *point spectra*, *compression/continuous spectra* and *residual spectra*, respectively.

1.4.4 Sparse identification (compressive sensing)

In many practical situations of scientific and engineering studies like image processing, sampling theory and signal processing, the problem of recovering signals from their measurements often appear (refer to [82] and references there). Suppose that $y \in \mathbb{K}^m$ is the measurement of signal $x \in \mathbb{K}^n$ measured by $A \in \mathbb{K}^{m\times n}$ where $\mathbb{K}$ is either $\mathbb{R}$ or $\mathbb{C}$, or

$$y = Ax.$$

Suppose that A has full rank. Traditionally, the problem of recovering x from the pair (A, y) is achieved by left-multiplying the pseudo-inverse of A to both sides, i.e., $A^\dagger x = A^\dagger A y$. Let $USV^* = A$ be the singular value decomposition of matrix A, then the following equation holds:

$$A^\dagger x = VS^\dagger SV^* y,$$

where $S \in \mathbb{K}^{m\times n}$ contains the singular values of A. In the case that $m > n$, $\text{rank}(S^\dagger S) = n$, and $S^\dagger S = I_n$. This allows x to be obtained as $x = A^\dagger y$. However, if $m < n$, then $S^\dagger S = \text{diag}\{I_m, \mathbf{0}_{(n-m)\times(n-m)}\} \neq I_n$, and the pseudo-inverse based method fails.

Sparse identification, first introduced in [83] and named *compressive sensing* in [53], is a method that recovers x from incomplete information, i.e., with $m < n$, under the constraint that x is a *sparse* vector. A vector (or a signal) is sparse if most of its components are zero, and the *sparsity* of a vector is evaluated by its 0-*norm* defined by

Definition 1.14. The 0-norm of vector $x \in \mathbb{K}^n$, denoted by $\|x\|_0$ is defined by

$$\|x\|_0 = \text{card}(\{x_i \mid x_i \neq 0, i = 1, \cdots, n\}),$$

where $\text{card}(S)$ denotes the *cardinality* of set S.

Note that $\|x\|_0$ does not satisfy property b) in Definition 1.6, and hence is not a norm or a quasi-norm (which are positive real scalar functions that satisfy property a) and property b) in Definition 1.6). Intrinsically, y can be considered as a linear combination of columns of A as basis and entries of x as coefficients. The sparsity of x means that y only has a small amount of basis, which makes the information contained in y sufficient for recovering the coefficients.

The sparse identification theory mainly considers two problems:

1) To design reconstruction algorithms for certain given (A, y) pairs.

2) To design the measuring process, i.e., matrix A, optimally.

Only problem 1) will be introduced here, and more details about problem 2) can be found in [53, 82, 84].

The recovery of x from (A, y) is achieved by minimizing the sparsity of x, i.e., to solve the ℓ_0-minimization problem

$$\begin{aligned} &x = \underset{z}{\text{argmin}} \|z\|_0, \\ &\text{subject to } Az = y. \end{aligned} \tag{1.7}$$

Since the ℓ_0-minimization problem is in general an NP-hard problem, the following ℓ_1-minimization is usually solved instead:

$$\begin{aligned} &x = \underset{z}{\text{argmin}} \|z\|_1, \\ &\text{subject to } Az = y. \end{aligned} \tag{1.8}$$

The problem can also be solved by considering the unconstrained form

$$x = \underset{z}{\operatorname{argmin}}(\frac{1}{2}\|Az - y\|_2^2 + \|z\|_1), \tag{1.9}$$

which is also known as the Lasso (least absolute shrinkage and selection operator, [85]).

Alternating direction method of multipliers (ADMM)

In this dissertation, the alternating direction method of multipliers (ADMM, [86]) is employed to solve optimization problems in the form of (1.9). The ADMM is a convex optimization algorithm that takes the advantages of *the dual ascent method* and *the augmented Lagrangian method* in the sense that the decomposability of dual ascent is preserved while a quadratic term is employed in the augmented Lagrangian to obtain higher order convergence ([86]). The ADMM solves problems in the form of

$$\begin{aligned} &\text{minimize } f(x_1, \cdots, x_n) + g(z) \\ &\text{s.t. } A_1x_1 + \cdots + A_nx_n + Bz = 0, \end{aligned} \tag{1.10}$$

where $x_i \in \mathbb{R}^{n_i}, z \in \mathbb{R}^m$, $A_i \in \mathbb{R}^{p\times n_i}$ and $B \in \mathbb{R}^{p\times m}$. The maps f and g are often assumed to be convex while it is shown in [87] that the ADMM can also handle non-convex non-smooth situations.

Consider optimization problem (1.10), and define the augmented Lagrangian by

$$\begin{aligned} L_\rho(x_1, \cdots, x_n, z, w) =& f(x_1, \cdots, x_n) + g(z) + w^\top(A_1x_1 + \cdots + A_nx_n + Bz) \\ &+ \frac{\rho}{2}\|A_1x_1 + \cdots + A_nx_n + Bz\|_2^2, \end{aligned} \tag{1.11}$$

where $\rho > 0$, $x_1, \cdots, x_n, z$ are the primal variables and w is the dual variable. An iterating algorithm for variable updating is given by

$$x_i^+ = \underset{x_i}{\operatorname{argmin}}\ L_\rho(x_1^+, \cdots, x_{i-1}^+, x_i, \cdots, x_n, z, w), \tag{1.12a}$$

$$z^+ = \underset{z}{\operatorname{argmin}}\ L_\rho(x_1^+, \cdots, x_n^+, z, w), \tag{1.12b}$$

$$w^+ = \underset{w}{\operatorname{argmin}}\ L_\rho(x_1^+, \cdots, x_n^+, z^+, w), \tag{1.12c}$$

for $i = 1, \cdots, n$, where x_i^+ denotes the update of variable x_i. For convergence analysis, applications, and more details about ADMM, refer to [86, 33, 87, 39] and references there.

1.4.5 Graph theory basics

This section introduces some basic concepts in graph theory.

Definition 1.15. A *graph* $\mathcal{G}$ is a structure of two sets $\mathcal{V}$ and $\mathcal{E}$, i.e., $\mathcal{G} = (\mathcal{V}, \mathcal{E})$, where $\mathcal{V}$ is a set of objects, and $\mathcal{E} \subseteq \mathcal{V} \times \mathcal{V}$.

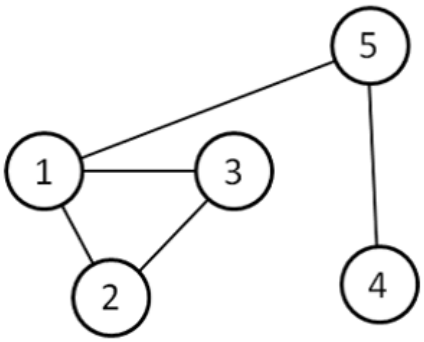

Fig. 1.2: Graph $\mathcal{G}$.

The elements in $\mathcal{V}$ are called the *nodes* or *vertices*, and the elements in $\mathcal{E}$ are called the *edges* of graph $\mathcal{G}$. Let v_i and e_{ij} denote the nodes and the edges, respectively. In this dissertation, only graphs with no self-loops are considered, i.e., $e_{ii} \notin \mathcal{E}$.

Definition 1.16. If $e_{ij} \in \mathcal{E}$, then nodes v_i and v_j are *adjacent*. A graph $\mathcal{G}$ is a *complete graph* if $e_{ij} \in \mathcal{E}$ for any $i \neq j$, and $\mathcal{G}$ is an *unconnected graph* if $\mathcal{E} = \varnothing$.

Definition 1.17. A graph $\mathcal{G}$ is an *undirected graph* if $e_{ij} \in \mathcal{E}$ indicates $e_{ji} \in \mathcal{E}$ for any $i \neq j$.

A graph is called a *directed graph* if it is not an undirected graph.

Definition 1.18. Consider a graph $\mathcal{G}$ such that $\text{card}\{\mathcal{V}\} = n$. The *adjacency matrix* $A = [a_{ij}] \in \mathbb{R}^{n\times n}$ of graph $\mathcal{G}$ is defined by

$$[A]_{ij} = \begin{cases} a_{ij}, & \text{if } (v_i, v_i) \in \mathcal{E}, \\ 0, & \text{else,} \end{cases}$$

where a_{ij} is the weight of edge (v_i, v_j), and the *degree matrix* $D = [d_{ij}] \in \mathbb{R}^{n\times n}$ of $\mathcal{G}$ is defined by

$$[D]_{ij} = \begin{cases} \sum_{j=1}^{n} a_{ij}, & \text{if } i = j, \\ 0, & \text{else.} \end{cases}$$

The *Laplacian matrix* L of $\mathcal{G}$ is defined by

$$L = D - A.$$

Example 1.5. Consider the graph shown in Fig.1.2, where the weights of all the edges are 1. The degree matrix and the adjacent matrix of graph $\mathcal{G}$ are given by

$$D = \begin{bmatrix} 3 & & & & \\ & 2 & & & \\ & & 2 & & \\ & & & 1 & \\ & & & & 2 \end{bmatrix}, \quad A = \begin{bmatrix} 0 & 1 & 1 & 0 & 1 \\ 1 & 0 & 1 & 0 & 0 \\ 1 & 1 & 0 & 0 & 0 \\ 0 & 0 & 0 & 0 & 1 \\ 1 & 0 & 0 & 1 & 0 \end{bmatrix}.$$

2 Identification of Network Structures for Network Systems with Measurable Full-states

2.1 Introduction

The network identification problem has been studied from various perspectives, and many identification methods have been developed based on Granger causality [23], noise injection [32, 29], data correlation [32, 88, 50, 36, 51, 49, 48, 89], sparse identification(compressive sensing) [39, 52, 35, 36, 34, 37], applied synchronization [25, 24], variable [28] or phase resetting [27], entropy transfer [16], just to name a few. However, a majority of the studies assume prior information on an unforced model of a system in networks[24, 35, 40, 90, 91, 48, 88, 41, 51, 32, 34, 41], and these assumptions usually do not hold in practice. Also, most of the existing methods estimate only the connectivity (in terms of the adjacency matrices) of the networks [32, 29, 49, 48], which fail to provide information on the exact possibly nonlinear coupling functions.

In this chapter, an approach is proposed that identifies both the connectivity and the nonlinear coupling functions of networks solely from measured data making use of Koopman operators. The proposed approach is realized by defining two Koopman operators associated with the original network and an unconnected virtual network, respectively, and obtaining the coupling function as the difference between the two Koopman operators acting on the state variables. To obtain the Koopman operator associated with the unconnected virtual network, it is assumed that a node can be isolated from the network so data of an unforced node can be measured. In addition, the problem is transformed into a standard LASSO [85] problem, and the sparse identification technique is employed to reduce the amount of required data, and improve robustness against measurement noise.

This chapter also shows that what the proposed method obtains is a projection of the true coupling function onto the space spanned by the pre-designed observables. The idea of employing observables is not new and can be found in, e.g., [92, 4, 38, 93, 51, 37]. These usages can be comprehended as variable changes or basis changes, as known that augmented variable sets using Taylor expansion series [37, 4] or trigonometric functions [92] of the states allow extracting higher-order approximations of nonlinearity. Instead

of approximations in point-wise manners, the proposed method focuses on the space spanned by the observables, which is considered invariant under the Koopman operator, to obtain global approximations of nonlinear coupling functions. It is also shown that the identification accuracy significantly depends on the design of the observable dictionary.

This chapter is organized as follows. In Section 2.1, technical details about the proposed method are described. Section 2.2 shows that the obtained result is a projection of the true coupling function onto the space spanned by the observables, and Section 2.3 gives numerical examples of a Kuramoto oscillator network and a Hindmarsh-Rose oscillators network with nonlinear coupling functions to illustrate the usefulness of the proposed method. In Section 2.4, the obtained results are summarized and some remarks are given.

2.2 Network identification via Koopman operator representations

2.2.1 Koopman operator representations of the problem

Consider a network system of N identical discrete-time systems described by

$$x_i^+ = f(x_i) + u_i, \tag{2.1a}$$

$$u_i = \sum_{j=1}^{N} a_{ij} g(x_i, x_j), \tag{2.1b}$$

where $x_i \in \mathbb{R}^n$, $f : \mathbb{R}^n \to \mathbb{R}^n$, a_{ij} is the (i, j) entry of the adjacency matrix associated with the network topology, and $g : \mathbb{R}^n \times \mathbb{R}^n \to \mathbb{R}^n$ describes the data exchange between two nodes via the network. Define $\boldsymbol{f}(x) := \mathrm{col}(f(x_1), \cdots, f(x_N))$, $\boldsymbol{g}(x) = \mathrm{col}(\sum_{j=1}^{N} a_{1j} g(x_1, x_j), \cdots, \sum_{j=1}^{N} a_{Nj} g(x_N, x_j))$. The dynamics of all the systems in the network is described by the following equation:

$$x^+ = \boldsymbol{f}(x) + \boldsymbol{g}(x), \tag{2.2}$$

where $\boldsymbol{g}(x)$ is called the *coupling function* of the nodes in the network. Note that $\boldsymbol{g}(x)$ contains both information about the network connectivity and the data exchange functions between nodes, which are considered together as the network structure.

Besides, if all the nodes are isolated, the dynamics of all the systems in the network can be described as

$$x^+ = \boldsymbol{f}(x). \tag{2.3}$$

Here, the goal of this chapter is then reduced to identifying $\boldsymbol{g}(x)$ from the time-series data of the connected network and the isolated nodes. Denote the space of all the observables

$\mathbb{R}^{Nn} \to \mathbb{C}$ by $\mathcal{F}$, and define Koopman operators K_1 and K_2 associated with dynamics (2.2) and (2.3) as follows.

$$\begin{aligned} K_1\psi(x) =& \psi(\boldsymbol{f}(x) + \boldsymbol{g}(x)), \\ K_2\psi(x) =& \psi(\boldsymbol{f}(x)), \end{aligned}$$

where $\psi \in \mathcal{F}$. Then, considering the states as observables, the dynamics of the network and the isolated nodes can be represented as

$$K_1 x = \boldsymbol{f}(x) + \boldsymbol{g}(x), \tag{2.4a}$$
$$K_2 x = \boldsymbol{f}(x), \tag{2.4b}$$

respectively, where the Koopman operators act on vectors in an entry-wise manner. Furthermore, defining a new operator K_g by the difference of K_1 and K_2 as

$$K_g = K_1 - K_2, \tag{2.5}$$

from (2.4a) and (2.4b), the following equations hold:

$$K_1 x = \boldsymbol{f}(x) + \boldsymbol{g}(x), \tag{2.6a}$$
$$K_2 x = \boldsymbol{f}(x), \tag{2.6b}$$

and

$$\begin{aligned} K_g x =& \boldsymbol{f}(x) + \boldsymbol{g}(x) - \boldsymbol{f}(x) \\ =& \boldsymbol{g}(x). \end{aligned} \tag{2.7}$$

Note that here K_g is defined by

$$K_g\psi(x) = \psi(\boldsymbol{f}(x) + \boldsymbol{g}(x)) - \psi(\boldsymbol{f}(x)),$$

for $\psi \in \mathcal{F}$.

As a result, the identification problem considered here is reduced to determining K_g. Since there is no information on $\boldsymbol{g}(x)$ or $\boldsymbol{f}(x)$, $\boldsymbol{g}(x)$ is approximated using a linear combination of the observables, which corresponds to a projection of $\boldsymbol{g}(x)$ onto the span of the observables. However, in general, an infinite amount of observables are needed to make the projection accurate, and practically, only a finite-dimensional approximation of K_g is numerically obtained.

Consider a set consisting of q observables $\{\psi_1(x), \cdots, \psi_q(x)\}$, and define $\Psi(x)$ as

$$\Psi(x) = \mathrm{col}(\psi_1(x), \ldots, \psi_q(x)) : \mathbb{R}^{Nn} \to \mathbb{C}^q. \tag{2.8}$$

Suppose that the data sequences $x[k]$ and $\bar{x}[k]$ for $k = 0, \dots, m$ are available, where $\bar{x}$ denotes data of a virtual network where all the nodes were isolated. Define data matrices $X_1, Y_1, X_2, Y_2 \in \mathbb{C}^{q\times m}$ as

$$X_1 = \begin{bmatrix} \Psi(x[0]) & \Psi(x[1]) & \cdots & \Psi(x[m-1]) \end{bmatrix}, \tag{2.9a}$$

$$Y_1 = \begin{bmatrix} \Psi(x[1]) & \Psi(x[2]) & \cdots & \Psi(x[m]) \end{bmatrix}, \tag{2.9b}$$

$$X_2 = \begin{bmatrix} \Psi(\bar{x}[0]) & \Psi(\bar{x}[1]) & \cdots & \Psi(\bar{x}[m-1]) \end{bmatrix}, \tag{2.9c}$$

$$Y_2 = \begin{bmatrix} \Psi(\bar{x}[1]) & \Psi(\bar{x}[2]) & \cdots & \Psi(\bar{x}[m]) \end{bmatrix}. \tag{2.9d}$$

Here, it is additionally assumed that all the nodes in the network do not synchronize. This assumption guarantees that $K_g x$ never vanishes. By the above definitions, Koopman operators K_1 and K_2 map X_1 to Y_1 and X_2 to Y_2 in a entry-wise manner, respectively, i.e.,

$$Y_1(m) = K_1 X_1(m),$$
$$Y_2(m) = K_2 X_2(m).$$

As a result, finite-dimensional approximations of the Koopman operators can be obtained as the matrices A_1 and A_2 that map X_1 and X_2 to Y_1 and Y_2, respectively, by solving the following optimization problems.

$$A_1 = \underset{A}{\operatorname{argmin}} \ \|AX_1 - Y_1\|_F, \tag{2.10a}$$

$$A_2 = \underset{A}{\operatorname{argmin}} \ \|AX_2 - Y_2\|_F. \tag{2.10b}$$

It follows that a finite-dimensional approximation of K_g is obtained by calculating $A_1 - A_2$, and the coupling function is identified as follows.

$$\boldsymbol{g}^{id}(x) = C_x(A_1 - A_2)\Psi(x), \tag{2.11}$$

where $C_x \in \mathbb{C}^{Nn\times q}$ is such that $x = C_x\Psi(x)$. Note that C_x can be obtained by designing the observable set $\Psi(x)$ to contain x, e.g., if one designs $\Psi(x) = \mathrm{col}(x, \psi_1, \cdots, \psi_{q-Nn})$, then C_x is obtained as $C_x = [I_{Nn}, \mathbf{0}_{Nn\times(q-Nn)}]$.

2.2.2 Calculation of K_g using sparse identification techniques

If m is sufficiently large, the solutions of the two minimization problems (2.10) may be solved explicitly by $A_1 = Y_1X_1^\dagger$ and $A_2 = Y_2X_2^\dagger$, respectively. However, considering the limited number of available data, a more effective calculation method is required from a practical point of view. In this subsection, a calculation method of the coupling function $K_g x$ is proposed based on the sparse identification techniques. To be specific, rows of

$A_1 - A_2$ are obtained by minimizing the sparsity of rows of $A_1 - A_2$, which corresponds to solving the following optimization problem:

$$\begin{aligned} \underset{a_{1i},a_{2i}}{\text{minimize}} \quad & \|a_{1i} - a_{2i}\|_1 \\ \text{subject to} \quad & a_{1i}X_1 = y_{i1}, \\ & a_{2i}X_2 = y_{i2}, \end{aligned} \tag{2.12}$$

or equivalently

$$\begin{aligned} \underset{a_{1i},a_{2i},v_i}{\text{minimize}} \quad & \left\| \begin{bmatrix} X_1^* & \\ & X_2^* \end{bmatrix} \begin{pmatrix} a_{1i}^* \\ a_{2i}^* \end{pmatrix} - \begin{pmatrix} y_{1i}^* \\ y_{2i}^* \end{pmatrix} \right\|_2^2 + \lambda \|v_i\|_1 \\ \text{subject to} \quad & a_{1i} - a_{2i} - v_i = 0, \end{aligned} \tag{2.13}$$

for $i = 1, \cdots, q$, where $\lambda > 0$, a_{1i} and $a_{2i} \in \mathbb{C}^{1\times q}$ are the ith rows of A_1 and A_2, and y_{1i} and $y_{2i} \in \mathbb{C}^{1\times m}$ are the ith rows of Y_1 and Y_2, respectively.

The optimization problem (2.13) can be solved via the alternating direction method of multipliers (ADMM) with the existing algorithm [86] as follows. First, define the augmented Lagrangian $L_{i\rho}$ by

$$\begin{aligned} L_{i\rho} :=& \|X_1^* a_{1i}^* - y_{1i}^*\|_2^2 + \|X_2^* a_{2i}^* - y_{2i}^*\|_2^2 \\ & + \lambda \|v_i\|_1 + w_i(a_{1i}^* - a_{2i}^* - v_i^*) + \frac{\rho}{2}\|a_{1i} - a_{2i} - v_i\|_2^2, \end{aligned} \tag{2.14}$$

where $\rho > 0$, and $w_i \in \mathbb{C}^{1\times q}$ is the dual variable. Next, update the optimization variables according to the following iterative algorithm:

$$(a_{1i}^*)^+ = -\frac{1}{2}(X_1X_1^* + \frac{\rho}{2}I_q)^{-1}(-2X_1y_{i1}^* + w_i^* - \rho(a_2^* + v_i^*)), \tag{2.15a}$$

$$(a_{2i}^*)^+ = -\frac{1}{2}(X_2X_2^* + \frac{\rho}{2}I_q)^{-1}(-2X_2y_{i2}^* - w_i^* + \rho(-(a_1^*)^+ + v_i^*)), \tag{2.15b}$$

$$(v_i^*)^+ = \mathcal{S}_{\lambda/\rho}((a_1^*)^+ - (a_2^*)^+ + \frac{1}{\rho}w_i^*), \tag{2.15c}$$

$$(w_i^*)^+ = w_i^* + \rho((a_{1i}^*)^+ - (a_{2i}^*)^+ - (v_i^*)^+), \tag{2.15d}$$

where a^+ denotes the update of variable a and I_q is the q-dimensional identity matrix. Here $\mathcal{S}_\gamma$ is a soft-thresholding function defined by

$$\mathcal{S}_\gamma(x) = \begin{cases} x - \gamma \text{sgn}(x), & |x| > \gamma, \\ 0, & |x| \le \gamma, \end{cases}$$

with $\gamma > 0$, and acts on a matrix (or a vector) in an entry-wise manner ([85, 87]).

Updating the variables under the above settings, the optimal solution of (2.13) can be obtained. Finally, the coupling function is obtained as

$$\boldsymbol{g}^{id}(x) = G\Psi(x), \tag{2.16}$$

where $G := C_x V$ in which $V = \mathrm{col}(v_1, \cdots, v_q) \in \mathbb{C}^{q\times q}$, and C_x is such that $x = C_x\Psi(x)$.

The identification method of network topology proposed above is summarized as an algorithm shown in Algorithm 2.1.

Algorithm 2.1 Proposed identification algorithm

Input: $x[k]$ and $\bar{x}[k]$ for $k = 0, 1, \ldots, m$, convergence criterion ε and $V = [0] \in \mathbb{C}^{q\times q}$

Output: $\boldsymbol{g}^{id}(x) = C_x V\Psi(x)$

1. **Define observables**: $\Psi(x) : \mathbb{R}^{Nn} \to \mathbb{C}^q$
2. **Define data sets**: X_1, Y_1, X_2, Y_2 in (2.9)
3. **Optimization**:

for $i \in \{1, \cdots, q\}$ **do**

while $\|v_i^+ - v_i\| \geq \varepsilon$ **do**

Update the optimization variables according to (2.15)

end while

Set $\boldsymbol{e}_i^\top V \leftarrow v_i^{opt}$, where $\boldsymbol{e}_i \in \mathbb{R}^q$ is the ith standard basis vector

end for

4. **Result:** obtain $\boldsymbol{g}^{id}(x) = C_x V\Psi(x)$

2.3 The obtained estimation as a projection

In this section, the relationship between the coupling functions estimated via the Koopman operators and the true coupling functions is considered. As mentioned above, if m is sufficiently large, the solution of the minimization problem (2.10) can be solved explicitly by $A_1 = Y_1 X_1^\dagger$ and $A_2 = Y_2 X_2^\dagger$, respectively, and the coupling function is obtained as $\boldsymbol{g}^{id}(x) = K_g x = C_x(A_1 - A_2)\Psi(x)$. This section shows that the obtained coupling function $\boldsymbol{g}^{id}(x)$ is an L_2 projection of the true coupling function onto the functional space spanned by the observables, such relationship is revealed by increasing the amount of data m, which is considered as a variable.

The following statement holds.

Proposition 2.1. Let $A_1(m) = Y_1(m)X_1^\dagger(m)$ and $A_2(m) = Y_2(m)X_2^\dagger(m)$ denote the transition matrices between $X_1(m), Y_1(m)$ and $X_2(m), Y_2(m)$, respectively, where the data matrices are defined by (2.9). Then,

$$\lim_{m\to\infty} \boldsymbol{e}_i^\top C_x(A_1(m) - A_2(m))\Psi(x) = \mathbb{P}_q^\mu\big(\boldsymbol{e}_i^\top \boldsymbol{g}(x)\big), \tag{2.17}$$

for $i = 1, \cdots, Nn$, where C_x is such that $x = C_x\Psi(x)$, $\boldsymbol{e}_i$ is the ith natural base of the Nn-dimensional Euclidean space, and $\mathbb{P}_q^\mu v$ denotes the $L_2(\mu)$ projection of $v \in \mathcal{F}$ onto $\mathcal{F}_q$.

Proof. Let $K_{1,q,m}$ and $K_{2,q,m}$ denote the q-dimensional approximations of K_1 and K_2 obtained from triplets $(\Psi(x), X_1(m), Y_1(m))$ and $(\Psi(x), X_2(m), Y_2(m))$, respectively, as

$$\begin{aligned} K_{1,q,m}\varphi(x) =& c_\varphi Y_1(m) X_1^\dagger(m)\Psi(x), \\ K_{2,q,m}\varphi(x) =& c_\varphi Y_2(m) X_2^\dagger(m)\Psi(x), \end{aligned}$$

where $\varphi \in \mathcal{F}_q$, and c_φ satisfies $c_\varphi \Psi(x) = \varphi$. Theorem 2 in [94] shows that if m goes to infinity, the following equations hold.

$$\lim_{m\to\infty} \int_{\mathcal{M}} |K_{1,q,m}\varphi - K_{1,q}\varphi|^2 \mathrm{d}\mu = 0, \tag{2.18a}$$

$$\lim_{m\to\infty} \int_{\mathcal{M}} |K_{2,q,m}\varphi - K_{2,q}\varphi|^2 \mathrm{d}\mu = 0, \tag{2.18b}$$

for all $\varphi \in \mathcal{F}_q$ where $\mathcal{M}$ is a subset of $\mathbb{R}^q$ and μ is a given positive measure on $\mathcal{M}$ (e.g., the Euclidean distance). Here $K_{1,q}, K_{2,q} : \mathcal{F}_q \to \mathcal{F}_q$ are the q-dimensional approximations of K_1, K_2 defined by

$$K_{1,q}\varphi = \mathbb{P}_q^\mu K_{1|F_q}\varphi, \quad K_{2,q}\varphi = \mathbb{P}_q^\mu K_{2|F_q}\varphi,$$

for all $\varphi \in \mathcal{F}_q$ where $K_{|F_q} : \mathcal{F}_q \to \mathcal{F}$ is the restriction of the operator K to $\mathcal{F}_q$, and $\mathbb{P}_q^\mu$ denotes the q-dimensional projection operator defined by

$$\mathbb{P}_q^\mu \phi = \operatorname*{argmin}_{f\in\mathcal{F}_q} \int_{\mathcal{M}} |f-\phi|^2 \mathrm{d}\mu = \left(\operatorname*{argmin}_{c\in\mathbb{C}^q} \int_{\mathcal{M}} |c^*\Psi - \phi|^2 \mathrm{d}\mu \right)^* \Psi.$$

It follows that, for $i = 1, \cdots, Nn$,

$$\begin{aligned} \lim_{m\to\infty} \boldsymbol{e}_i^\top C_x (A_1(m) - A_2(m))\Psi(x) &= \lim_{m\to\infty} \boldsymbol{e}_i^\top C_x \big(Y_1(m)X_1^\dagger(m) - Y_2(m)X_2^\dagger(m)\big)\Psi(x) \\ &= \lim_{m\to\infty} K_{1,q,m}x_i - \lim_{m\to\infty} K_{2,q,m}x_i \\ &= K_{1,q}x_i - K_{2,q}x_i \\ &= \mathbb{P}_q^\mu K_{1|\mathcal{F}_q}x_i - \mathbb{P}_q^\mu K_{2|\mathcal{F}_q}x_i \\ &= \mathbb{P}_q^\mu \left(\boldsymbol{e}_i^\top (\boldsymbol{f}(x) + \boldsymbol{g}(x) - \boldsymbol{f}(x))\right), \end{aligned} \tag{2.19}$$

where $\Psi(x)$ is designed such that $x \in \Psi(x)$, so $K_{1|\mathcal{F}_q}x_i = K_1 x_i$ and $K_{2|\mathcal{F}_q}x_i = K_2 x_i$. If, further, $\boldsymbol{g}(x)$ lies in the span of entries of $\Psi(x)$, then there exists a $G \in \mathbb{C}^{Nn\times q}$ such that $\mathrm{col}_{i=1}^{Nn}(\mathbb{P}_q^\mu(\boldsymbol{e}_i^\top \boldsymbol{g}(x))) = \boldsymbol{g}(x) = G\Psi(x)$, i.e.,

$$\lim_{m\to\infty} C_x(A_1 - A_2)\Psi = G\Psi = \boldsymbol{g}(x), \tag{2.20}$$

where C_x is such that $C_x\Psi(x) = x$. In such case, the set of observables $\Psi(x)$ is said *complete*. □

It should be mentioned that DMD-like methods could only extract the point spectra of the Koopman operator and do not apply to systems with continuous spectra. However, as stated in Proposition 2.1, the proposed method estimates the coupling function as a projection onto the span of q observables, i.e., obtaining $K_g x$ directly as the difference between $K_1 x$ and $K_2 x$. As a result, the estimated coupling function may be just a finite-dimensional approximation based on the observables. Therefore, although the identification accuracy depends on the construction of the observables, the proposed method is expected to apply to a larger class of nonlinear systems.

Remark 2.1. If data are abundant, then A_1, A_2 and in turn K_g can be obtained directly by calculating pseudo-inverse matrices, i.e., let $\lambda = 0$ and

$$A_1 = Y_1 X_1^\dagger, \quad A_2 = Y_2 X_2^\dagger. \tag{2.21}$$

The method can be regarded as performing EDMD proposed in [65] twice for K_1 and K_2, respectively, and will be valid if the data are abundant. However, the proposed method would show better performance in the sense of robustness and accuracy when applied with noisy measurements.

Remark 2.2. Although theoretically, the proposed method can also identify the models of the unforced nodes, i.e., the $\boldsymbol{f}(x)$ function, by obtaining approximations of K_2, such model identification may not reach high accuracy because $K_2 x$ is not required to be in $\mathcal{F}_q^{Nn}$. To make the proposed method applicable to identifying $\boldsymbol{f}(x)$, further requirements on $\Psi(x)$ are needed.

2.4 Numerical examples

In this section, two numerical examples show the usefulness and validity of the proposed method. The first example shows details of the proposed method in the case that functions included in the coupling function are contained in a pre-designed observable dictionary, and the second example considers the case that the functions in the coupling function are not in the dictionary. In addition, the second example shows that the proposed method can estimate the coupling by approximating the coupling function with functions in the dictionary. For both examples, the proposed method is compared with the pseudo-inverse-based method concerning the accuracy of the identification results.

In addition, throughout these examples, the vectors of observable functions $\Psi(x)$ are designed to be real-valued functions instead of complex-valued functions. This restriction comes from that the proposed method can be considered as an embedding of the true coupling function $\boldsymbol{g}(x)$ into the space spanned by the observables in $\Psi(x)$, or an approximation of $\boldsymbol{g}(x)$ using the entries of $\Psi(x)$.

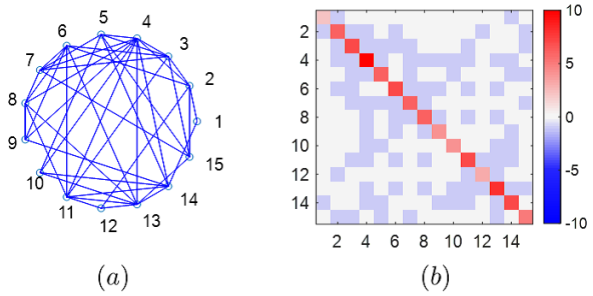

Fig. 2.1: The topology of the Kuramoto model. (a) the connections between nodes, and (b) the graph Laplacian matrix shown in color.

2.4.1 The Kuramoto model: identification with a complete observable set

The proposed method is based on Koopman operators defined in discrete-time settings, so only discrete-time models are obtained. In this example, the identified discrete-time models are transformed into continuous-time manually using the first-order Euler method for the simplicity of visualizing and comparing with the original systems.

Consider the Kuramoto model consisting of $N = 15$ oscillators whose dynamical models are given by

$$\dot{\theta}_i = \omega + \sum_{j=1}^{15} a_{ij} \sin(\theta_j - \theta_i),$$

for $i = 1, \cdots, 15$, where $\theta_i \in \mathbb{R}$, ω is the constant oscillating frequency of all the nodes, and a_{ij} is the (i, j) entry of the adjacency matrix associated with the network topology. The topology of the network shown in Fig.2.1 is an undirected unweighted graph randomly generated such that the probability of $a_{ij} = a_{ji} = 1$ is 50%. Note that it is not required that the connections in the network be sparse, but it is required to design the observables such that the rows of matrices G in (2.16) are sparse. In most cases, this condition is naturally satisfied since the observables should be designed sufficiently rich to contain the coupling function in the spanned space.

As for measured data, each node system is assigned an initial state randomly in the range $[-\pi, \pi]$, and the time series data from those initial states are then obtained by numerical simulations. Suppose that 200 trajectories, each consisting of 51 steps from $k = 0$ to 50 with a sampling time of 0.01s for each node in the network, are available. Also, suppose that another 200 trajectories of 51 steps from $k = 0$ to 50 of an isolated node are available. All the data are measured with random noise uniformly distributed in some range.

Here, let $\theta^j[k] \in \mathbb{R}^{15}$ and $\bar{\theta}^j[k] \in \mathbb{R}$ denote the values of the kth steps of the jth measured trajectories of the network system and the isolated node, respectively, where

$\theta := (\theta_1, \cdots, \theta_{15})^\top$. Then, the measured states are described as the following signals with noise, $\theta^j[k] + \delta^{i,j}$, where $\delta^{i,j} \in \mathbb{R}^{15}$ denotes a noise vector whose elements are assumed to be uniformly distributed in the range $[-0.005, 0.005]$.

The observable set $\Psi(\theta) : \mathbb{R}^{15} \to \mathbb{R}^{241}$ is defined as

$$\Psi(\theta) = \mathrm{col}(1, \theta, \mathrm{col}_{i=1}^{15}(\mathrm{col}_{j=1}^{15}(\cos\theta_j \sin\theta_i))), \tag{2.22}$$

and data matrices $X_1, Y_1 \in \mathbb{R}^{241\times 10^4}$ are then constructed using $\theta^{i,j}$ for $j = 0$ to 49 and $j = 1$ to 50, respectively, as

$$X_1 = \begin{bmatrix} \Psi(\theta^1[0] + \delta^{1,0}) & \cdots & \Psi(\theta^1[49] + \delta^{1,49}) & \cdots & \Psi(\theta^{200}[49] + \delta^{200,49})) \end{bmatrix},$$
$$Y_1 = \begin{bmatrix} \Psi(\theta^1[1] + \delta^{1,1}) & \cdots & \Psi(\theta^1[50] + \delta^{1,50}) & \cdots & \Psi(\theta^{200}[50] + \delta^{200,50})) \end{bmatrix}.$$

On the other hand, data series $\bar{\theta}^j[k]$ is insufficient in dimensions to be the argument of function $\Psi(\cdot)$, so an unconnected network with dynamics (2.3) is imitated using $\bar{\theta}^{i,j}$. The time order of $\bar{\theta}^{i,j}$ is shuffled randomly 15 times while preserving the information on the time evolution of data, i.e., define

$$\xi := \begin{bmatrix} \bar{\theta}^1[0] & \cdots & \bar{\theta}^1[49] & \bar{\theta}^2[0] & \cdots & \bar{\theta}^{200}[49] \\ \bar{\theta}^1[1] & \cdots & \bar{\theta}^1[50] & \bar{\theta}^2[1] & \cdots & \bar{\theta}^{200}[50] \end{bmatrix} \in \mathbb{R}^{2\times 10^4},$$

and define a column shuffling operator $s_i(\xi)$ which shuffles the columns of ξ into some random order i. Let $\xi_{i-} \in \mathbb{R}^{1\times 10^4}$ and $\xi_{i+} \in \mathbb{R}^{1\times 10^4}$ denote the first and the second row of $s_i(\xi)$, respectively, and define

$$\bar{\theta}_- = \mathrm{col}(\xi_{1-}, \cdots, \xi_{15-}), \quad \bar{\theta}_+ = \mathrm{col}(\xi_{1+}, \cdots, \xi_{15+}).$$

Data matrices X_2 and Y_2 are then constructed as

$$X_2 = \begin{bmatrix} \Psi(\bar{\theta}_-^1) & \Psi(\bar{\theta}_-^2) & \cdots & \Psi(\bar{\theta}_-^{10^4}) \end{bmatrix} \in \mathbb{R}^{241\times 10^4},$$
$$Y_2 = \begin{bmatrix} \Psi(\bar{\theta}_+^1) & \Psi(\bar{\theta}_+^2) & \cdots & \Psi(\bar{\theta}_+^{10^4}) \end{bmatrix} \in \mathbb{R}^{241\times 10^4},$$

where $\bar{\theta}_-^i, \bar{\theta}_+^i$ denote the ith columns of $\bar{\theta}_-, \bar{\theta}_+$, respectively.

The coupling function of the network is then obtained by solving (2.13) and substituting the solution into (2.16), where the parameters are set to $\lambda = 0.1$ and $\rho = 3$. Denote the coefficient matrix of the observable vector $\Psi(\theta)$ in the identified coupling function by G, i.e.,

$$\boldsymbol{g}^{id}(\theta) = G\Psi(\theta).$$

As a comparison, let $\tilde{\boldsymbol{g}}^{id}(\theta) = \tilde{G}\Psi(\theta)$ denote the identification results obtained by the pseudo-inverse based method, i.e., let

$$\tilde{G} = C_\theta(Y_1 X_1^\dagger - Y_2 X_2^\dagger).$$

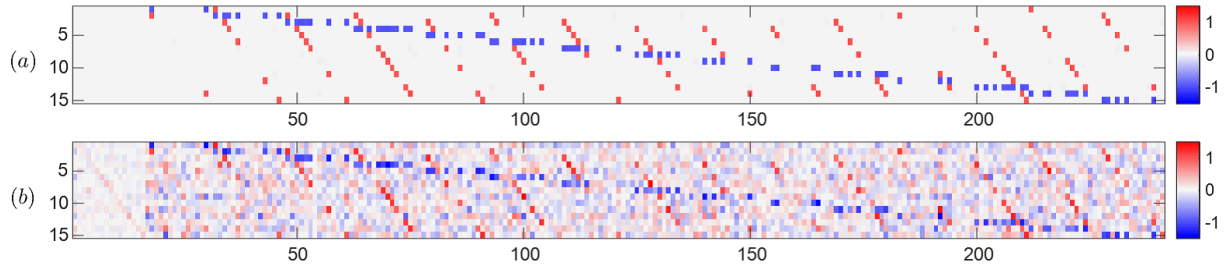

Fig. 2.2: The entries of the identified coefficient matrices: the value of each entry is indicated in color. (a) the values of all the entries in matrix $G \in \mathbb{R}^{15\times 241}$; (b) the values of all the entries in matrix $\tilde{G} \in \mathbb{R}^{15\times 241}$.

Fig.2.2 shows the calculated values of the entries of $G \in \mathbb{R}^{15\times 241}$ and $\tilde{G} \in \mathbb{R}^{15\times 241}$ in color. As the figures show, the identification result obtained with the proposed method shown in Fig.2.2(a) is less noisy than that of the pseudo-inverse based method shown in Fig.2.2(b). As an example of reading Fig.2.2, the first entry of $\boldsymbol{g}^{id}(\theta)$ is obtained as the first row of matrix G multiplying the observable vector $\Psi(\theta)$, which reads

$$\begin{aligned}\boldsymbol{e}_1^\top \boldsymbol{g}^{id}(\theta) =& -1.00\psi_{18} - 0.99\psi_{30} + 0.99\psi_{32} + 0.96\psi_{212},\\ =& -1.00\cos\theta_2 \sin\theta_1 - 0.99\cos\theta_{14}\sin\theta_1 + 0.99\cos\theta_1\sin\theta_2\\ &+ 0.96\cos\theta_1\sin\theta_{14},\end{aligned}$$

where all the values are rounded to 10^{-2}. The estimated coupling function almost coincides with the original function $\boldsymbol{e}_1^\top \boldsymbol{g}(\theta) = \sin(\theta_2 - \theta_1) + \sin(\theta_{14} - \theta_1)$.

To verify the correctness of the identified coupling functions, the true coupling function $\boldsymbol{g}(\theta) = \mathrm{col}_{i=1}^{15} \sum_{j=1}^{15} a_{ij}\sin(\theta_j - \theta_i)$ is projected onto the space spanned by the entries of $\Psi(\theta)$ to obtain a *correct* coefficient matrix $G^{true} \in \mathbb{R}^{15\times 241}$ such that $\boldsymbol{g}(\theta) = G^{true}\Psi(\theta)$. Note that the projection is unique, and the equality holds strictly with $\Psi(\theta)$ designed in (2.22). The relationship between all the entries in G^{true} and the respective identified values in $G, \tilde{G}$ are plotted in Fig.2.3. As the figures show, the coefficient matrix obtained with the proposed method achieves better accuracy.

Although this example considers the case where measurement noises are present, it should be mentioned that the presence of larger noises would disable the proposed method. The method extracts the coupling function from the dynamics of the network, which is obtained by finding the optimal nonlinear function that governs the evolution of measured data. In the presence of large noises, the obtained function would differ from the original dynamics, and the proposed method fails. Due to the same reason, the proposed method requires that the data are sampled simultaneously and no packet loss occurs.

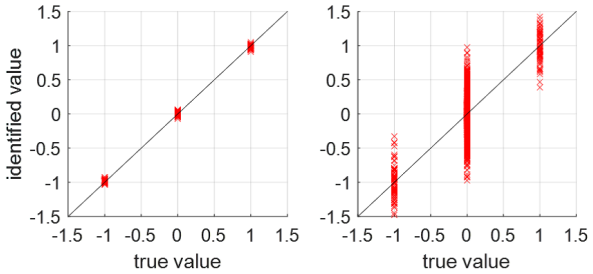

(a) (b)

Fig. 2.3: The relationship between the true values and the identified values of all the entries in the obtained coefficient matrices: (a) entries in G obtained using the proposed method, and (b) entries in $\tilde{G}$ obtained using the pseudo-inverse based method. An entry is perfectly identified if the associated '$\times$' marker is on the black line.

2.4.2 A network of Hindmarsh-Rose neuron systems: identification with an incomplete observable set

Consider a network consisting of 10 Hindmarsh-Rose neuron models, which are chaotic oscillators modeled by

$$\begin{aligned}
x_{i,1}^{+} =& 0.01(-x_{i,1}^3 + 3x_{i,1}^2 + x_{i,2} - x_{i,3} + 3.25 + u_i),\\
x_{i,2}^{+} =& 0.01(1 - 5x_{i,1}^2 - x_{i,2}),\\
x_{i,3}^{+} =& 0.01(0.005(4(x_{i,1} + 1.618) - x_{i,3})),
\end{aligned}$$

for $i = 1, \cdots, 10$. Here, suppose that each coupling input u_i is given by

$$u_i = \frac{2}{\pi} \sum_{j=1}^{10} a_{ij} \mathrm{atan}(x_{j,1} - x_{i,1}),$$

where a_{ij} denotes the (i, j) entry of the adjacency matrix associated with the network. From this equation, it is known that each input is in the range $(-1, 1)$. The topology of the network shown in Fig.2.4 is also randomly generated as an undirected unweighted graph with a 25% probability of $a_{ij} = a_{ji} = 1$.

As original measurements, suppose that measured data of 300 trajectories consisting of 51 steps from both all the nodes in the network and an isolated node are available, respectively. The initial values of all the trajectories are randomly taken in the range $[-2, 2]$, and all the measured data were generated by numerical simulations. Denote the kth step of the jth trajectory of the two time-series by $x^j[k] \in \mathbb{R}^{30}, \bar{x}^j[k] \in \mathbb{R}^3$, respectively, where $x := (x_{1,1}, \cdots, x_{10,1}, x_{1,2}, \cdots, x_{10,2}, x_{1,3}, \cdots, x_{10,3})^\top$.

Define the observables $\Psi(x) : \mathbb{R}^{30} \to \mathbb{R}^{186}$ to be all the states as well as the combinations

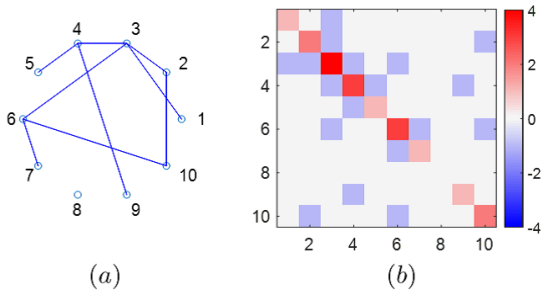

Fig. 2.4: The topology of the Hindmarsh-Rose neuron network. (a) the connection between neurons, and (b) the graph Laplacian matrix shown in color.

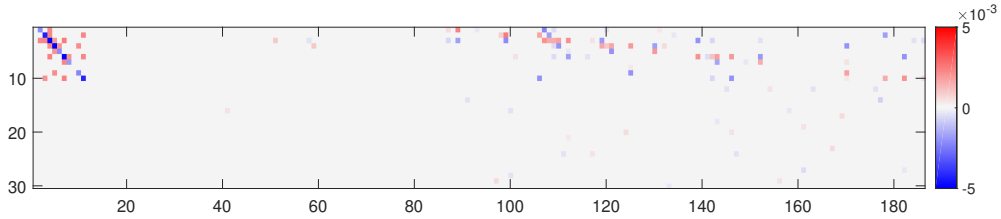

Fig. 2.5: The values of the entries of the identified coefficient matrix G with the proposed method shown in color.

of the first components $x_{i,1}, x_{j,1}$ up to the third power, i.e.,

$$\Psi(x) = \mathrm{col}\big(1, \mathrm{col}_{i=1}^{10}(x_{i,1}), \mathrm{col}_{i=1}^{10}(x_{i,2}), \mathrm{col}_{i=1}^{10}(x_{i,3}), \\ \mathrm{col}_{i=1}^{10}(\mathrm{col}_{j=i}^{10}(\frac{x_{i,1}x_{j,1}}{2})), \mathrm{col}_{i=1}^{10}(\mathrm{col}_{j=i}^{10}(\frac{x_{i,1}^2 x_{j,1}}{6}, \frac{x_{i,1}x_{j,1}^2}{6}))\big), \tag{2.23}$$

from which all the duplicate elements are removed. Then data matrices X_1, Y_1 are calculated directly from $\Psi(x)$ and $\{x^{i,j}\}$, while data matrices X_2, Y_2 are obtained by shuffling the time order of $\bar{x}^{i,j}$ to imitate an unconnected network. Also, suppose that measurement noise exists which is modeled as uniformly distributed random variables in the range $[-0.005, 0.005]$. The optimization problem (2.13) is then solved with $\lambda = 0.1, \rho = 4$.

Figure 2.6 shows the true and the identified coupling function of the first node restricted to the space spanned by $x_{3,1}$ and $x_{1,1}$, respectively. To compare the identified coupling function with the true coupling function $\boldsymbol{e}_1^\top \boldsymbol{g}(x) = \frac{2}{\pi}\mathrm{atan}(x_{3,1} - x_{1,1})$, $\boldsymbol{e}_1^\top \boldsymbol{g}(x) - \boldsymbol{e}_1^\top \boldsymbol{g}^{id}(x)$ is plotted restricted to the space spanned by $x_{1,1}$ and $x_{3,1}$ in Fig.2.7. As the figure shows, the identified coupling function matches the true coupling function in the domain where data are measured (as indicated by the frame) and deviates otherwise. This is the best one can get with the designed observables and the measured data, while better identification accuracy can be obtained if the observable dictionary contains elements that approximate $\boldsymbol{g}(x)$ better, e.g., including $\mathrm{atan}(x_{j,1} - x_{i,1}), \forall i, j = 1, \cdots, N,\ j \neq i$ as entries of $\Psi(x)$.

Next, simulation results about how the identification accuracy is influenced by the amount of measured data are shown. The identification results are also compared with

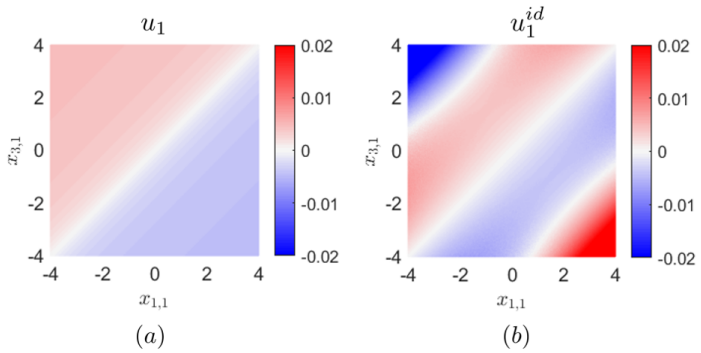

Fig. 2.6: (a) The true coupling function and (b) the identified coupling function restricted to the space spanned by $x_{1,1}$ and $x_{3,1}$.

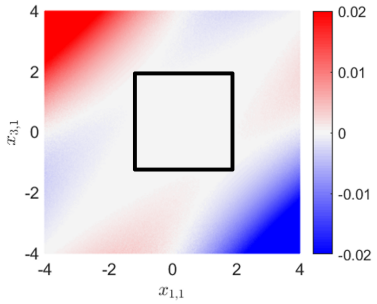

Fig. 2.7: The difference of the true coupling function $\boldsymbol{e}_1^\top \boldsymbol{g}(x)$ and the identified coupling function $\boldsymbol{e}_1^\top \boldsymbol{g}^{id}(x)$ of the first state plotted near the origin of the space spanned by $x_{1,1}$ and $x_{3,1}$. The true coupling function is correctly approximated over $[-1, 2] \times [-1, 2]$ (i.e., the area within the frame), which is the domain where data are measured from.

those obtained with the pseudo-inverse-based method.

Here, the set of observables is also defined by (2.23) as in the previous simulation. The set is incomplete, in the sense that the spanned space of its entries does not contain the coupling function $\boldsymbol{g}(x)$ which are arc-tangent functions. As a result, obtaining a G^{true} could be hard, and the identification accuracy is quantified in terms of the identified network connectivity, instead of some other metrics that are related to every entry in G. In the case that the coupling strength $\frac{2}{\pi}$ is known, the connectivity of the network can be extracted from the coefficients of the x observables, i.e., the $\mathrm{col}_{i=1}^{10}(x_{i,1}), \mathrm{col}_{i=1}^{10}(x_{i,2}), \mathrm{col}_{i=1}^{10}(x_{i,3})$ terms in (2.23). Here, the connectivity identification accuracy of the proposed method and the pseudo-inverse-based method are compared.

Suppose that M trajectories each consisting of 11 steps (with a sampling time of 0.01[s]) from both the nodes in the network and an isolated node are available where $M \in \mathbb{N}$. To

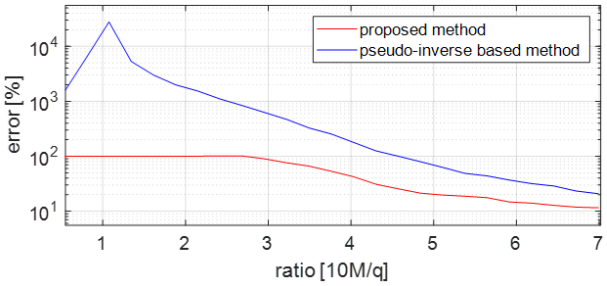

Fig. 2.8: The relationship between the identification accuracy and the amount of measurement data plotted in logarithmic scale. The proposed method can identify the network connectivity with smaller errors and achieves better identification accuracy.

quantify the identification accuracy, define the identification error by

$$e = \frac{\|L^{id} - L^{true}\|_F}{\|L^{true}\|_F} \times 100\%,$$

where L^{true} and L^{id} are the true and the identified graph Laplacian matrices, respectively, associated with the network.

Let $M = 10, 25, 20, \cdots, 130$. For each M, the identification is performed 5 times with different random initial data, and the average identification error is recorded. The topology of the network is generated randomly in each identification where the probability of two nodes being directly connected is 25%, and the parameters of the optimization algorithm are set to $\lambda = 0.1, \rho = 4$. Fig.2.8 shows the identification errors obtained via the proposed method and the pseudo-inverse based method as functions of the *data ratio*, which is defined to be the ratio of the amount of data pairs to the number of observables, i.e., $\frac{10M}{q}$.

As Fig.2.8 shows, both the two methods reach higher identification accuracy with more data, while the proposed method provides relatively higher accuracy. Also, the identification accuracy of the proposed method converges to that of the pseudo-inverse matrix method, as shown in Proposition 2.1. On the other hand, the identification error of the proposed method is bounded, while the error blows up in the pseudo-inverse-based method case. This is because the pseudo-inverses are calculated via the singular value decomposition (SVD) method, i.e., $A_1 = Y_1 X_1^\dagger = Y_1(V\Sigma^\dagger U^*)$ where

$$\Sigma^\dagger = \begin{bmatrix} \mathrm{diag}(\sigma_i^\dagger) & \mathbf{0} \end{bmatrix} \text{ or } \begin{bmatrix} \mathrm{diag}(\sigma_i^\dagger) \\ \mathbf{0} \end{bmatrix}, \quad \sigma_i^\dagger = \begin{cases} \sigma_i^{-1}, & \sigma_i \neq 0, \\ 0, & \sigma_i = 0, \end{cases}$$

and $\Sigma^\dagger = \mathrm{diag}(\sigma_i^\dagger)$ when $\frac{10M}{q} = 1$. As a result, a small singular value could lead to a large identification error. While in the proposed method, the identity matrix I_q is introduced to the first terms in (2.15a) and (2.15b), which ensures that the matrices are invertible.

2.5 Conclusions and discussions

In this chapter, the identification problem of network structures is considered, and an identification method is proposed. The structural characteristics are formulated as the coupling function of the nodes and extracted as a linear combination of manually defined observables using Koopman analysis and sparse identification techniques. Two identification examples are shown to verify the usefulness of the proposed algorithm. The comparisons with the pseudo-inverse-based method show that the proposed method remains valid even under the influence of measurement noise.

The proposed method does not require that all the measured data belong to the same trajectory, because what matters is how data evolves, i.e., the pair $(x^{i,j}, x^{i,j+1})$. Actually in the identification process, the time order of $\bar{x}^{i,j}$ is randomly, but the pair $\bar{x}^{i,j}, \bar{x}^{i,j+1}$ is kept bound. A similar consideration can be found in the EDMD method proposed in [65] where only randomly taken data pairs are required.

There are still drawbacks and problems that remain to be solved in the future. The method proposed in this chapter requires data from isolated nodes, which is a very strict assumption from a practical point of view. If the nodes in the network fully synchronize, then the dynamics on the synchronization manifold can be considered as that of the isolated nodes, however, such synchronization would make the network structure unidentifiable as shown in [25], because $\boldsymbol{g}(x)$ vanishes. The proposed method also requires that the full states of all the nodes be measurable, although generally, only output data of the nodes may be available in practice. Also, the proposed method does not apply to networks whose topology is time-varying such as networks with switching topology.

On the other hand, as mentioned in Proposition 2.1, the proposed method obtains a projection of the coupling function over the space spanned by the observables. The design of the observable set $\Psi(x)$ greatly influences the identification accuracy, but it lacks an optimal design method for the coupling function. In the numerical examples, combinations of basis functions constructed out of the states of all the nodes are employed, which ensures accurate approximation over certain domains, but also leads to high computational costs. Design of the observables can be performed theoretically by using GLA methods, or by considering the physical characteristics of the network and measured data.

3 Identification of Network Structure Changes Using Streaming Data Sets of Measurable Full-states

3.1 Introduction

In the previous chapter, an identification method for network structures is proposed based on Koopman analysis and sparse identification. The proposed method treats the structure of a network as the coupling function that describes the data flow in the network and approximates the coupling function using linear combinations of pre-defined observables. However, the proposed method has two significant drawbacks. First, the coupling function is obtained as the difference between two Koopman operators corresponding to the network and some isolated nodes, respectively, to approximate which both data from the network and the isolated nodes are required. However, it is generally difficult to obtain a large amount of data from an isolated node, especially in the case where networks are in operation. Second, the method solves the problem in a post-processing manner, so it cannot be applied to cases in which the network structures change during data recording.

In this chapter, an identification algorithm for network structures is proposed by adding some restrictions to the network structures to overcome these drawbacks. In particular, under the assumptions that the network topology is an undirected graph and that the data flows between any two nodes are symmetric, the first drawback is solved. To solve the second drawback, the previous algorithm is modified so it employs streaming data sets to detect changes in network structures. Similar implementations can be found in the streaming dynamical mode decomposition (sDMD) method proposed in [77]. Such implementations can also be found in, e.g., [24, 25, 77]. In [24], assuming the dynamics and the coupling functions to be known, an observer-like auxiliary system is designed to synchronize with the network system, and the variables converge to the coupling strengths practically. In [25], a dynamical coupling input to the auxiliary system replaces the static input in [24] which makes the convergence asymptotic. Besides, [77] performs the DMD method with streaming data sets which bring the DMD in real-time. In this chapter, design *nonlinear* observables are designed to identify nonlinear coupling functions accurately. From the viewpoint of Koopman analysis, the proposed method can be considered

as obtaining and updating an approximation of a Koopman operator at every time step using newly measured data. The relationship between the identification result and the actual coupling function is also theoretically verified, and derive conditions under which a time-invariant approximation of the Koopman operator can be obtained using time-varying data matrices.

This chapter is organized as follows. Section 3.2 proposes a modification of the method proposed in the previous chapter to relax some requirements and construct an identification algorithm that detects network structure changes. Convergence conditions of the proposed method are also derived in Section 3.2. Section 3.3 presents numerical examples to illustrate the validity of the modified algorithm and in Section 3.4, a summary of the results obtained in this chapter and some additional remarks are given.

3.2 Identification of Network Structure Changes

Consider a network system consisting of N identical discrete-time systems described by

$$x_i^+ = f(x_i) + \sum_{j=1}^{N} a_{ij} g(x_i, x_j), \tag{3.1}$$

for $i = 1, \cdots, N$, where $x_i \in \mathbb{R}^n, f : \mathbb{R}^n \to \mathbb{R}^n$, and $g : \mathbb{R}^n \times \mathbb{R}^n \to \mathbb{R}^n$. The function g denotes the coupling function between any two systems, and a_{ij} is the (i, j) entry of the adjacency matrix associated with the network topology.

To simplify the description, define $x = \mathrm{col}(x_1, \cdots, x_N) \in \mathbb{R}^{Nn}$ and rewrite the dynamics of the network as the following compact form:

$$x^+ = \boldsymbol{f}(x) + \boldsymbol{g}(x), \tag{3.2}$$

where $\boldsymbol{f}(x) = \mathrm{col}_{i=1}^{N}(f(x_i))$ and $\boldsymbol{g}(x) = \mathrm{col}_{i=1}^{N}(\sum_{j=1}^{N} a_{ij} g(x_i, x_j))$. Here, $\boldsymbol{g}(x)$ is called the *coupling function* of the network, which contains information about both the data flow in the network and the network topology, and corresponds to the network structure to be identified. On the other hand, N uncoupled systems can be described as

$$x^+ = \boldsymbol{f}(x). \tag{3.3}$$

Let $\mathcal{F}$ denote the functional space consisting of all of the observables $\psi(x)$, i.e., $\mathcal{F} = \{\psi \mid \psi : \mathbb{R}^{Nn} \to \mathbb{C}\}$. Now, define two Koopman operators $K_1 : \mathcal{F} \to \mathcal{F}$ and $K_2 : \mathcal{F} \to \mathcal{F}$ corresponding to systems (3.2) and (3.3) as follows:

$$K_1\psi(x) = \psi(\boldsymbol{f}(x) + \boldsymbol{g}(x)), \tag{3.4}$$

$$K_2\psi(x) = \psi(\boldsymbol{f}(x)). \tag{3.5}$$

Then, the evolution of the state of each system can be described as $K_1 x = \boldsymbol{f}(x)+\boldsymbol{g}(x)$ and $K_2 x = \boldsymbol{f}(x)$, respectively. In addition, defining the difference operator for two operators as $K_g = K_1 - K_2$, one has

$$\begin{aligned} K_g x =& \boldsymbol{f}(x) + \boldsymbol{g}(x) - \boldsymbol{f}(x) \\ =& \boldsymbol{g}(x). \end{aligned} \tag{3.6}$$

This equation means that the identification problem for the network structure can be solved by determining K_1 and K_2 from the measured data.

As a result, as shown in the previous Chapter, if measured data for the states of both the coupled system (3.2) and the completely uncoupled system (3.3) could be obtained, then the network structure of system (3.2) could be detected as an approximation of the difference operator K_g.

3.2.1 Detection of K_g from measured data

In the previous Chapter, it is assumed that data can be measured from at least one isolated node to obtain an approximation of K_2 corresponding to system (3.3), but this assumption is not realistic in practical situations. Therefore, this chapter considers relaxing the assumption by adding some restrictions to the network structure.

Throughout this chapter, the following assumptions are made for the coupling function $g(x_i, x_j)$ and the adjacency matrix associated with network system (3.1).

Assumption 3.1. The coupling function $g(x_i, x_j)$ is skew-symmetric, i.e., $g(x_i, x_j) = -g(x_j, x_i)$ for any x_i and x_j.

Assumption 3.2. The adjacency matrix $[a_{ij}]$ satisfies $a_{ij} = a_{ji}$ and $a_{ii} = 0$.

Assumption 3.1 means that the numerical summation of $g(x_i, x_j)$ and $g(x_j, x_i)$ is always 0, and it is well known that diffusive couplings in reaction-diffusion systems satisfy this assumption. Assumption 3.2 means that the graph representation of the network topology is undirected and has no self-loop. Under these assumptions, it is shown show that K_g, which is the difference between K_1 and K_2, can be obtained approximately without any data for the completely uncoupled systems.

The coupling function is identified following two steps: first to obtain an approximation of $K_1 x$, and then to determine $K_2 x$ from $K_1 x$.

In the first step, to obtain an approximation of $K_1 x$ from data, assume that a time series of the states of system (3.1) for $m + 1$ steps is measured as $\{x[0], \cdots, x[m]\}$. In addition, define a set of q observables as $\Psi(x) = \mathrm{col}(\psi_1(x), \cdots, \psi_q(x)) : \mathbb{R}^{Nn} \to \mathbb{C}^q$ where

$\psi_i : \mathbb{R}^{Nn} \to \mathbb{C}$ for $i = 1, \cdots, q$, and define data matrices X and Y as

$$X = \begin{bmatrix} \Psi(x[0]) & \Psi(x[1]) & \cdots & \Psi(x[m-1]) \end{bmatrix},$$
$$Y = \begin{bmatrix} \Psi(x[1]) & \Psi(x[2]) & \cdots & \Psi(x[m]) \end{bmatrix}.$$

For K_1 satisfying (3.4), $\Psi(x[k+1]) = K_1\Psi(x[k])$, and, in turn, the following equation hold:

$$\begin{bmatrix} \Psi(x[1]) & \cdots & \Psi(x[m]) \end{bmatrix} = \begin{bmatrix} K_1\Psi(x[0]) & \cdots & K_1\Psi(x[m-1]) \end{bmatrix}.$$

As a result, a q-dimensional approximation of $K_1 x$ is obtained as

$$K_1 x \approx A_1 \Psi(x), \tag{3.7}$$

where $A_1 := C_x A_0$, $C_x \in \mathbb{C}^{Nn \times q}$ is such that $x = C_x \Psi(x)$, and A_0 is a transition matrix that maps X to Y, i.e.,

$$A_0 = \underset{A}{\operatorname{argmin}} \, \|AX - Y\|_F. \tag{3.8}$$

Note that although C_x contains the expansion coefficients of x from $\Psi(x)$, one can design $\Psi(x)$ such that the expansion is trivial, i.e., let $\Psi(x) = \operatorname{col}(x, \psi_1, \cdots, \psi_{q-Nn})$, then $C_x = [I_{Nn}, \mathbf{0}_{Nn \times (q-Nn)}]$.

Next, as the second step, it is shown that $K_2 x$ can be obtained from $K_1 x$ without using the data for the completely uncoupled system (3.3). The core idea here is that, under Assumptions 3.1 and 3.2, $a_{ij} g(x_i, x_j)$ always cancels out $a_{ij} g(x_j, x_i)$ numerically for any $j \neq i$. This means that the terms describing data transmissions vanish if added, and what remains is the unforced dynamical models of the node systems corresponding to $K_2 x$. Under the assumptions, $a_{ij} g(x_i, x_j) + a_{ji} g(x_j, x_i) = 0$ holds, and

$$\begin{aligned} \sum_{i=1}^{N} \sum_{j=1}^{N} a_{ij} g(x_i, x_j) &= \sum_{i=1}^{N} \sum_{j=1}^{i-1} a_{ij} g(x_i, x_j) + \sum_{j=1}^{N} \sum_{i=1}^{j-1} a_{ij} g(x_i, x_j) \\ &= \sum_{i=1}^{N} \sum_{j=1}^{i-1} \big(a_{ij} g(x_i, x_j) + a_{ji} g(x_j, x_i) \big) = 0, \end{aligned} \tag{3.9}$$

where $a_{ii} = 0$ is substituted to the first equality. Equation (3.9) indicates that if $x_i[k] = \bar{x}_i[k]$ for $i = 1, \cdots, N$, then $\sum_{i=1}^{N} x_i[k+1] = \sum_{i=1}^{N} \bar{x}_i[k+1]$ holds with respect to dynamics (3.2) and (3.3). Using the definitions of Koopman operators K_1 and K_2, the following equation holds

$$\sum_{i=1}^{N} K_1 x_i = \sum_{i=1}^{N} K_2 x_i, \tag{3.10}$$

which acts as a bridge between K_2x and K_1x. Defining matrices $C_1, \cdots, C_N \in \mathbb{R}^{n\times Nn}$ such that $x_i = C_i x$ for $i = 1, \cdots, N$, and substituting (3.7) into (3.10), the following equation holds

$$\sum_{i=1}^{N} K_2 x_i \approx \sum_{i=1}^{N} C_i A_1 \Psi(x). \tag{3.11}$$

Note that the right-hand side of (3.11) has already been identified from data and is considered known.

Next, individuals, i.e., K_2x_i, from the summation based on the known right-hand side of (3.11) are extracted from the summation. Note that $\sum_{i=1}^{N} K_2x_i$ is a summation of the same function $f(\cdot)$ mapping different variables $x_1, \cdots, x_N$, which is highly symmetric. As a result, if an approximation of K_2x in terms of a linear combination of the observables $\Psi(x)$ is desired, as one of K_1x, then all of the coefficients of *multi-variable* observables, e.g., $\psi_k(x_i, x_j)$, in such a linear combination must have 0 as coefficients. As a result, equation (3.11) can be rewritten as

$$\sum_{i=1}^{N} K_2 x_i \approx D + B_1\Psi_1'(x_1) + \cdots + B_N\Psi_2'(x_N) + \mathbf{0}_{n\times(q-\sum_{i=1}^{N} p_i)}\Psi_o'(x), \tag{3.12}$$

where $D \in \mathbb{R}^n$ is a vector of constants, $\Psi_i'(x_i) : \mathbb{R}^n \to \mathbb{C}^{p_i}$ with some $p_i \leq q/N$ is a sub-vector of observables contained in $\Psi(x)$, which contains all of the observables that *only* have x_i as variables, and $\Psi_o'(x)$ contains observables of multiple variables. Here, $B_i \in \mathbb{C}^{n\times p_i}$ is the coefficient matrix of the linear combination $B_i\Psi_i'(x_i)$, and D will appear if the observable set $\Psi(x)$ is designed to contain a constant observable. It follows (3.12) that

$$f(x_i) = K_2x_i \approx \frac{D}{N} + B_i\Psi_i'(x_i),$$

which is an approximation of K_2x_i. To obtain matrix A_2 such that $K_2x \approx A_2\Psi(x)$, rewrite $K_2x_i = D/N + B_i\Psi_i'(x_i)$ for $i = 1, \cdots, N$ as a linear combination of $\Psi(x)$. Since $\Psi_i'(x_i)$ is a sub-vector of $\Psi(x)$, there always exists $B_i' \in \mathbb{C}^{n\times q}$ such that $K_2x_i = D/N + B_i\Psi_i'(x_i) = B_i'\Psi(x)$. Then A_2 can be obtained as

$$A_2 = \mathrm{col}(B_1', \cdots, B_N') \in \mathbb{C}^{Nn\times q}. \tag{3.13}$$

Finally, to obtain K_g, recall that K_g is defined as the difference between K_1 and K_2. As a result, the coupling function $\boldsymbol{g}(x)$ can be identified from the approximations of K_1x and K_2x, i.e.,

$$\boldsymbol{g}^{id}(x) = K_g x \approx (A_1 - A_2)\Psi(x). \tag{3.14}$$

3.2.2 Detecting Network Structure Changes using Streaming Data Sets

To detect changes in network structure, the identification procedures are performed over an $(m+1)$-step-long horizon making use of newly measured data at every time step. At step k, define data matrices $X[k]$ and $Y[k]$ by

$$\begin{aligned} X[k] &= \begin{bmatrix} \Psi(x[k-m]) & \Psi(x[k-2]) & \cdots & \Psi(x[k-1]) \end{bmatrix}, \\ Y[k] &= \begin{bmatrix} \Psi(x[k-m+1]) & \Psi(x[k-m]) & \cdots & \Psi(x[k]) \end{bmatrix}. \end{aligned} \tag{3.15}$$

Then, an approximation of $K_1 x$ at step k, i.e., $A_1[k]\Psi(x)$, can be calculated with $X[k]$ and $Y[k]$. For the case in which $m \gg q$, $A_1[k]$ can be directly obtained by

$$A_1[k] = C_x \underset{A}{\operatorname{argmin}} \|AX[k] - Y[k]\|_F = C_x A_0[k] = C_x Y[k] X^\dagger[k], \tag{3.16}$$

where $X^\dagger$ denotes the Moore-Penrose inverse of matrix X, and C_x is such that $C_x \Psi(x) = x$. However, if the amount of data is limited due to practical reasons such as the capacity of data storage systems, then $A_1[k]$ cannot be detected with high accuracy. In such a case, sparse identification techniques are employed to obtain $A_1[k]$ and hence K_g. For $i = 1, \cdots, q$, consider the optimization problem

$$\begin{aligned} a_{0i}[k] = \underset{a}{\operatorname{argmin}} \ & \|a\|_1 \\ \text{subject to} \ \ & aX[k] = y_i[k], \end{aligned}$$

or equivalently ([85]),

$$a_{0i}[k] = \underset{a}{\operatorname{minimize}} \ \ \|X^*[k]a^* - y_i^*[k]\|_2^2 + \lambda \|a\|_1, \tag{3.17}$$

where $\lambda > 0$, $a_{0i}[k]$ is the ith row of $A_0[k]$, and $y_i[k]$ is the ith row of $Y[k]$.

To solve the optimization problem (3.17), ADMM ([87]) is employed. A vector-wise updating algorithm of the variables is given explicitly by

$$a_{0i}^*[k] = -\frac{1}{2}(X[k]X^*[k] + \frac{\rho}{2} I_q)^{-1}(-2X[k]y_i^*[k] + w_i^*[k-1] - \rho v_i^*[k-1]), \tag{3.18a}$$

$$v_i^*[k] = \mathcal{S}_{\lambda/\rho}(a_{0i}^*[k] + \frac{1}{\rho} w_i^*[k-1]), \tag{3.18b}$$

$$w_i^*[k] = w_i^*[k-1] + \rho(a_{0i}^*[k] - v_i^*[k]), \tag{3.18c}$$

for $i = 1, \cdots, q$ where a_{0i}, v_i are the primal variables, w_i is the dual variable and $\rho > 0$. Here, $\mathcal{S}_\gamma$ is a soft-thresholding operator defined by

$$\mathcal{S}_\gamma(x) = \begin{cases} x - \gamma \operatorname{sgn}(x) & |x| > \gamma \\ 0 & |x| \leq \gamma \end{cases}$$

for some $\gamma > 0$, and the operator acts on a vector or a matrix in an entry-wise manner. Furthermore, update the variables in a matrix-wise manner to reduce computational costs:

$$A_0^*[k] = -\frac{1}{2}(X[k]X^*[k] + \frac{\rho}{2}I_q)^{-1}(-2X[k]Y^*[k] + W^*[k-1] - \rho V^*[k-1]), \tag{3.19a}$$

$$V^*[k] = \mathcal{S}_{\lambda/\rho}(A_0^*[k] + \frac{1}{\rho}W^*[k-1]), \tag{3.19b}$$

$$W^*[k] = W^*[k-1] + \rho(A_0^*[k] - V^*[k]). \tag{3.19c}$$

The optimal $A_0^\star$ is used for constructing A_1, A_2 and $\boldsymbol{g}^{id}(x)$ via $A_1 = C_x A_0^\star$, (3.13) and (3.14), respectively.

Finally, an algorithm for the above-mentioned network identification approach is constructed in Algorithm 3.1.

Remark 3.1. Assumptions 3.1 and 3.2 ensure that the influence of $\boldsymbol{f}(x)$ can be totally removed, and the coupling function $\boldsymbol{g}(x)$ can be accurately identified. If the assumptions do not hold, the equation (3.10) does not hold and $K_2 x_i$ cannot be extracted, so the coupling function could not be accurately identified. However, the information sent from node j to node i can still be identified as a linear combination of the observables that are *dependent* on x_j, which may be a coupling function to be identified.

Algorithm 3.1 Proposed identification algorithm

Input: Observables $\Psi(x) \in \mathbb{C}^q$, matrix $C_x \in \mathbb{C}^{Nn \times q}$ such that $x = C_x \Psi(x)$, parameters ρ, λ, m and convergence criteria $L, \varepsilon > 0$

Output: $\boldsymbol{g}^{id}(x) = C_x(A_1 - A_2)\Psi(x)$

1. Initialization: Define variables $A_0, V, W \in \mathbb{R}^{q \times q}$ and data matrices $X, Y \in \mathbb{R}^{q \times m}$ as zero matrices.

2. At time step k: Construct data matrices $X[k]$, $Y[k]$ with (3.15)

Update A_0, V, and W with (3.19a), (3.19b) and (3.19c), respectively.

4. Convergence verification:

if $\frac{1}{L}\sum_{i=k}^{k-L+1} \|A_0[i] - A_0[i-1]\| < \varepsilon$ **then**

record $A_0[k]$ as $A_0^\star$ and go to step **5**

else

set $k \leftarrow k+1$ and go to step **2**

end if

5. Result: Calculate A_1, A_2 and $\boldsymbol{g}^{id}(x)$ via $A_1 = C_x A_0^\star$, (3.13), and (3.14), respectively.

3.2.3 Error and convergence analysis

In this subsection, a brief theoretical analysis of the proposed identification method is given. It is first shown that the identified result is a projection of the actual coupling

function, and then conditions are derived under which a time-invariant solution to the optimization problem (3.8) can be obtained using time-varying data matrices $X[k]$ and $Y[k]$.

Proposition 3.1. If the obtained data sequence is sufficiently long and distributes uniformly, then the identified coupling function $\boldsymbol{g}^{id}(x) = (A_1 - A_2)$ is an L_2 projection of the coupling function $\boldsymbol{g}(x)$ onto the space spanned by the entries of $\Psi(x)$, i.e.,

$$\boldsymbol{g}^{id}(x) = \mathbb{P}_{\text{span}\{\Psi(x)\}^{Nn}}\boldsymbol{g}(x),$$

on the manifold where the data are measured.

Proof. It is known that if $m \to \infty$, then A_0 obtained by solving (3.8) is the optimal approximation of Koopman operator K_1 in the sense that A_0 minimizes $\|A_0\Psi - K\Psi\|_{L_2}$ ([94, 95]). For any observable $\varphi \in \mathcal{F} = \{f \mid f : \mathbb{R}^{Nn} \to \mathbb{C}\}$, $K\varphi$ can be approximated as $K\varphi \approx c_\varphi A_0\Psi$, where c_φ minimizes $\|c_\varphi\Psi - \varphi\|_{L_2}$. As a result,

$$\begin{aligned} A_1\Psi(x) =& C_x A_0\Psi(x) = C_x(\text{argmin}_A\|A\Psi(x) - K\Psi(x)\|_{L_2})\Psi(x) \\ =& C_x\mathbb{P}_{\text{span}\{\Psi(x)\}^{Nn}}(K\Psi(x)) = \mathbb{P}_{\text{span}\{\Psi(x)\}^{Nn}}(Kx) \\ =& \mathbb{P}_{\text{span}\{\Psi(x)\}^{Nn}}(\boldsymbol{f}(x) + \boldsymbol{g}(x)), \end{aligned}$$

for $i = 1, \cdots, Nn$ where C_x satisfies $C_x\Psi(x) = x$. On the other hand, the construction of A_2 indicates

$$\begin{aligned} A_2\Psi(x) =& \text{col}_{i=1}^{N}\big(\mathbb{P}_{\text{span}\{\Psi_i'\}^n}(\sum_{j=1}^{N}(C_j A_1\Psi(x) + D/N))\big) \\ =& \text{col}_{i=1}^{N}\big(\mathbb{P}_{\text{span}\{\Psi_i'\}^n}(\mathbb{P}_{\text{span}\{\Psi(x)\}^n}(\sum_{j=1}^{N} C_j\boldsymbol{f}(x) + \sum_{j=1}^{N} C_j\boldsymbol{g}(x)))\big) \\ =& \mathbb{P}_{\text{span}\{\Psi(x)\}^{Nn}}K_2 x, \end{aligned}$$

where the fact that $\mathbb{P}_{\text{span}\{\Psi_i'\}^n}f(x_i) = \mathbb{P}_{\text{span}\{\Psi(x)\}^n}f(x_i)$ is used. As a result,

$$\begin{aligned} \boldsymbol{g}^{id}(x) =& (A_1 - A_2)\Psi(x) = \mathbb{P}_{\text{span}\{\Psi(x)\}^{Nn}}K_1 x - \mathbb{P}_{\text{span}\{\Psi(x)\}^{Nn}}K_2 x \\ =& \mathbb{P}_{\text{span}\{\Psi(x)\}^{Nn}}\boldsymbol{g}(x). \end{aligned}$$

□

Next, conditions on the number of measured data and the design of observables are derived under which a time-invariant approximation of Koopman operator K_1, i.e., $A_1[k]$ in (3.16), exists.

Proposition 3.2. Assume that the network structure is time-invariant over an interval $[T_1, T_2]$, where $T_2 - T_1 > m + 1$. In the case where $m \geq q$, if the observable set $\Psi(x)$ is sufficiently rich, i.e., there exists a matrix F such that $F\Psi(x) = \boldsymbol{f}(x) + \boldsymbol{g}(x)$, then the optimality of (3.16) is time-invariant over $[T_1 + m + 1, T_2]$.

Proof. Note that $\boldsymbol{f}(x[k]) + \boldsymbol{g}(x[k]) = x[k+1] = C_x\Psi(x[k+1])$ holds and consider the matrix A_1 obtained at step k:

$$\begin{aligned} A_1[k] = C_x A_0[k] =& \underset{(C_x A)}{\operatorname{argmin}}(\|C_x AX[k] - C_x Y[k]\|_F^2) \\ =& \underset{(C_x A)}{\operatorname{argmin}}(\|(C_x A)X[k] - FX[k]\|_F^2), \end{aligned}$$

where $C_x Y[k] = \left[\cdots, \boldsymbol{f}(x[k+j]) + \boldsymbol{g}(x[k+j]), \cdots\right]_{j=0,\cdots,m-1} = FX[k]$ is used. The optimization problem becomes time-invariant with a globally unique optimality as long as $X[k]$ has full rank. □

Note that in the case where data are not sufficient, $(C_x A)X[k] - FX[k] = 0$ may not indicate $C_x A - F = 0$. In such a case, the algorithm (3.19) is used to solve the inverse problem to find $A_0[k]$ using sparsity. The fixed point of the algorithm also minimizes $\|A_0\Psi(x) - \Psi(\boldsymbol{f}(x) + \boldsymbol{g}(x))\|_{L_2}$, but would deviate slightly from A_0^{true}. The deviation depends on the parameters ρ and λ.

3.3 Numerical examples

In this section, three numerical examples are given to show the validity of the obtained results. Specifically, the first example is a detailed example of determining $K_2 x$ and $\boldsymbol{g}(x)$ from $K_1 x$, and the second example shows that the proposed method successfully detects and records changes in network topology. In the third example, data generated using a SPICE model are employed, which are sampled aperiodically, to simulate measured real data.

3.3.1 A network of chaotic scalar oscillators

This example shows in detail how matrices A_1 and A_2 are constructed and how the coupling function is obtained.

Consider a network of 10 scalar oscillators ([96]), the ith node of which is modeled by

$$x_i^+ = \beta I(x_i) + \delta + u_i, \tag{3.20}$$

$$u_i = \sum_{j=1}^{10} l_{ij} I(x_i), \tag{3.21}$$

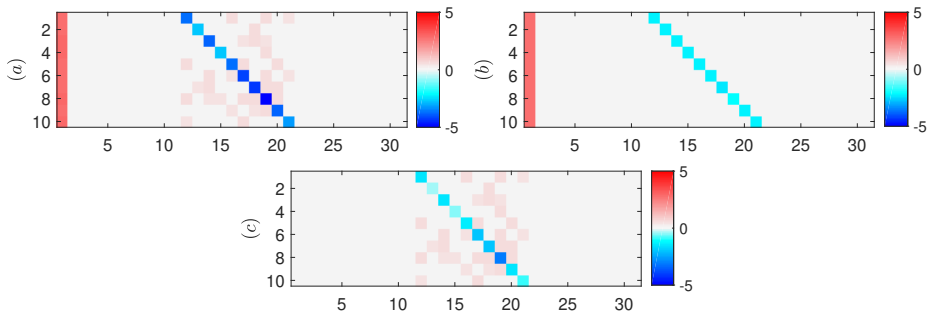

Fig. 3.1: The identification results at $k = 250$: (a) matrix A_1 which corresponds to dynamics (3.20). The color plotted at coordinate (i, j) in the figure corresponds to the (i, j) entry in matrix A_1; (b) matrix A_2 constructed based on A_1 which corresponds to the dynamics of all the nodes when isolated and (c) matrix $A_1 - A_2$ which corresponds to the coupling function.

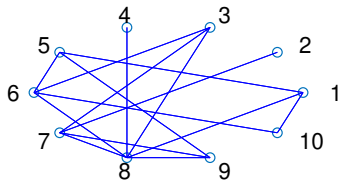

Fig. 3.2: The identified network topology.

for $i = 1, \cdots, 10$, where $x_i \in \mathbb{R}$, $I(x) = 0.5(1 - \cos x)$ and l_{ij} is the (i, j) entry of the Laplacian matrix $\mathcal{L}$ associated with the network topology. Each oscillator behaves chaotically when the parameters are set to $\beta = 1.45\pi$ and $\delta = 0.525$. The network is a randomly generated undirected unweighted graph in which the probability of $a_{ij} = a_{ji} = 1$ is 50%.

Suppose that the data storage system is capable of storing 36 steps of measured data from all of the nodes, i.e., $m = 35$. Define the observable set $\Psi(x) : \mathbb{R}^{10} \to \mathbb{R}^{31}$ by

$$\Psi(x) = \mathrm{col}(1, x, \mathrm{col}_{i=1}^{10}(\cos x_i), \mathrm{col}_{i=1}^{10}(\sin x_i)), \tag{3.22}$$

and initialize data matrices $X, Y \in \mathbb{R}^{31\times 35}$ as zero matrices. Specifically, let the data be measured with some measurement noises, which are random signals distributed uniformly in $[-0.05, 0.05]$. At each time step of the simulation process, optimization (3.19a)-(3.19c) is performed with parameters set to $\rho = 3$ and $\lambda = 10^{-4}$.

The time evolution of the states is obtained in terms of $K_1 x$ as $A_1\Psi(x)$. In addition, A_2 is constructed based on $A_1\Psi(x)$. Here, take $A_1[250]$ obtained at the last step of the simulation as an example. The entries of $A_1 \in \mathbb{R}^{10\times 31}$ are shown in Figure 3.1(a) in color,

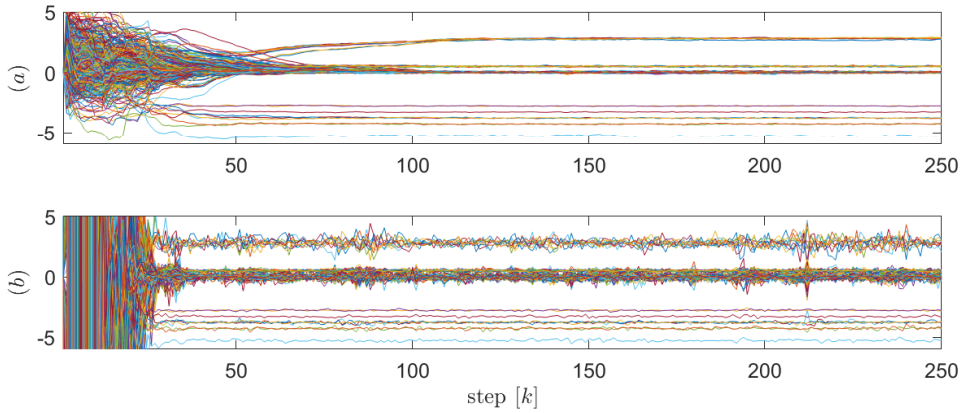

Fig. 3.3: Time evolution of all the entries in A_1 and A_1^p. (a) Time evolution of entries in A_1, which is obtained by the proposed method and (b) time evolution of entries in A_1^p, which is obtained by calculating the pseudo-inverses.

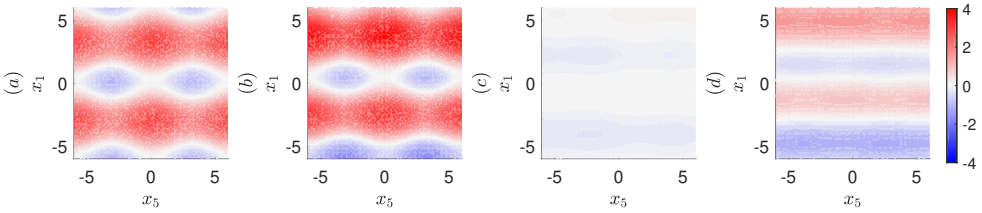

Fig. 3.4: A comparison between the obtained coupling function of the first node using the proposed method and pseudo-inverse restricted to the space spanned by x_1 and x_5. (a) $\boldsymbol{e}_1^\top \boldsymbol{g}^{id}(x)$ obtained with the proposed method; (b) $\boldsymbol{e}_1^\top \boldsymbol{g}^{id}(x)$ obtained with pseudo-inverse; (c) the identification error $\boldsymbol{e}_1^\top(\boldsymbol{g}^{id}(x) - \boldsymbol{g}(x))$ of the proposed method and (d) the identification error $\boldsymbol{e}_1^\top(\boldsymbol{g}^{id}(x) - \boldsymbol{g}(x))$ of using pseudo-inverse.

and the identified $K_1 x = A_1 \Psi(x)$ reads

$$\begin{aligned}
\boldsymbol{e}_1^\top A_1 \Psi(x) =& 2.783\psi_1 - 3.751\psi_{12} + 0.512\psi_{16} + 0.517\psi_{19} + 0.478\psi_{21} \\
=& 2.783 - 3.751\cos x_1 + 0.512\cos x_5 + 0.517\cos x_8 + 0.478\cos x_{10}, \\
&\vdots \\
\boldsymbol{e}_{10}^\top A_1 \Psi(x) =& 2.805\psi_1 + 0.492\psi_{12} + 0.495\psi_{20} - 3.270\psi_{21} \\
=& 2.805 + 0.492\cos x_1 + 0.495\cos x_9 - 3.270\cos x_{10},
\end{aligned}$$

where $\boldsymbol{e}_i^\top \in \mathbb{R}^{10}$ is the ith standard basis vector, and entries of $\mathcal{O}(10^{-1})$ are omitted. By adding all of the entries of $K_1 x$, the following equation holds

$$\sum_{i=1}^{10} K_1 x_i = 27.933 - 2.306\cos x_1 - 2.176\cos x_2 - 2.245\cos x_3 \cdots - 2.305\cos x_{10}.$$

The above equation corresponds to (3.12) with $D = 27.933$, $B_1 = (0, -2.306, 0)$, $\cdots$, $B_{10} = (0, -2.305, 0)$ and $\Psi_i'(x_i) = (x_i, \cos x_i, \sin x_i)^\top$. Then, for $i = 1, \cdots, 10$, $K_2 x_i$ is

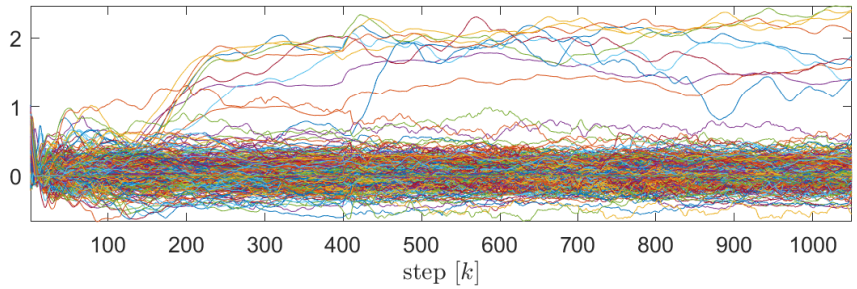

Fig. 3.5: Time evolution of entries in $A_1 - A_2$ using observables defined in (3.24). The entries fail to converge to constant values.

extracted as

$$\begin{aligned} f(x_1) =& K_2 x_1 = 27.933/10 - 2.306 \cos x_1 = B_1' \Psi(x), \\ & \vdots \\ f(x_{10}) =& K_2 x_{10} = 27.933/10 - 2.305 \cos x_{10} = B_{10}' \Psi(x), \end{aligned}$$

where

$$\begin{aligned} B_1' &= \begin{bmatrix} 2.793 & \mathbf{0}_{1\times 10} & -2.306 & \mathbf{0}_{1\times 19} \end{bmatrix}, \\ & \vdots \\ B_{10}' &= \begin{bmatrix} 2.793 & \mathbf{0}_{1\times 19} & -2.305 & \mathbf{0}_{1\times 10} \end{bmatrix}. \end{aligned}$$

Matrix A_2 is then constructed using (3.13) as $A_2 = \mathrm{col}(B_1', \cdots, B_{10}')$, and the values of the entries are shown in Figure 3.1(b) in color. The coupling function is then identified as $\boldsymbol{g}^{id}(x) = (A_1 - A_2)\Psi(x)$, and the entries of matrix $A_1 - A_2$ are shown in Figure 3.1(c) in color. As the figure shows, the coupling function is identified as

$$\begin{aligned} \boldsymbol{e}_1^\top \boldsymbol{g}^{id}(x) =& -1.445 \cos x_1 + 0.512 \cos x_5 + 0.517 \cos x_8 + 0.478 \cos x_{10}, \\ & \vdots \\ \boldsymbol{e}_{10}^\top \boldsymbol{g}^{id}(x) =& 0.492 \cos x_1 + 0.495 \cos x_9 - 0.965 \cos x_{10}, \end{aligned}$$

which approximately match the true inputs of $\boldsymbol{g}(x) = \mathcal{L}\mathrm{col}_{i=1}^{10}(I(x_i))$, where $\mathcal{L}$ is the Laplacian matrix associated with the network structure, and $I(x) = 0.5(1 - \cos x)$. The connectivity of the network is identified as shown in Figure 3.2.

In addition, the identification results are compared with the results obtained in a comparison simulation in which sparse identification techniques are not used, and A_1 is obtained with (3.16), which is denoted by A_1^p. The time evolution of all of the entries of A_1 and A_1^p is shown in Figure 3.3. As the figures show, the proposed method obtains higher accuracy. Figure 3.4 shows the identified coupling function of the first node restricted to

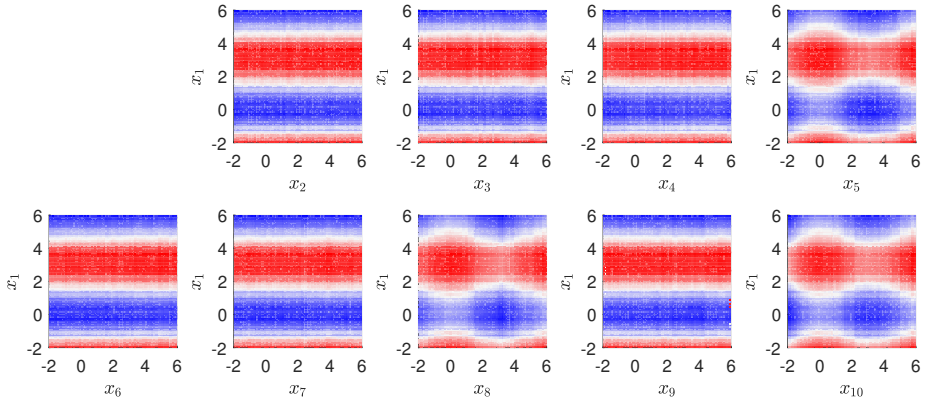

Fig. 3.6: The first component of the identified coupling function restricted to the spaces spanned by x_1 and x_j for $j = 1, \cdots, 10$. It can be seen that $\boldsymbol{e}_1^\top \boldsymbol{g}^{id}(x)$ is only dependent on x_1, x_5, x_8 and x_{10}.

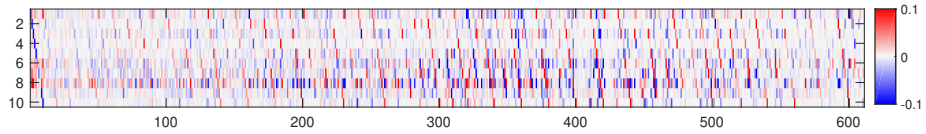

Fig. 3.7: The obtained $A_1 - A_2 \in \mathbb{R}^{61\times 611}$ shown in color, which fails to reveal a direct relationship as in Figure 3.1.

the space spanned by x_1 and x_5, where both the results obtained with pseudo-inverse and the proposed method are plotted. As the figure shows, the identification error obtained using the proposed method is smaller compared to that obtained using the pseudo-inverse. To quantify the identification errors, introduce the error index $\mathcal{I}(A_1)$ defined by

$$\mathcal{I}(A_1[k]) = \frac{\|\boldsymbol{g}(x) - \boldsymbol{g}^{id}(x)\|_{L_2}}{\|\boldsymbol{g}(x)\|_{L_2}} \times 100\%, \tag{3.23}$$

where the L_2 norm is approximated by dividing the space into lattices of side length 0.1 and calculating the average error for every grid. Here, the error index restricted to $\text{span}\{x_1, x_5\}$ for both results are $\mathcal{I}(A_1[250])|_{x_1,x_5} = 9.815\%$ and $\mathcal{I}(A_1^p[250])|_{x_1,x_5} = 55.049\%$.

As stated in Proposition 3.2, the observable set $\Psi(x)$ contains the true coupling function $g(x_i, x_j) = I(x_i) - I(x_j) = \cos x_j - \cos x_i$, and all the entries in $A_1 - A_2$ converge to constant values. Next, consider the case where the coupling function is not contained in $\Psi(x)$.

Define the observable set $\Psi(x)$ by

$$\Psi(x) = \text{col}\big(1, x, \text{col}_{t\in\mathcal{T}}\text{col}_{i=1}^{10}(s_o(x_i,t)), \text{col}_{t\in\mathcal{T}}\text{col}_{i=1}^{10}(s_e(x_i,t))\big) : \mathbb{R}^{10} \to \mathbb{R}^{611}, \tag{3.24}$$

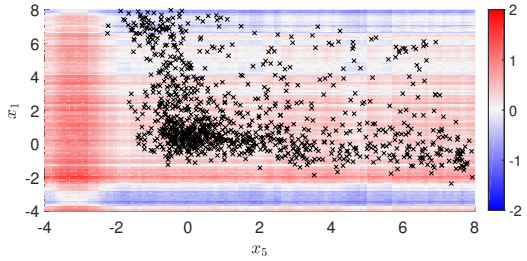

Fig. 3.8: The identification error of the first component of the coupling function, where a black $\times$ represents a pair $(x_1[i], x_5[i])$ for $i \in \{0, 1, 2, \cdots, 250\}$. As the figure shows, the identification error is relatively small over the manifold where the data are measured and deviates elsewhere.

where $\mathcal{T} = \{0.1\pi, 0.2\pi, \cdots, 3\pi\}$ and $s_o(x,t)$, $s_e(x,t)$ are square waves with periods $t > 0$ that are odd functions and even functions, respectively, i.e.,

$$s_o(x,t) = \begin{cases} 1, & \mathrm{mod}(x,t) \in [0, \frac{1}{2}t) \\ -1, & \mathrm{mod}(x,t) \in [\frac{1}{2}t, t) \end{cases}, s_e(x,t) = \begin{cases} 1, & \mathrm{mod}(x,t) \in [0, \frac{1}{4}t) \cup [\frac{3}{4}t, t) \\ -1, & \mathrm{mod}(x,t) \in [\frac{1}{4}t, \frac{3}{4}t) \end{cases}.$$

Let $m = 350$ and perform the proposed identification method for 1050 steps, where the parameters are set to $\lambda = 0.5$ and $\rho = 5$. Figure 3.5 shows the time evolution of entries in $A_1 - A_2$, and the entries fail to converge. However, Figure 3.6 shows the identified coupling function of the first node at $k = 1050$ restricted to the space spanned by x_1 and x_j for $j = 2, \cdots, 10$. It can be seen from the figures that $\boldsymbol{e}_1^\top \boldsymbol{g}^{id}(x)$ depends solely on x_1, x_5, x_8 and x_{10}, which indicates that the network topology is correctly identified. The obtained $A_1 - A_2 \in \mathbb{R}^{10\times 611}$ matrix is shown in Figure 3.7. Here, the entries fail to show a direct relationship with the Laplacian matrix. Figure 3.8 shows the identification error restricted to $\mathrm{span}\{x_1 \in [-4, 8], x_5 \in [-4, 8]\}$, and it can be seen that the proposed method guarantees the error to be small over the manifold where data are measured, i.e., $\mathrm{span}\{x_1 \in [-2, 6], x_5 \in [-2, 6]\}$. In conclusion, although the entries in $A_1 - A_2$ did not converge, the coupling function is still identified numerically. Nevertheless, convergence is still considered as the stop criterion of the proposed algorithm, because the above comparison is not available in practical situations, and therefore, there lacks an indication to end the process.

The influence of parameter m is revealed in Figure 3.9(a) where the identification error defined by (3.23) is plotted, which is also restricted to $\mathrm{span}\{x_1, x_5\}$. For every $m \in \{100, 150, 200, \cdots, 800\}$, the identification is performed 10 times and the average values of the errors are plotted. Specifically, for each m the result at $k = 3m$ is taken, the observable set is defined as in (3.24), and the parameters λ and ρ remain the same. As the figure shows, the identification error decreases as m becomes larger, however, the error would not converge to 0 because no linear combination of the observables could

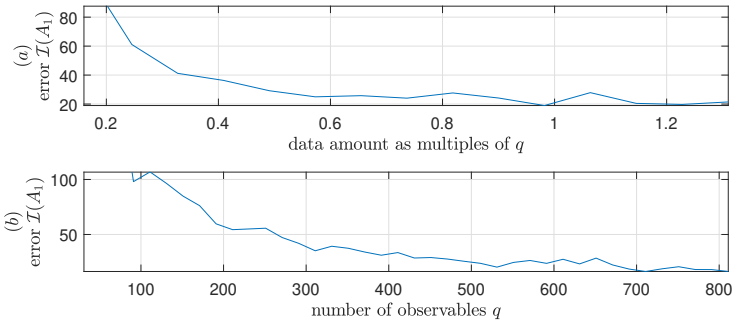

Fig. 3.9: (a) The relationship between the identification error and the parameters m which is represented as multiples of q, the number of observables. Note that if $m > 1.0q$, then A_0 could be obtained using pseudo-inverse. (b) The relationship between the identification error and q, the number of observables.

approximate the coupling function perfectly. On the other hand, to show the influence of the richness of the observable set, define another observable set $\Psi(x) : \mathbb{R}^{10} \to \mathbb{R}^{11+20a}$ by

$$\Psi(x) = \mathrm{col}\big(1, x, \mathrm{col}_{t\in\mathcal{T}_a}\mathrm{col}_{i=1}^{10}(s_o(x_i,t)), \mathrm{col}_{t\in\mathcal{T}_a}\mathrm{col}_{i=1}^{10}(s_e(x_i,t))\big), \tag{3.25}$$

where $\mathcal{T}_a = \{1\frac{3\pi}{a}, 2\frac{3\pi}{a}, 3\frac{3\pi}{a}, \cdots, a\frac{3\pi}{a}\}$. Let $a = 1, \cdots, 40$ and perform the identification with $m(a) = \lceil 0.8(11{+}20a)\rceil$ for $3m(a)$ steps. For each parameter setting, the identification is repeated 10 times with different trajectories, and the average values of the errors defined by (3.23) are recorded. The identification result is shown in Figure 3.9(b). As the figure shows, as the number of square wave functions grows, the observables approximate the true coupling functions better and the error becomes smaller.

3.3.2 A network of Lorenz systems

In this example, the availability of the proposed method for multi-dimensional chaotic system networks with topology changes is shown. Since the convergence of the entries greatly depends on the design of the observable set, the case where the assumptions of Proposition 3.2 are satisfied is considered, i.e., the span of the observable set contains the coupling function. Consider the Lorenz oscillators discretized with the first-order Euler method with sampling intervals $h = 0.01$s.

Consider a network of 10 Lorenz systems modeled by

$$\begin{aligned}
x_{i,1}^+ &= x_{i,1} + h\cdot(-10x_{i,1} + 10x_{i,2}),\\
x_{i,2}^+ &= x_{i,2} + h\cdot(-x_{i,1}x_{i,3} + 28x_{i,1} - x_{i,2} + u_i),\\
x_{i,3}^+ &= x_{i,3} + h\cdot(x_{i,1}x_{i,2} - 8/3x_{i,3}),\\
u_i &= \sigma\sum_{j=1}^{10} c_{ij}(x_{j,2} - x_{i,2}),
\end{aligned} \tag{3.26}$$

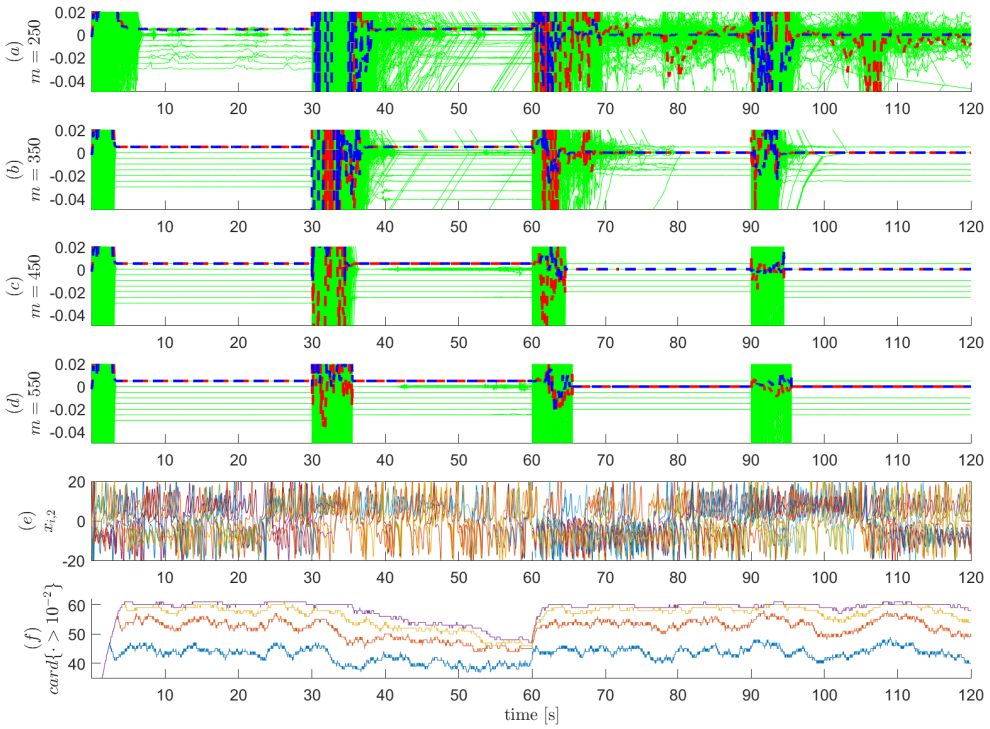

Fig. 3.10: (a)-(d) Time evolution of entries in matrix $A_1 - A_2$ obtained with parameter $m = 250, 230, 450$ and 550, respectively. Specifically, the entries correspond with c_{13} and c_{31} are emphasized with bold red lines and bold blue lines, respectively; (e) the second state components of the trajectories of the Lorenz oscillators, i.e., $x_{i,2}$, used for identification and (f) time evolution of $\text{card}\{\text{eig}(X[k]X^*[k]) > 10^{-2}\}$, which is approximately $\text{rank}(X[k])$. From the top to the bottom, the four lines correspond to $m = 550, 450, 350$ and 250, respectively.

for $i = 1, \cdots, 10$, c_{ij} is the (i, j) entry of the adjacency matrix associated with the network topology, and $\sigma = 1$ is the coupling strength. Consider the case that the network topology changes randomly every 30 seconds where the probability of $c_{ij} = c_{ji} = 1$ is 40% for any $i \neq j$, and perform identifications with $m = 250, 350, 450$ and 550, i.e., using recorded trajectories of 2.5s, 3.5s, 4.5s and 5.5s. The observable set $\Psi(x) : \mathbb{R}^{30} \to \mathbb{R}^{61}$ is defined by

$$\Psi(x) = \text{col}(1, \text{col}_{j=1}^{3}\text{col}_{i=1}^{N}(x_{i,j}), \text{col}_{i=1}^{10}(x_{i,1}x_{i,2}), \text{col}_{i=1}^{10}(x_{i,1}x_{i,3}), \text{col}_{i=1}^{10}(x_{i,2}x_{i,3})). \quad (3.27)$$

The identification process is performed for 120s, and the parameters are set to $\rho = 10^{-3}$ and $\lambda = 10^{-7}$. The identification results are shown in Figure 3.10. Figure 3.10(a)-(d) show the time evolution of entries in the identified $A_1 - A_2$ matrix for $m = 250, \cdots, 550$, respectively, and the entries associated with the connection between node 1 and node 3 are emphasized with bold lines. It can be confirmed that node 1 and node 3 are

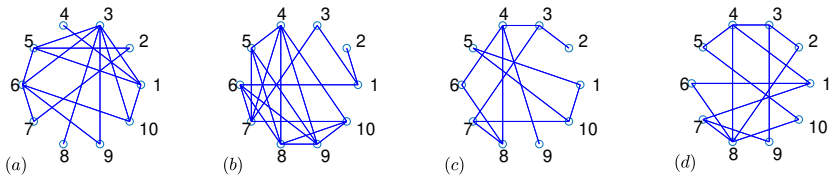

Fig. 3.11: The actual topology of the network, where (a)-(d) correspond to $t = [0, 30)$, $t = [30, 60)$, $t = [60, 90)$ and $t = [90, 120]$, respectively.

directly connected for approximately $t = [3, 30] \cup [36, 60]$ and not directly connected for $t \in [65, 90] \cup [95, 120]$. As shown by Figure 3.11, the topology is correctly identified. Figure 3.10(e) shows the second state components of all the nodes, and Figure 3.10(f) plots the number of eigenvalues of $X[k]X^*[k]$ that are larger than 10^{-2}, i.e., card$\{\text{eig}(X[k]X^*[k]) > 10^{-2}\}$, which can be considered the rank of the matrix. As stated in Proposition 3.2, the span of the observables in $\Psi(x)$ contains the coupling function, and there exists a time-invariant optimality for each period that the network topology does not change. Convergence to the optimality is also highly related to the rank of matrix $X[k]X^*[k]$, which depends on both m and the distribution of measured data. For $t \in [-30, 60]$, some of the nodes synchronize practically, so the rank of $X[k]X^*[k]$ falls and more data are required to achieve convergence. Note that in the case $x_i \approx x_j$, the optimal solution described in Proposition 3.2 is not unique since $X[k]$ no longer has full rank, as shown in Figure 3.10(b)-(d) where the entries converge to different values. For $t \in [60, 120]$, a comparison of the figures indicates that convergence can be ensured by enlarging m, however, at least $m + 1$ steps are required for X and Y to be filled with data measured after the topology change. Note that as an exception, the reason that the entries converge with less than m steps for $t \in [0, 30]$ is that X and Y are initialized as zero matrices. Figure 3.12 shows the obtained A_1, A_2 and $A_1 - A_2$ matrices at $t = 120$ in the case where $m = 450$, and the network topology can be revealed from Figure 3.12(c).

Generally speaking, dynamical mode decomposition (DMD)-like methods could not reach high accuracy when applied to systems with continuous spectra, such as a chaotic system ([65]). However, intrinsically, the proposed method obtains a projection of the coupling function onto the span of the observables and is expected to be applicable to a large class of nonlinear systems.

3.3.3 A network of Chua's Circuits simulating real data identifications

Consider a network of 4 Chua's circuits shown in Fig.3.13, which are realized in an inductor-less manner ([97]). The parameters of the components are shown in the fig-

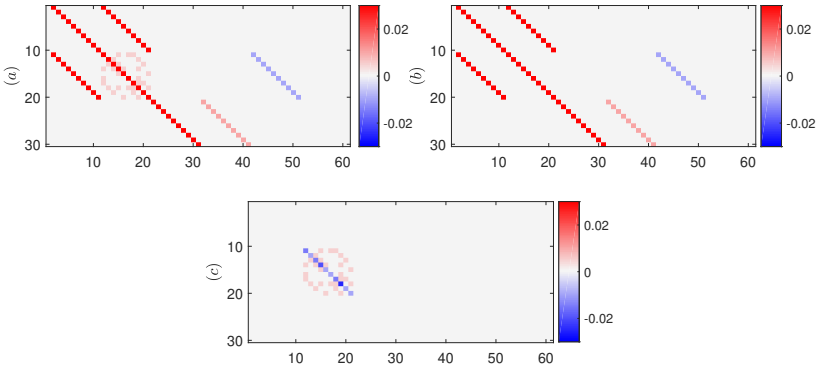

Fig. 3.12: Matrices obtained at $t = 120$ in the case where $m = 450$. (a) The A_1 matrix; (b) the A_2 matrix and (c) the $A_1 - A_2$ matrix.

ure, where the units of the resistors, the capacitors and the voltage sources are Ohm (Ω), Farad (F) and Volt (V), respectively.

As measured signals, let the voltages at nodes $x11, x12, x21, x22, \cdots, x41, x42, P1, P2$, $P3$ and $P4$ marked in Fig.3.13 be recorded as $x_{11}(t), \cdots, p_4(t)$, respectively. The currents of the equivalent inductors, i.e., the third components of the Chua's circuits, are then calculated as $x_{3j} = (x_{2j} - p_j)/1,000$ for $j = 1, \cdots, 4$ with units Ampere (A, [97]). Consider the case that a 0.5-second long trajectory is recorded, as shown in Fig.3.14 where the first 0.1s of the trajectories are plotted. Here, the raw data are generated strongly aperiodically, as shown in Fig.3.15(a) where the sampling intervals of the raw data are plotted. As a result, data for identification are re-sampled with approximately 0.00005s intervals. Fig.3.16 shows a comparison of the raw signals $x_{11}, \cdots, x_{41}$ and the sampled signals for identification. Note that the data used for identification is still slightly aperiodic, as shown in Fig.3.15(b). Such misalignment is then considered measurement noise.

Also, consider the situation that one has basic knowledge about Chua's circuits, but does not know the specific parameters. Define $\xi = \mathrm{col}(x_{11}, \cdots, x_{41}, x_{12}, \cdots, x_{42}, x_{13}, \cdots, x_{43}) \in \mathbb{R}^{12}$ to be a permutation of x and define the observables set $\Psi(x) : \mathbb{R}^{12} \to \mathbb{R}^{49}$ for identification by

$$\Psi(x) = \mathrm{col}\big(1, \xi, \mathrm{atan}(0.8\xi), \mathrm{atan}(\xi), \mathrm{atan}(1.2\xi)\big),$$

where the atan functions act on every entry of a vector, and are used to approximate Chua's diode. Specifically, the observables are defined using x_{i3} in microAmpere (mA) units considering the scales of the data. Other parameters of the identification are set to $m = 450, \rho = 12$ and $\lambda = 15$. The convergence criteria is $\|A_0[k] - A_0[k-1]\| + \|A_0[k-1] - A_0[k-2]\| \leq \varepsilon = 0.05$.

As the identification result, the identification algorithm ends at $k = 3495$, i.e., approximately $t = 0.175$s. The time evolution of the coefficients which correspond to the states

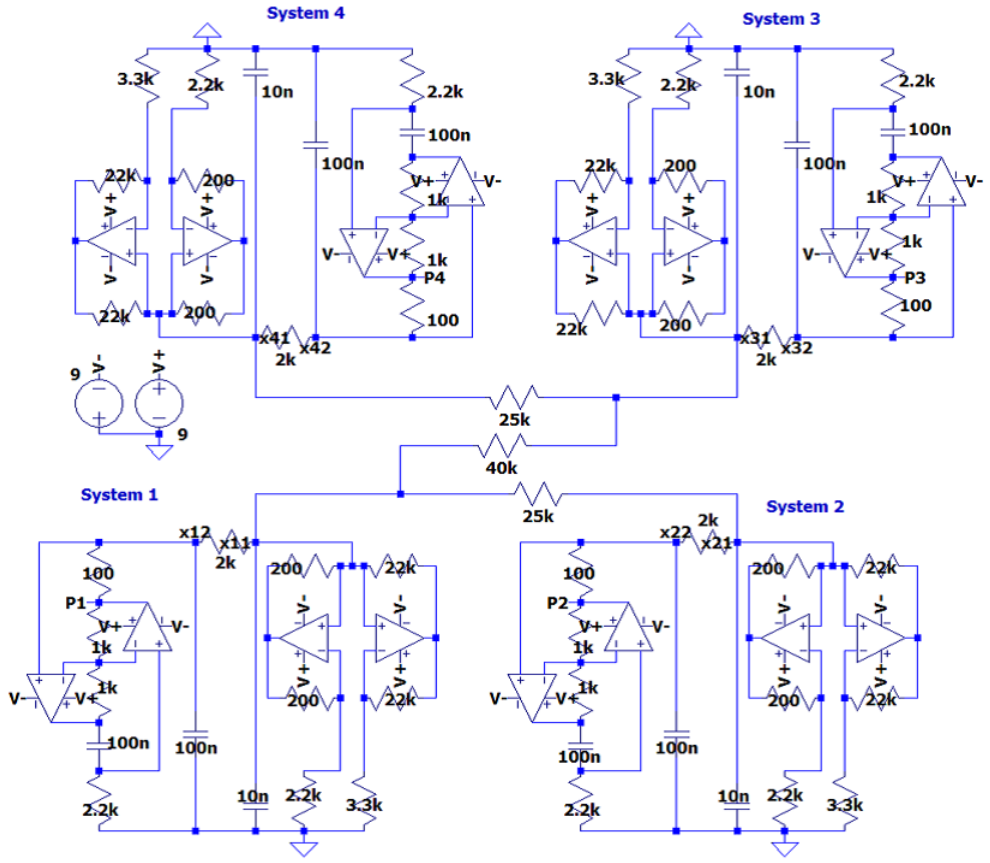

Fig. 3.13: The circuit diagram of 4 coupled Chua's systems. Here, 'k' denotes 'kilo' and 'n' denotes 'nano', i.e., 2k denotes $2,000$ and 10n denotes 10×10^{-9}.

as observables are plotted in Fig.3.17. As the figure shows, the convergence of zero-value entries is achieved, while the nonzero entries fail to converge to constant values. Still, the convergence criterion is satisfied at $k = 3495$, where the algorithm ends. The obtained matrix $A_1 - A_2$ is shown in Fig.3.18 in color, which indicates that the Chua's systems are coupled by the first components x_{i1}, and the network structure can be inferred from the sub-block $(A_1 - A_2)_{(1:4,2:5)}$. On the other hand, small identification errors exist which are considered to be caused by two factors that the data are samples of a continuous system, and that the data are sampled aperiodically. Using the obtained result and assuming Assumptions 3.1 and 3.2 hold, the Laplacian matrix is identified as

$$
\begin{aligned}
L^{id} =& \frac{1}{2}\left((A_1 - A_2)^{\top}_{(1:4,2:5)} + (A_1 - A_2)_{(1:4,2:5)}\right) \\
=& \begin{bmatrix} -0.1823 & 0.1532 & 0.0542 & 0 \\ 0.1532 & -0.1976 & 0 & 0 \\ 0.0542 & 0 & -0.1574 & 0.1327 \\ 0 & 0 & 0.1327 & -0.1839 \end{bmatrix},
\end{aligned}
$$

where terms smaller than 0.01 were omitted. The obtained result matches the circuit

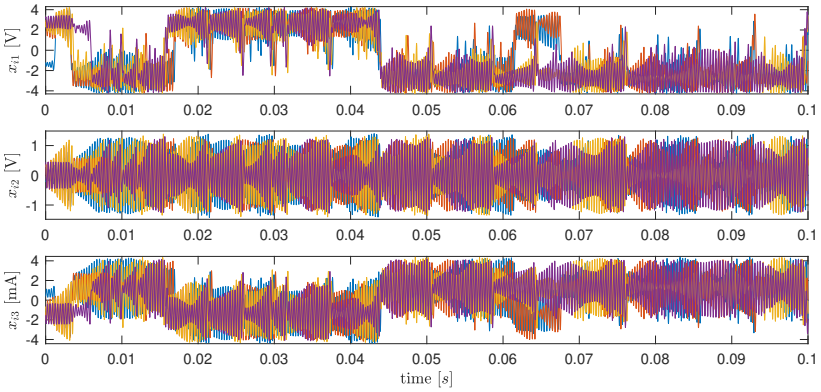

Fig. 3.14: Raw data measured from the circuit diagram shown in Fig.3.13. Note that the third components $x_{i3}(t)$ are plotted with units microAmpere (mA).

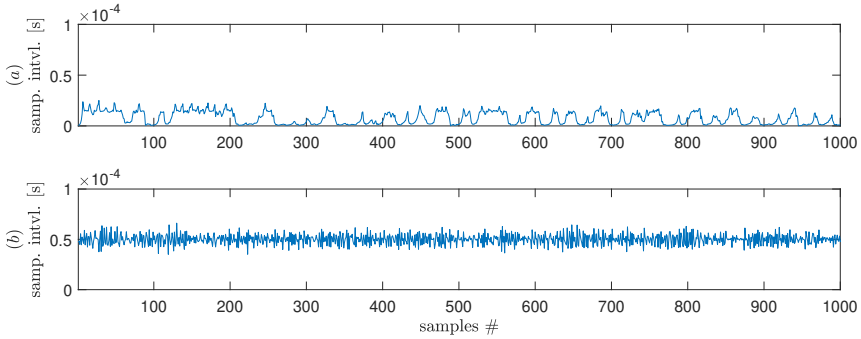

Fig. 3.15: The sampling intervals of (a) the raw signals and (b) the re-sampled data.

diagram in Fig.3.13, and the weights of the edges are identified qualitatively correctly.

3.4 Conclusions and discussions

In this chapter, the identification problem of network structures was considered and the identification method proposed in Chapter 2 was modified to detect structure changes in networks. The requirement on measured data for isolated nodes was released by posing some restrictions to the network structures. An identification algorithm is constructed that performs optimization at each time step to detect network structure changes. The modified method can detect possibly nonlinear coupling functions and is applicable to networks with topology changes. Numerical simulation results demonstrated the validity and applicability of the proposed method.

Generally, Assumptions 3.1 and 3.2 are satisfied in networks where data transmissions between nodes are symmetric. Therefore, these assumptions hold for undirected networks with linear diffusive couplings and electric circuits coupled by linear resistors in practical structures. As a result, the proposed method will be applicable for a wide range of actual

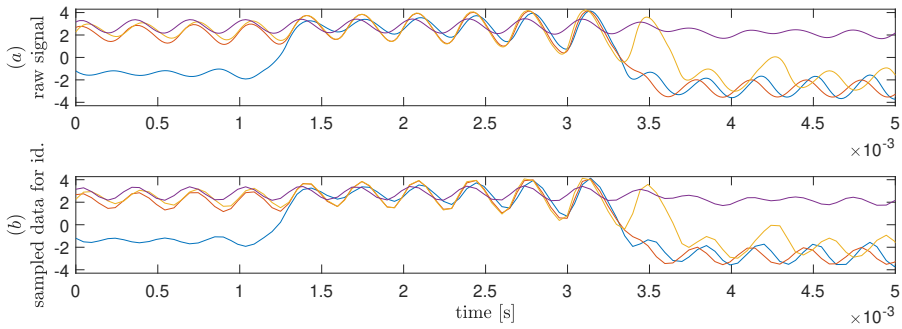

Fig. 3.16: A comparison of the first components $x_{11}(t), \cdots, x_{41}(t)$ between (a) the raw signals and (b) the re-sampled data.

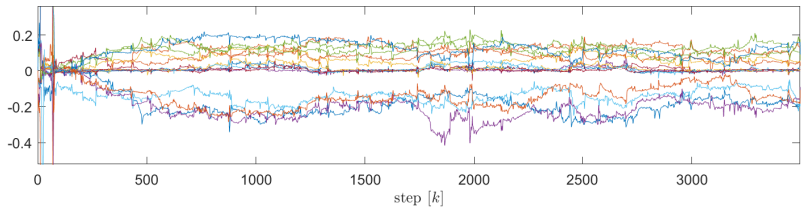

Fig. 3.17: Time evolution of the entries in $A_1 - A_2$ associated with the states as observables, i.e., $\psi_2, \cdots, \psi_{13}$.

network systems for purposes such as fault detection and monitoring in power supply systems, multi-robot communication and electric circuit networks.

To apply the proposed method, the is no theoretical limitation on the size of networks N, but for accurate identification, the observable set should be designed sufficiently rich, and the computational cost would blow up. On the other hand, although sparsity-based methods are employed, it is not required that the network be sparsely connected since the sparsity of rows of A_0 can be manually manipulated by the design of the observable set $\Psi(x)$. However, since small values are simply set to 0 by the sparse identification method, there exists a trade-off between the accuracy of identification and the amount of required data in the case where the coupling function is not contained in the span of the observables.

There are still drawbacks remaining as future tasks. The optimal values of the optimization parameters λ, ρ, and the record length m are not clear, and there is no design method for the observable set $\Psi(x)$. As stated in Chapter 2.3, the proposed method obtains a projection of $\boldsymbol{g}(x)$ onto $\mathrm{span}\{\psi_i\}^{Nn}$. Thus, theoretically, there is no need to require entries of $\boldsymbol{f}(x)$ to be in the span. However, the identification accuracy may decrease in such a case. Moreover, it is also assumed that all the states of the nodes were measurable, but, in practical situations, only the outputs of the nodes may be available. On the other hand, compared to the sDMD method ([77]), the proposed method requires

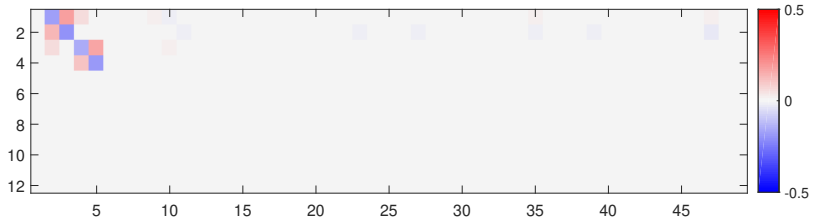

Fig. 3.18: The obtained $A_1 - A_2$ matrix shown in color.

higher computational capability, since data matrices are updated and matrix inverses are calculated at every step. It remains a future task to develop an algorithm that detects changes in network structures. Also, the proposed method does not apply to networks whose structure changes continuously with time. When the network structure changes, the proposed method requires the network structure to not change in the following at least m steps for the data matrices to be filled with data corresponding to the dynamics after the structure change. If the network structure changes again within the m step window, then the first structure change will not be identified. If the network structure changes continuously, then the proposed method fails.

4 Identification of Networks Structures for Networks with Partially-measurable States and Known Dynamical Models

4.1 Introduction

Including the identification methods described in the previous chapters, although most of the above-mentioned methods assume that all the states of the nodes are measurable, in practical cases, there may exist states that cannot be measured, which are known as hidden variables. In [32, 89, 98], the hidden variables are considered colored noises, and the identification is performed in the subspace spanned by the measurable states. In [90], networks with hidden nodes are identified by reconstructing the adjacency matrix corresponding to the network and calculating the covariance of the obtained results, where inputs signals from hidden nodes would enlarge the covariance, and [52] extends the results to networks with transmission time delays.

On the other hand, in [24], the problem of identifying the topology of networks is considered assuming both the dynamics of isolated nodes and the coupling function is known. A drive-response system is designed whose variables converge practically to the states of the original network system, and the topology of the network is obtained as the coefficients of the coupling functions in the dynamics of the network. [25] designed a dynamical input for the drive-response system to make the convergence to the states asymptotic. In [47], the method is extended to the situation where nodes synchronize. However, a problem exists that the convergence of the variables in the drive-response system to the coefficients of the coupling function in the network dynamics is not strictly ensured.

Although the adaptive-synchronization-based method achieved much success, there are still open problems that remain to be solved. First, the method requires both the unforced dynamics and the coupling function of all the nodes to be known, which is sometimes impractical. Second, the auxiliary system is designed such that some of its states converge to those of the original, and others converge to the to-be-identified parameters. In previous efforts, the convergence of the former is ensured by constructing Lyapunov functions, and the latter is ensured by applying the invariance principle. However, the equilibrium of the

error dynamics of the latter may not be uniquely the origin, so the identification may fail even in the case where all the state variables are correctly identified. Third, as described in [25], the method fails in the case where the nodes synchronize and no inputs are allowed to be applied to the original. In other words, it lacks explanations for the results obtained by applying the method.

This chapter proposes an identification method that solves the above-mentioned problems. The case where only the outputs of all the nodes can be measured is considered, and only the unforced dynamical models of the nodes are assumed known. An auxiliary system is constructed where the unknown coupling function is modeled as a linear combination of pre-defined basis functions, and the auxiliary system uses a streaming data set of past data to obtain the gain matrix of the linear combination. Also, the auxiliary system tracks past values of the original state variables, and the current values of the original states are then obtained by iterating the states of the auxiliary system using the identified dynamics. It is shown theoretically that under certain assumptions, the identification results converge to the respective true values asymptotically. This chapter also shows that if the nodes synchronize partially, then the proposed method obtains a reduction of the original network.

This chapter is organized as follows. Section 4.2 describes the proposed drive-response-system-based network identification method, and Section 4.3 gives numerical examples to show the usefulness of the obtained results. Section 4.4 summarizes this chapter and gives some remarks.

4.2 Identification using a drive-response system

Consider a network of N interconnected systems described by

$$\begin{aligned} x_i^+ =& f(x_i) + Bu_i(x), \\ u_i(x) =& \sum_{j=1}^{N} a_{ij} g(x_i, x_j), \quad w_i = Cx_i, \end{aligned} \tag{4.1}$$

for $i = 1, \cdots, N$, where $x_i \in \mathbb{R}^n$ denotes the states, $w_i \in \mathbb{R}^m$ denotes the output and $u_i(x) : \mathbb{R}^{Nn} \to \mathbb{R}^m$ denotes the to-be-identified coupling function of node i. Suppose that $f : \mathbb{R}^n \to \mathbb{R}^n$ is known, and the goal of this chapter is to identify $u_i(x)$ from $f(x_i)$ and measured data of w_i.

Define $\bar{f}(x, u) = f(x) + Bu$, and let $\bar{f}^{i+1}(x, u)$ denote $\bar{f}(\bar{f}^i(x, u)) + Bu$ for $i = 0, 1, \cdots$. Specifically, $\bar{f}^0(x, u) = x$. For $\ell = 1, \cdots, m$, let r_ℓ denote the relative degree of the ℓ-th output $w_{i\ell}$, which is defined as the minimum of the relative degrees of $(w_{i\ell}, u_{i1}), \cdots,$

$(w_{i\ell}, u_{im})$ pairs. Define $y_{i\ell} \in \mathbb{R}^{r_\ell}$ by

$$\begin{aligned} y_{i\ell} =& \mathrm{col}(w_{i\ell}, w_{i\ell}^{+}, \cdots, w_{i\ell}^{(r_\ell-1)+}) \\ =& \mathrm{col}(C_\ell x_i, C_\ell \bar{f}(x_i, u), \cdots, C_\ell \bar{f}^{r_\ell-1}(x_i, u)), \end{aligned}$$

and define $y_i \in \mathbb{R}^{r_\Sigma} = \mathrm{col}(y_{i1}, \cdots, y_{im})$. Define $r_M = \max\{r_1, \cdots, r_m\}$ and $r_\Sigma = \sum_{\ell=1}^{m}(r_\ell)$. Assume that the following statements hold.

Assumption 4.1. The following matrix has full rank for all $x \in \mathbb{R}^n$, i.e.,

$$\mathrm{rank}\left[(\frac{\partial C_1 \bar{f}^{r_1}(x,u)}{\partial u})^\top \quad \cdots \quad (\frac{\partial C_m \bar{f}^{r_m}(x,u)}{\partial u})^\top \right] = m, \tag{4.2}$$

where $C_\ell \in \mathbb{R}^{1\times n}$ is the ℓ-th row of C in (4.1).

Assumption 4.2. There exists a mapping $\xi_i = S(x_i) : \mathbb{R}^n \to \mathbb{R}^{n-r_\Sigma}$ defined globally such that there exists an invertible transformation ϕ such that

$$x_i = \phi(\mathrm{col}(y_i, \xi_i)) \;\Leftrightarrow\; \phi^{-1}(x_i) = \mathrm{col}(y_i, \xi_i).$$

Assumptions 4.1 and 4.2 ensure that the dynamical model (4.1) can be decoupled into the following form

$$y_{i\ell}^{+} = A_0^\ell y_{il} + B_0^\ell b_{i\ell}(y, \xi), \tag{4.3a}$$

$$\xi_i^{+} = a(y_i, \xi_i), \tag{4.3b}$$

$$A_0^\ell = \begin{bmatrix} \mathbf{0} & I_{r_\ell-1} \\ 0 & \mathbf{0} \end{bmatrix}, \quad B_0^\ell = \begin{pmatrix} \mathbf{0}_{(r_\ell-1)\times 1} \\ 1 \end{pmatrix},$$

for $i = 1, \cdots, N$ where $y = \mathrm{col}(y_1, \cdots, y_N) \in \mathbb{R}^{Nr_\Sigma}$, $\xi = \mathrm{col}(\xi_1, \cdots, \xi_N) \in \mathbb{R}^{N(n-r_\Sigma)}$ and

$$\begin{aligned} b_{i\ell} =& C_\ell \bar{f}^{r_\ell}\big(x_i, u_i(x)\big) \\ =& C_\ell \bar{f}^{r_\ell}\big(\phi(\mathrm{col}(y_i, \xi_i)), u_i(\mathrm{col}_{i=1}^{N}(\phi(\mathrm{col}(y_i, \xi_i))))\big). \end{aligned}$$

Assumption 4.3. For any $y^* \in \mathbb{R}^{r_\Sigma}$ and $\xi_1, \xi_2 \in \mathbb{R}^{n-r_\Sigma}$, the following inequality holds:

$$\|a(y^*, \xi_1) - a(y^*, \xi_2)\| \le \gamma_0(y^*)\|\xi_1 - \xi_2\|, \tag{4.4}$$

with $\gamma_0 : \mathbb{R}^{r_\Sigma} \to [0, 1)$ and $\sup \gamma_0(y^*) = \gamma < 1$.

The problem of obtaining the coupling function $u_i(x)$ is then reduced to identifying the $b_{i\ell}$ function from data. Throughout this chapter, suppose that the measured outputs are bounded, and the time series of the outputs are recorded for certain steps.

4.2.1 Construction of a response system

Consider a drive-response system that is designed to track past values of the original full states of (4.3), and identify the coupling function in terms of a linear combination of pre-defined basis functions. Define

$$w_{i\ell}^d[k] = w_{i\ell}[k - r_M], \quad \xi_i^d[k] = \xi_i[k - r_M],$$

where r_M denotes the largest relative degree of all the outputs. Also, define $y_{i\ell}^d[k] = y_i[k - r_M], y_i^d[k] = y_i[k - M]$ and $\xi^d[k] = \xi[k - r_M]$, and note that $y_i^d[k]$ is numerically available at step k. Consider the response system

$$\hat{\xi}_i^+ = a(y_i^d, \hat{\xi}_i), \tag{4.5}$$

for $i = 1, \cdots, N$ where $\hat{\xi}_i \in \mathbb{R}^{n-r_\Sigma}$. For a set of basis functions $\Psi(y, \xi) : \mathbb{R}^{Nr_\Sigma} \times \mathbb{R}^{N(n-r_\Sigma)} \to \mathbb{R}^q$ where $q > Nm$, suppose that the to-be-identified functions $b_{i\ell}(y, \xi)$ admits an approximation

$$\mathrm{col}_{i=1}^N(b_{i\ell}(y, \xi)) \approx H^\top \Psi(y, \xi),$$

where $H \in \mathbb{R}^{q \times Nm}$ is a constant matrix. Define $\hat{H} \in \mathbb{R}^{q \times Nm}$ to be a variable updated by

$$\hat{H}^+ = \hat{H} + G[k](Y[k] - X[k]\hat{H}), \tag{4.6}$$

where $G[k] \in \mathbb{R}^{q \times M}$ is to be designed, and $X[k] \in \mathbb{R}^{M \times q}$, $Y[k] \in \mathbb{R}^{M \times Nm}$ are data matrices defined by

$$X[k] = \begin{bmatrix} \Psi(y^d[k - M + 1], \hat{\xi}[k - M + 1]) & \cdots & \Psi(y^d[k], \hat{\xi}[k]) \end{bmatrix}^\top, \tag{4.7a}$$

$$Y[k] = \begin{bmatrix} \boldsymbol{b}[k - M + 1 - r_M] & \cdots & \boldsymbol{b}[k - r_M] \end{bmatrix}^\top, \tag{4.7b}$$

where $M > q$ is a constant and

$$\begin{aligned} \boldsymbol{b}[j] =& \mathrm{col}_{i=1}^N \mathrm{col}_{\ell=1}^m (b_{i\ell}(y[j], \xi[j])) \\ =& \mathrm{col}_{i=1}^N \mathrm{col}_{\ell=1}^m (w_{i\ell}[j + r_\ell]) \end{aligned}$$

for $j = k - r_M - M + 1, \cdots, k - r_M$.

On the other hand, let $F(\hat{H}, \mathrm{col}(y, \xi))$ denote the estimated dynamics of the network as

$$F(\cdot, \cdot) = \begin{pmatrix} \mathrm{col}_{i=1}^N \mathrm{col}_{\ell=1}^m (A_0^\ell y_{i\ell} + B_0^\ell \hat{H}_{i\ell}^\top \Psi(y, \xi)) \\ \mathrm{col}_{i=1}^N (a(y_i, \xi_i)) \end{pmatrix}, \tag{4.8}$$

where $\hat{H}_{i\ell} \in \mathbb{R}^q$ denotes the $(m(i-1)+\ell)$-th column of $\hat{H}$. Let $F^{i+1}(\hat{H}, \mathrm{col}(y, \xi))$ denote $F(\hat{H}, F^i(\hat{H}, \mathrm{col}(y, \xi)))$, and define

$$\theta[k] = F^{r_M}(\hat{H}[k], \mathrm{col}(y^d[k], \hat{\xi}[k])), \tag{4.9}$$

as an estimation of the original states $\xi[k]$ and $y[k]$ at the current step where $\theta \in \mathbb{R}^{Nn}$.

Let $\boldsymbol{\phi} : \mathbb{R}^{Nn} \to \mathbb{R}^{Nn}$ be an invertible transformation such that

$$x = \boldsymbol{\phi}(\mathrm{col}(y, \xi)) \;\Leftrightarrow\; \boldsymbol{\phi}^{-1}(x) = \mathrm{col}(y, \xi).$$

The dynamics of the outputs, i.e., $\mathrm{col}_{i=1}^{N}\mathrm{col}_{\ell=1}^{m}(b_{i\ell}(y, \xi))$, is then identified as $\hat{H}^\top \Psi(y, \xi)$, and the dynamics of the network is then identified as

$$x^{+,id} = \boldsymbol{\phi}(F(\hat{H}, \mathrm{col}(y, \xi))).$$

The coupling function is then obtained as

$$\mathrm{col}_{i=1}^{N}(u_i^{id}(x)) = \boldsymbol{B}^\dagger\big(x^{+,id} - \mathrm{col}_{i=1}^{N}(f(x_i))\big), \tag{4.10}$$

where $\boldsymbol{B} = I_N \otimes B$.

4.2.2 Stability analysis of the identification errors

Suppose that the states of the original network system are uniformly bounded, i.e., $\|x\| \leq \mathcal{B}$ for some $\mathcal{B} < \infty$. Then the following statement holds.

Proposition 4.1. If $X[k]$ is column full-rank and there exists a matrix $H \in \mathbb{R}^{q \times Nm}$ such that

$$\mathrm{col}_{i=1}^{N}\mathrm{col}_{\ell=1}^{m}\big(b_{i\ell}(y, \xi)\big) = H^\top \Psi(y, \xi) \tag{4.11}$$

holds strictly, then

$$\lim_{k\to\infty} \|\xi^d[k] - \hat{\xi}[k]\| = 0, \tag{4.12a}$$

$$\lim_{k\to\infty} \|\mathrm{col}(y[k], \xi[k]) - \theta[k]\| = 0, \tag{4.12b}$$

$$\lim_{k\to\infty} \|H - \hat{H}[k]\| = 0, \tag{4.12c}$$

hold with $G[k]$ in (4.6) given by $G[k] = \rho X^\dagger[k]$ where $0 < \rho < 1$ is a constant and † denotes the pseudo-inverse.

Proof. To account for the delayed data in matrices X, two extended systems are constructed based on $\hat{\xi}$ and ξ, respectively. Define $\eta, \hat{\eta} \in \mathbb{R}^{NM(n-r_\Sigma)}$ by

$$\eta[k] = \mathrm{col}(\xi^d[k], \xi^d[k-1], \cdots, \xi^d[k-M+1]),$$
$$\hat{\eta}[k] = \mathrm{col}(\hat{\xi}[k], \hat{\xi}[k-1], \cdots, \hat{\xi}[k-M+1]).$$

Define the estimation errors by $\varepsilon = \eta - \hat{\eta}$, $E = H - \hat{H}$ and $e = \mathrm{col}(y, \xi) - \theta$, and consider the error dynamics:

$$\varepsilon^+ = \mathrm{col}_{j=k}^{k-M+1}\big(a(\xi^d[j], y_i^d[j]) - a(\hat{\xi}[j], \hat{y}^d[j])\big), \tag{4.13a}$$
$$E^+ = E - G(Y[k] - X[k]\hat{H}), \tag{4.13b}$$
$$e^+ = F^{r_M+1}(\hat{H}, \mathrm{col}(\hat{\xi}, y^d)) - F^{r_M+1}(H, \mathrm{col}(\xi^d, y^d)). \tag{4.13c}$$

For the simplicity of denotation, let $X^d[k]$ denote $[Psi(\xi^d[k-M+1], y^d[k-M+1]), \cdots, \Psi(\xi^d[k], y^d[k])]$ which contains the true past data of the original network system. By the construction of $Y[k]$ and $X[k]$,

$$\begin{aligned} Y[k] - X[k]\hat{H}[k] =& X^d[k]H - X[k]\hat{H}[k] \\ =& (X^d[k] - X[k])H + X[k](H - \hat{H}[k]). \end{aligned}$$

Thus, it can be verified that $\varepsilon = 0, E = 0$ and $e = 0$ is an equilibrium of (4.13):

$$\begin{aligned} 0 =& \mathrm{col}_{j=k}^{k-M+1}\big(a(\xi^d[j], y_i^d[j]) - a(\xi^d[j], y_i^d[j])\big), \\ 0 =& 0 - G((X^d[k] - X^d[k])H + X[k](H - H)), \\ 0 =& F^{r_M+1}(H, \mathrm{col}(\xi^d, y^d)) - F^{r_M+1}(H, \mathrm{col}(\xi^d, y^d)), \end{aligned}$$

where $\hat{\xi} = \xi^d$, $X = X^d$ and $\hat{H} = H$ are substituted.

Under the assumptions that $M > q$ and $X[k]$ having full column rank, define $G[k] = \rho X^\dagger[k]$ and (4.13b) is transformed into

$$E^+ = (1 - \rho)E + \rho X^\dagger[k](X^d[k] - X[k])H.$$

Here, the second term is bounded by

$$\rho X^\dagger[k](X^d[k] - X[k])H \le c_1' \|y^d\| \|\varepsilon\|,$$

for some constant $c_1' > 0$. Since y^d contains the measured output data of the original network which are bounded, and H is a constant matrix, there exists a $c_1 > 0$ such that $c_1' \|y^d\| \le c_1$. As a result,

$$\|E[k+1]\| \le (1 - \rho)\|E[k]\| + c_1 \|\varepsilon[k]\|$$

holds. On the other hand, by Assumption 4.3 the following inequality holds:

$$\|\varepsilon[k+1]]\| \le \gamma \|\hat{\eta}[k] - \eta[k]\|.$$

Also, since $f(x_i)$ is locally Lipschitz, dynamic (4.3) is also Lipschitz continuous and there exists a positive constant L with which the following inequalities hold.

$$\begin{aligned}
&\|F^{r_M+1}(\hat{H}, \mathrm{col}(\hat{\xi}, y_i^d)) - F^{r_M+1}(H, \mathrm{col}(\xi^d, y_i^d))\| \\
\leq & L\|F^{r_M}(\hat{H}, \mathrm{col}(\hat{\xi}, y_i^d)) - F^{r_M}(H, \mathrm{col}(\xi^d, y_i^d))\| \\
\leq & \cdots \\
\leq & L^{r_M+1}\|\mathrm{col}(\hat{\xi}, y_i^d) - \mathrm{col}(\xi^d, y_i^d)\| \\
& + L^{r_M}\|H - \hat{H}\|\|\Psi(\hat{\xi}, y^d) - \Psi(\xi^d, y^d)\| \\
\leq & L^{r_M+1}\|y^d\|\|\varepsilon\| + L^{r_M}L_p\|y^d\|\|E\|\|\varepsilon[k]\|,
\end{aligned}$$

where L_p is a constant depending on $\Psi(y, \xi)$ and $\|B_0 v\| = \|v\|$ for any $v \in \mathbb{R}^{Nm}$. As a result, there exists a positive constant c_2 with which

$$\|e[k+1]\| \leq c_2\|\varepsilon[k]\| + c_2\|E[k]\|\|\varepsilon[k]\|$$

holds.

Next, define auxiliary variables $z_1 = \|E\|\|\varepsilon\|$, $z_2 = \|\varepsilon\|^2$, and it follows that

$$\begin{aligned}
\|z_1[k+1]\| \leq & \gamma\|\varepsilon[k]\|\big((1-\rho)\|E[k]\| + c_1\|\varepsilon[k]\|\big) \\
= & \gamma(1-\rho)\|z_1[k]\| + c_1\gamma\|z_2[k]\|, \\
\|z_2[k+1]\| \leq & \gamma^2\|\varepsilon[k]\|^2 = \gamma^2\|z_2[k]\|.
\end{aligned}$$

Now, consider the stability of the origin of (4.13). Consider the augmented error dynamics:

$$\begin{pmatrix} \|e[k+1]\| \\ \|E[k+1]\| \\ \|\varepsilon[k+1]\| \\ \|z_1[k+1]\| \\ \|z_2[k+1]\| \end{pmatrix} \leq \begin{bmatrix} 0 & 0 & c_2 & c_2 & 0 \\ 0 & \rho' & c_1 & 0 & 0 \\ 0 & 0 & \gamma & 0 & 0 \\ 0 & 0 & 0 & \gamma\rho' & c_1\gamma \\ 0 & 0 & 0 & 0 & \gamma^2 \end{bmatrix} \begin{pmatrix} \|e[k]\| \\ \|E[k]\| \\ \|\varepsilon[k]\| \\ \|z_1[k]\| \\ \|z_2[k]\| \end{pmatrix}, \tag{4.14}$$

where $\rho' = 1 - \rho$. Here the inequality holds in an entry-wise manner. It can be verified that the origin of (4.13) is globally asymptotically stable since all the diagonal elements of the above upper-triangle matrix are positive and smaller than 1. □

Remark 4.1. Let K be the Koopman operator which corresponds to dynamics (4.3), then $K(\boldsymbol{e}_{r_\ell}^\top y_{i\ell}) = b_\ell(y_i, \xi_i, u_i(y, \xi))$ holds, where $\boldsymbol{e}_{r_\ell}^\top y_{i\ell}$ is the r_ℓth entry of $y_{i\ell} \in \mathbb{R}^{r_\ell}$. On the other hand, if (4.11) holds, then $K\mathrm{col}_{i=1}^N\mathrm{col}_{\ell=1}^m(\boldsymbol{e}_{r_\ell}^\top y_{i\ell}) = H\Psi(w, y)$ holds. Since $\hat{H} \to H$ holds, from the perspective of identification using Koopman mode decomposition, the obtained $\hat{H}^\top\Psi(y, \xi)$ corresponds to the approximation of $K\mathrm{col}_{i=1}^N\mathrm{col}_{\ell=1}^m(\boldsymbol{e}_{r_\ell}^\top y_{i\ell})$.

The identification algorithm is summarized in Algorithm 4.1.

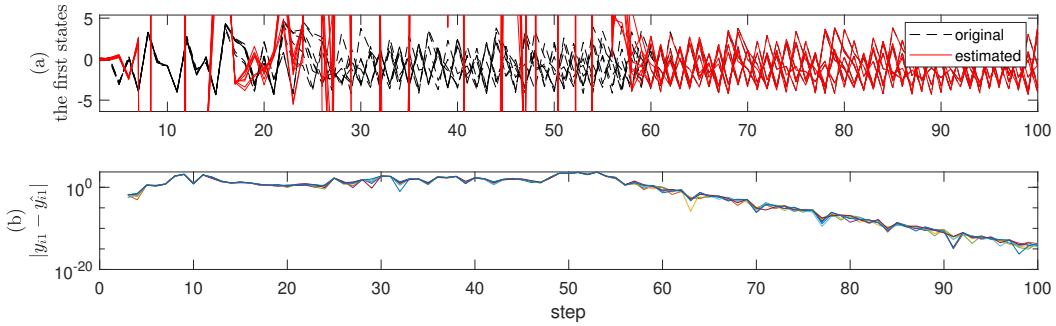

Fig. 4.1: (a). A comparison between the estimated first states y_{i1} estimated with $\theta_1, \theta_4, \cdots, \theta_{22}$, and their true values. (b). The estimation errors plotted in logarithmic scales.

Algorithm 4.1 Proposed identification algorithm

Input: Model $f(x_i), B$, C, parameter M, observable set $\Psi(\xi, y)$ and stop criteria $L \in \mathbb{N}$ and $\varepsilon > 0$

Output: $\boldsymbol{g}^{id}(x)$ and $x^{id}[k]$

1. Initialization: Obtain model (4.3) according to $f(x_i), B$ and C. Define $X \in \mathbb{R}^{M\times q}$, $Y \in \mathbb{R}^{M\times Nm}$ and $\hat{H} \in \mathbb{R}^{q\times Nm}$ as zero matrices

2. Matrices update: At time step k, construct $X[k]$ and $Y[k]$ with (4.7)

3. Variables update: Update $\hat{\xi}$ and $\hat{H}$ with (4.5) and (4.6), respectively

4. Convergence Verification:

if $\sum_{j=0}^{L-1} \|\hat{H}[k-j] - \hat{H}[k-j-1]\| \leq \varepsilon$ **then**

go to step **5**

else

set $k \leftarrow k+1$ and repeat steps **2-4**

end if

5. Result: Obtain $\boldsymbol{g}^{id}(x)$ with (4.10). Obtain $x^{id}[k] = \boldsymbol{\phi}(\theta[k])$

4.3 Numerical examples

4.3.1 Identification of a network of SISO nodes

Consider a network of 8 generalized Hénon maps described by

$$x_{i1}^{+} = -0.3x_{i3} \tag{4.15a}$$

$$x_{i2}^{+} = x_{i1} + 0.3x_{i3} + 0.1\sin^2 x_{i2} \tag{4.15b}$$

$$x_{i3}^{+} = 1 + x_{i2} - 1.07x_{i3}^2 + u_i, \tag{4.15c}$$

$$w_i = 10x_{i1},$$

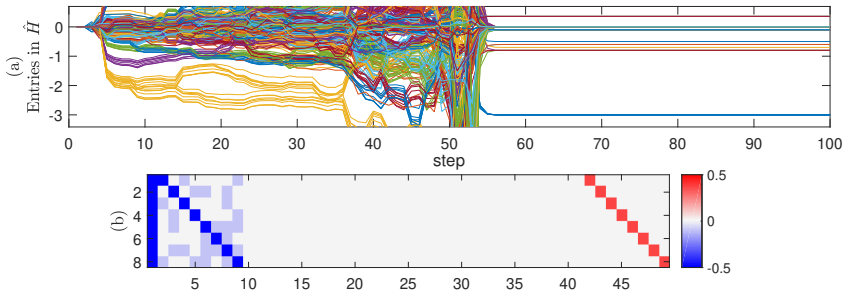

Fig. 4.2: (a). Time evolution of the entries in $\hat{H}$. (b) The $\hat{H}^\top \in \mathbb{R}^{8\times 49}$ matrix obtained at $k = 100$ shown in color, where the color at row i and column j corresponds with $[\hat{H}[100]]^\top_{(i,j)}$.

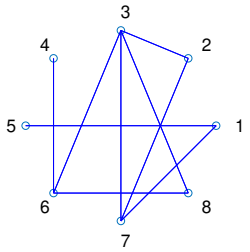

Fig. 4.3: The topology of the network.

for $i = 1, \cdots, 8$ where a_{ij} is the (i, j) entry of the adjacency matrix associated with the network topology. Define $y_i = (10x_{i1}, -3x_{i3})^\top$, $\xi_i = 3x_{i2}$ and rewrite (4.15) into

$$y_i^+ = \begin{bmatrix} 0 & 1 \\ 0 & 0 \end{bmatrix} y_i + \begin{pmatrix} 0 \\ 1 \end{pmatrix} b_i(\xi_i, y_i, u_i), \tag{4.16a}$$

$$\xi_i^+ = 0.3y_{i1} - 0.3y_{i2} + 0.3\sin^2(\xi_i/3), \tag{4.16b}$$

where $b_i(\xi_i, y_i, u_i) = (-3 - \xi_i + \frac{1.07}{3}y_{i2}^2 - 3u_i)$. It can be verified that Assumptions 4.1 and 4.2 are satisfied. Noting that $0.1|\sin^2 a - \sin^2 b| \le 0.1\sqrt{2}|a - b|$, Assumption 4.3 is satisfied with $\gamma = 0.1\sqrt{2}/3$.

First, construct the drive-response system described in (4.5). Let $y_{i1}^d[k]$ and $y_{i2}^d[k]$ denote $y_{i1}[k-2]$ and $y_{i2}[k-2]$, respectively, and define

$$\hat{\xi}_i^+ = 0.3y_{i1}^d - 0.3y_{i2}^d + 0.3\sin^2(\hat{\xi}_i/3).$$

Next, $\mathrm{col}_{i=1}^8(b(\xi_i, y_i, u_i))$ is approximated with $\hat{H}^\top\Psi(\hat{\xi}, y^d)$, where $\hat{H} \in \mathbb{R}^{49\times 8}$,

$$\Psi(\xi, y) = \mathrm{col}\big(1, y, \xi, \mathrm{col}_{i=1}^8(y_{i1}^2), \mathrm{col}_{i=1}^8(y_{i2}^2), \mathrm{col}_{i=1}^8(\xi_{i1}^2)\big) : \mathbb{R}^{24} \to \mathbb{R}^{49},$$

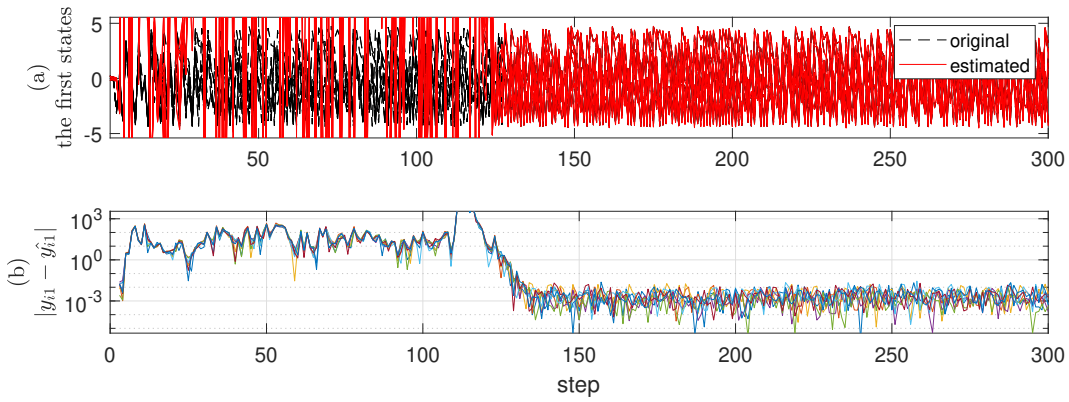

Fig. 4.4: (a). A comparison between the estimated first states y_{i1} estimated with $\theta_1, \theta_2, \cdots, \theta_8$, and their true values in the case where the coupling function is not contained in the span of $\Psi(\xi, y)$. (b). The estimation errors plotted in logarithmic scales.

and the dynamics of $\hat{H}$ follows (4.6) where the data matrices X, Y consist of data of 50 steps, i.e., $M = 50$. Also, define a variable $\theta \in \mathbb{R}^{24}$ as described in (4.9) to estimate the states $(\xi^\top, y^\top)^\top$ in real-time.

The parameter ρ is set to 0.5 and the results of the identification are shown in Fig.4.1. In Fig.4.1(a) a comparison between the estimated first states using $\theta_1, \cdots, \theta_8$ defined in (4.9) and the original states is shown, and Fig.4.1(b) plots the estimation errors in logarithmic scales. As the figure shows, the errors converge exponentially which matches the results of Proposition 4.1. However, note that the convergence starts after $k = M = 50$, which is the time step when X becomes full-rank. Fig.4.2(a) shows the evolution of the entries in H, and Fig.4.2(b) shows the $\hat{H}$ matrix obtained at $k = 100$. The function $\mathrm{col}_{i=1}^{N} b(\xi_i, y_i, u_i)$ is obtained as $\hat{H}^\top \Psi(\xi, y)$, and a brief example of obtaining the coupling function from $\hat{H}$ is given as follows. The first row of $\hat{H}^\top \Psi(\xi, y)$ reads

$$\boldsymbol{e}_1^\top \hat{H}^\top = \begin{pmatrix} -0.300 & -0.270 & \mathbf{0} & -0.030 & \mathbf{0} & 3.567 & \mathbf{0} \end{pmatrix},$$

which means that $b(\xi_1, y_1, u_1)$ is identified as

$$\begin{aligned} b^{id}(\xi_1, y_1, u_1) =& \boldsymbol{e}_1^\top \hat{H}^\top \Psi(\xi, y) \\ =& -3.000\psi_1 - 0.800\psi_2 - 0.100\psi_6 - 0.100\psi_8 + 0.357\psi_{42} \\ =& -3.000 - 0.800\xi_1 - 0.100\xi_5 - 0.100\xi_7 + 0.357y_{i2}^2. \end{aligned}$$

Combining $b^{id}(\xi_1, y_1, u_1)$ with (4.16a), it can be obtained that

$$\begin{aligned} \boldsymbol{e}_1^\top \hat{H}^\top \Psi(\xi, y) =& -3 - \xi_1 + \frac{1.07}{3} y_{12}^2 - 3u_1^{id} \\ 3u_1^{id} =& -0.200\xi_1 + 0.100\xi_5 + 0.100\xi_7, \end{aligned}$$

which matches the true input $u_1 = 0.1(x_{52} - x_{12}) + 0.1(x_{72} - x_{12})$. Finally, the topology of the network is obtained as shown in Fig.4.3.

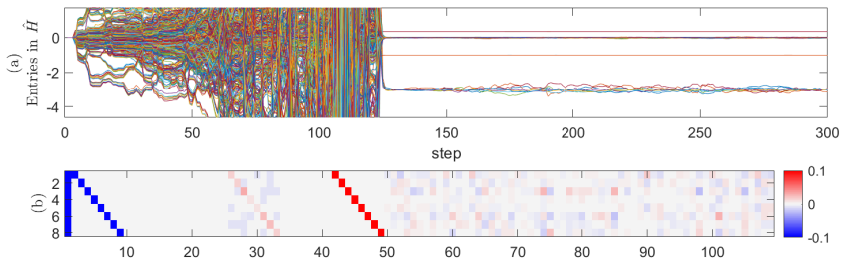

Fig. 4.5: (a). Time evolution of the entries in $\hat{H}$. (b) The $\hat{H}^\top \in \mathbb{R}^{8\times 49}$ matrix obtained at $k = 300$ shown in color, which unclear readings appear.

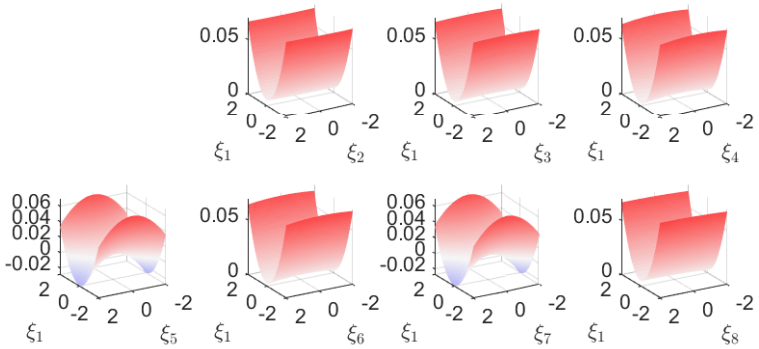

Fig. 4.6: The identified coupling function associated with y_{12}^+ restricted to the spaces spanned by ξ_1 and ξ_i for $i = 2, \cdots, 8$.

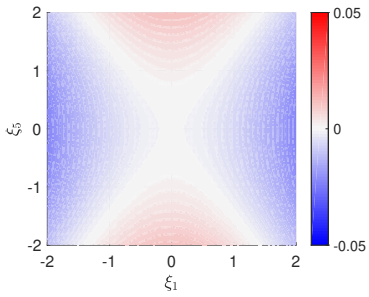

Fig. 4.7: The identification error of the coupling function associated with y_{12}^+ calculated in the space spanned by ξ_1 and ξ_5.

Next, consider the case where the coupling function is not contained in the span of $\Psi(\xi, y)$. Suppose that u_i in (4.15c) is given by

$$u_i = \sum_{j=1}^{N} a_{ij}(I(x_{j2}) - I(x_{i2})),$$

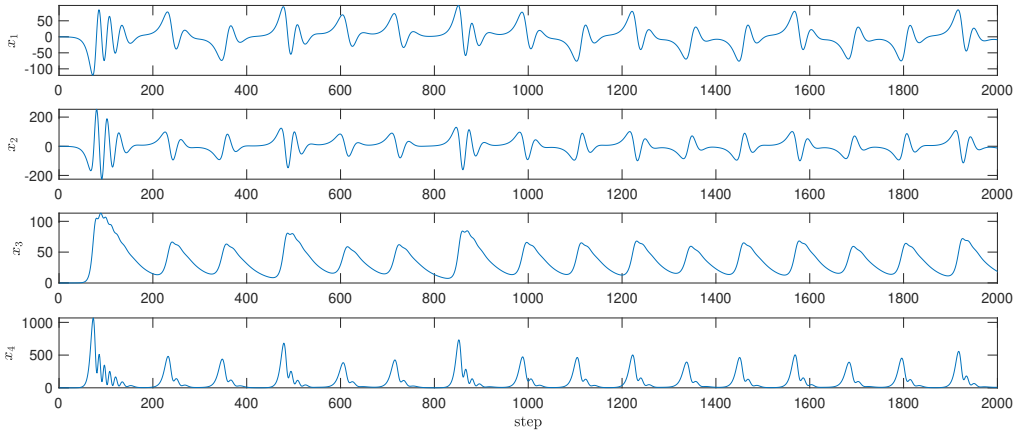

Fig. 4.8: Trajectory of system (4.17) with $u_{i1} = 0$ and $u_{i2} = 0$.

where $I(x) = 0.5(1 - \cos x)$. Redefine $\Psi(\xi, y)$ as

$$\begin{aligned}\Psi(\xi, y) =& \mathrm{col}\big(1, y, \xi, \mathrm{col}_{i=1}^{8}(y_{i1}^2), \mathrm{col}_{i=1}^{8}(y_{i2}^2), \mathrm{col}_{i=1}^{8}(\xi_{i1}^2),\\ & \mathrm{col}_{j=1}^{60}(\log \|(z^\top, y^\top)^\top - c_j\|^2)\big) : \mathbb{R}^{24} \to \mathbb{R}^{109},\end{aligned}$$

where $c_j \in \mathbb{R}^{24}$ for $j = 1, \cdots, 60$ are snapshots taken from the trajectories of 8 unforced generalized Hénon maps using k-means clustering. Let $M = 300$ and other parameters remain the same. Fig.4.4(a) shows a comparison between the y_{i1} states estimated with θ and their true values, and Fig.4.4(b) plots the errors in logarithmic scales, from which one can verify that the errors are not asymptotically stable, but still ultimately bounded. Fig.4.5(a) shows the time-evolution of the entries in $\hat{H}$. The coupling function cannot be completely represented by any linear combination of Ψ, so the origin of the error dynamics (4.13) is no longer an equilibrium. Nevertheless, the obtained values stay in small neighborhoods of the true values. Fig.4.5(b) shows the $\hat{H}$ matrix obtained at $k = 200$, and unclear readings that are hard to comprehend appear. To verify the correctness of the obtained results, the obtained coupling function associated with y_{12}^+ restricted to the spaces spanned by ξ_1 and ξ_j for $j = 2, \cdots, 8$ is shown in Fig.4.6. As the figures show, the coupling function shows a clear dependence on ξ_1, ξ_5 and ξ_7, and is not sensitive to the changes in other states. The fact matches the topology of the network shown in Fig.4.3, and the topology can be correctly inferred. Fig.4.7 shows a comparison between the obtained and the true coupling function associated with y_{12}^+ restricted to $\mathrm{span}\{\xi_1 \in [-2, 2], \xi_5 \in [-2, 2]\}$, i.e., $\big(u_1 - u_1^{id}\big)|_{[-2,2]^2}$, which indicates that the nonlinear coupling function is correctly identified in the region where data are measured, i.e., approximately $[-1, 1]^2$. This example indicates that if u_i is not contained in $\mathrm{span}\{\Psi\}$, then the proposed method can only identify the nonlinear coupling function locally over the manifold where data are measured.

4.3.2 Identification of a network of MIMO nodes

Consider the network of 15 nodes described by

$$\begin{aligned}
x_{i,1}^+ =& x_{i,1} + h(-10x_{i,1} + 10x_{i,2}), && (4.17a)\\
x_{i,2}^+ =& x_{i,2} + h(-x_{i,1}x_{i,3} + 28x_{i,1} - x_{i,2} + u_{i,1}), && (4.17b)\\
x_{i,3}^+ =& x_{i,3} + h(x_{i,4} - 8/3x_{i,3} + u_{i,2}) && (4.17c)\\
x_{i,4}^+ =& x_{i,4} + h(-10x_{i,4} + x_{i,1}x_{i,2}), && (4.17d)\\
w_{i,1} =& x_{i,1}, \qquad w_{i,2} = x_{i,3},
\end{aligned}$$

which are modified Lorenz oscillators discretized using the 1st order Euler method where $h = 0.01$. The trajectory of an oscillator described by (4.17) when $u_{i,1} = 0$ and $u_{i,2} = 0$ is shown in Fig.4.8. Here $u_{i,1} = \sum_{j=1}^N a_{ij}(x_{j2} - x_{i,2})$ and $u_{i,2} = \sum_{j=1}^N a_{ij}\sin(x_{j3} - x_{i,3})$.

Consider the time-evolution of the outputs:

$$\begin{aligned}
w_{i,1}^+ =& 0.9x_{i,1} + 0.1x_{i,2}\\
w_{i,1}^{2+} =& 0.9(0.9x_{i,1} + 0.1x_{i,2}) + 0.1(0.28x_{i,1} + 0.99x_{i,2} - 0.01x_{i,1}x_{i,3} + 0.01u_{i,1})\\
w_{i,2}^+ =& 2.92/3x_{i,3} + 0.01x_{i,4} + 0.01u_{i,2},
\end{aligned}$$

which indicates that the relative degrees of $w_{i,1}$ and $w_{i,2}$ are 2 and 1, respectively. Define $\xi_i = x_{i,4}$ and $\phi(x_i) = (x_{i,1}, 0.9x_{i,1} + 0.1x_{i,2}, x_{i,3}, x_{i,4})^\top$, and it can be verified that the requirements of all the assumptions are satisfied. Define $y_{i,11} = x_{i,1}, y_{i,12} = 0.9x_{i,1} + 0.1x_{i,2}, y_{i,1} = (y_{i,11}, y_{i,12})^\top$ and $y_{i,2} = x_{i,3}$. Noting that

$$\|(0.9\xi_i + 0.01x_1^*x_2^*) - (0.9\xi_j + 0.01x_1^*x_2^*)\| = 0.9\|\xi_i - \xi_j\|,$$

the requirement of Assumption 4.3 is also satisfied. Rewrite (4.17) into the following form:

$$\begin{aligned}
y_{i,1}^+ =& \begin{bmatrix}0 & 1\\ 0 & 0\end{bmatrix} y_{i,1} + \begin{pmatrix}0\\1\end{pmatrix}(-0.863y_{i,11} + 1.89y_{i,12} - 0.001y_{i,11}y_{i,2} + 0.001u_{i,1}), && (4.18a)\\
y_{i,2}^+ =& 2.92/3y_{i,2} + 0.01\xi_i + 0.01u_{i,2}, && (4.18b)\\
\xi_i^+ =& 0.9\xi_i + 0.01y_{i,11}(10y_{i,12} - 9y_{i,11}). && (4.18c)
\end{aligned}$$

Define $y_i^d[k] = y_i[k-2], \xi_i^d[k] = \xi_i[k-2]$ and define a drive-response system as described in (4.5) by

$$\hat{\xi}_i^+ = 0.9\hat{\xi}_i + 0.01y_{i,11}^d(10y_{i,12}^d - 9y_{i,11}^d). \tag{4.19}$$

Define $\Psi(\xi, y) : \mathbb{R}^{45} \to \mathbb{R}^{376}$ by

$$\begin{aligned}
\Psi(\xi, y) =& \mathrm{col}\big(1, \xi, y, \mathrm{col}_{i=1}^{15}(y_{i,11}y_{i,12}), \mathrm{col}_{i=1}^{15}(y_{i,11}y_{i,2}), \mathrm{col}_{i=1}^{15}(y_{i,11}\xi_i), \mathrm{col}_{i=1}^{15}(y_{i,12}y_{i,2}),\\
& \mathrm{col}_{i=1}^{15}(y_{i,12}\xi_i), \mathrm{col}_{i=1}^{15}(y_{i,2}\xi_i), \mathrm{col}_{i=1}^{15}\mathrm{col}_{j=1}^{15}(\cos y_{j,2}\sin y_{i,2})\big), && (4.20)
\end{aligned}$$

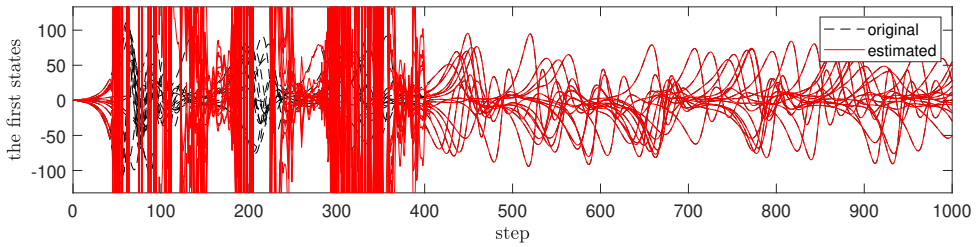

Fig. 4.9: A comparison between the estimated first states $\theta_1, \cdots, \theta_{15}$ and the original $y_{1,11}, \cdots, y_{15,11}$.

and let the inputs $u_{i,1}, u_{i,2}$ be approximated by

$$\begin{pmatrix} \mathrm{col}_{i=1}^{15}(u_{i,1}) \\ \mathrm{col}_{i=1}^{15}(u_{i,2}) \end{pmatrix} = \hat{H}^\top \Psi(\hat{\xi}, y_i^d),$$

where $\hat{H} \in \mathbb{R}^{376\times 30}$. Let $M = 400$ and define data matrices $X[k] \in \mathbb{R}^{400\times 376}$ and $Y[k] \in \mathbb{R}^{20\times 376}$ by

$$\begin{aligned} X[k] &= \begin{bmatrix} \cdots & \Psi(\hat{\xi}[j], y^d[j]) & \cdots \end{bmatrix}, \\ Y[k] &= \begin{bmatrix} \cdots & \mathrm{col}\big(\mathrm{col}_{i=1}^{15}(w_{i,1}[j]), \mathrm{col}_{i=1}^{15}(w_{i,2}[j-1])\big) & \cdots \end{bmatrix}, \end{aligned}$$

for $j = k, k-1, \cdots, k-399$. Then, matrix $\hat{H}$ is updated according to (4.6) using the above-defined $X[k]$ and $Y[k]$ matrices. The parameter ρ is set to 0.5. On the other hand, Let $F(H[k], \xi, y)$ defined by

$$F(H[k], \xi, y) = \begin{pmatrix} \mathrm{col}_{i=1}^{15}(y_{i,12}) \\ H[k]\Psi(\xi, y) \\ \mathrm{col}_{i=1}^{15}(0.9\xi_i + 0.01 y_{i,11}(10 y_{i,12} - 9 y_{i,11})) \end{pmatrix}$$

denote the dynamics of the drive response system obtained at step $[k]$, and define $\theta \in \mathbb{R}^{60}$ by

$$\theta = F \circ F(H[k], \hat{\xi}[k], y^d[k])$$

to estimate $(y^\top, \xi^\top)^\top$ in real-time.

The result of state estimation is shown in Fig.4.9, where the estimated and the original of the two inputs of the nodes are plotted. As shown by the figures, the states are correctly estimated for $k > M$, which indicates that the dynamics of the nodes are correctly identified. Time-evolution of the entries in $\hat{H}$ is shown in Fig.4.10, and as the figure shows, the entries converge to constant values for $k > M$. The obtained $\hat{H}^\top[1000] \in \mathbb{R}^{30\times 376}$ matrix obtained at the end of the identification process is shown in Fig.4.11, where the top 15 rows correspond to $v_{i,1}$ and the bottom 15 rows corresponds to

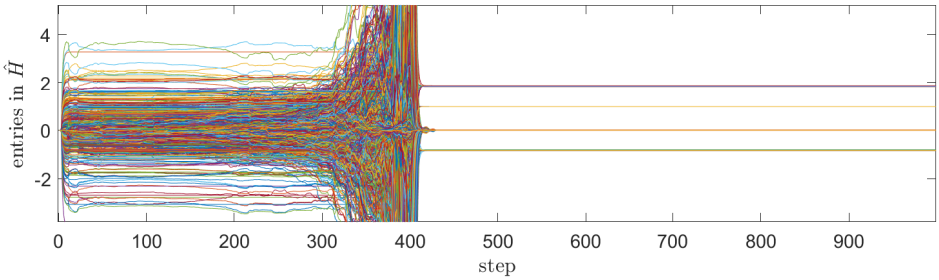

Fig. 4.10: Time-evolution of the entries in $\hat{H}$.

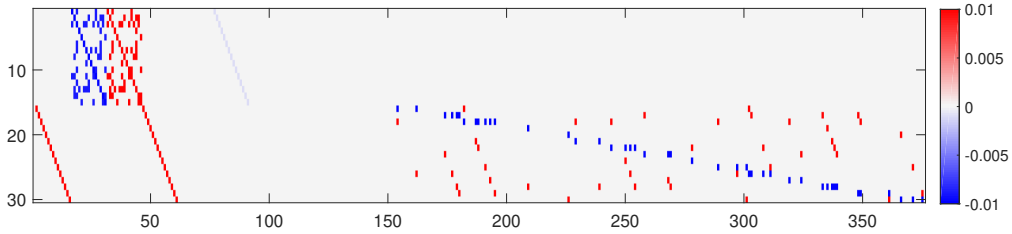

Fig. 4.11: The $\hat{H}^\top[1000]$ matrix shown in color.

$v_{i,2}$ for $i = 1, \cdots, 15$, respectively. As an illustrative example, the 1st row and the 16th row read

$$\begin{aligned}
b_1^{id}(\xi_1, y_1, u_1) =& \boldsymbol{e}_1^\top \hat{H}^\top[1000]\Psi(\xi, y) \\
=& -0.845\psi_{17} - 0.009\psi_{19} - 0.009\psi_{27} + 1.870\psi_{32} + 0.010\psi_{34} \\
&+ 0.010\psi_{42} - 0.001\psi_{77} \\
=& -0.845y_{1,11} - 0.009y_{3,11} - 0.009y_{11,11} + 1.870y_{1,12} + 0.010y_{3,12} \\
&+ 0.010y_{11,12} - 0.001y_{1,11}y_{1,2}, \\
b_2^{id}(\xi_1, y_1, u_1) =& \boldsymbol{e}_{16}^\top \hat{H}^\top[1000]\Psi(\xi, y) \\
=& 0.010\psi_2 + 0.973\psi_{47} - 0.010\psi_{154} - 0.010\psi_{162} + 0.010\psi_{182} + 0.010\psi_{302} \\
=& 0.010\xi_1 + 0.973y_{1,2} - 0.010\cos y_{3,2} \sin y_{1,2} \\
&- 0.010\cos y_{11,2} \sin y_{1,2} + 0.010\cos y_{1,2} \sin y_{3,2} + 0.010\cos y_{1,2} \sin y_{11,2}.
\end{aligned}$$

On the other hand, it can be obtained from (4.18) that

$$\begin{aligned}
b_1(\xi_1, y_1, u_1) =& -0.863y_{1,11} + 1.89y_{1,12} - 0.001y_{1,11}y_{1,2} + 0.001u_{1,1} \\
b_2(\xi_1, y_1, u_1) =& 2.92/3y_{1,2} + 0.01\xi_1 + 0.01u_{1,2},
\end{aligned}$$

which results in

$$\begin{aligned}
0.001u_{1,1}^{id} =& 0.018y_{1,11} - 0.02y_{1,12} - 0.009y_{3,11} - 0.009y_{11,11} + 0.010y_{3,12} + 0.010y_{11,12} \\
u_{i,1}^{id} =& -2(10y_{1,12} - 9y_{1,11}) + (10y_{3,12} - 9y_{3,11}) + (10y_{11,12} - 9y_{11,11}),
\end{aligned}$$

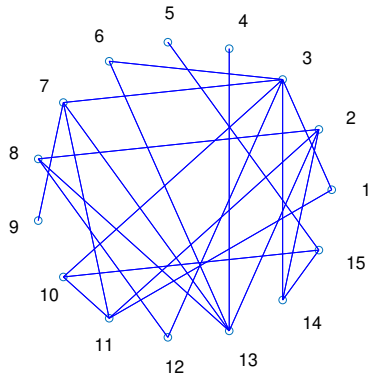

Fig. 4.12: The identified network topology.

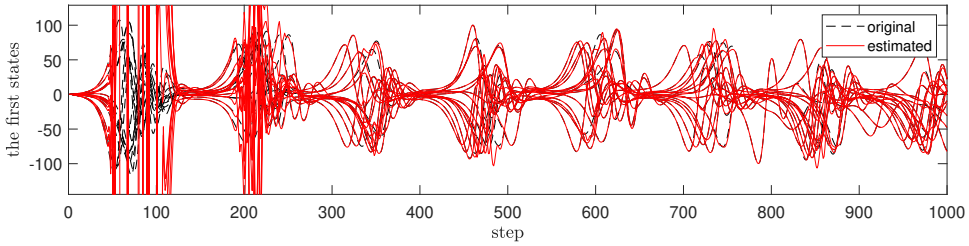

Fig. 4.13: A comparison between the estimated and the original first states in the case where the span of the observables does not contain the coupling function.

and

$$\begin{aligned} 0.01u_{1,2}^{id} =& -0.010\cos y_{3,2}\sin y_{1,2} - 0.010\cos y_{11,2}\sin y_{1,2} + 0.010\cos y_{1,2}\sin y_{3,2} \\ &+ 0.010\cos y_{1,2}\sin y_{11,2} \\ u_{1,2}^{id} =& \sin(y_{3,2} - y_{1,2}) + \sin(y_{11,2} - y_{1,2}). \end{aligned}$$

Note that by definition, $x_{i,1} = y_{i,11}$ and $x_{i,2} = -9y_{i,11} + 10y_{i,12}$ hold. As a result, the inputs are transformed into

$$\begin{aligned} u_{1,1}^{id} =& (x_{3,2} - x_{1,2}) + (x_{11,2} - x_{1,2}), \\ u_{1,2}^{id} =& \sin(x_{3,3} - x_{1,3}) + \sin(x_{11,3} - x_{1,3}), \end{aligned}$$

which match the true inputs and the identification is considered successful. The identified network topology is shown in Fig.4.12.

Next, consider the case where the coupling function is not contained in the span of the observables. Define $\Psi(\xi, y) : \mathbb{R}^{60} \to \mathbb{R}^{151}$ by

$$\begin{aligned} \Psi(\xi, y) =& \mathrm{col}\big(1, \xi, y, \mathrm{col}_{i=1}^{15}(y_{i,11}y_{i,12}), \mathrm{col}_{i=1}^{15}(y_{i,11}y_{i,2}), \mathrm{col}_{i=1}^{15}(y_{i,11}\xi_i), \mathrm{col}_{i=1}^{15}(y_{i,12}y_{i,2}), \\ & \mathrm{col}_{i=1}^{15}(y_{i,12}\xi_i), \mathrm{col}_{i=1}^{15}(y_{i,2}\xi_i)\big), \end{aligned}$$

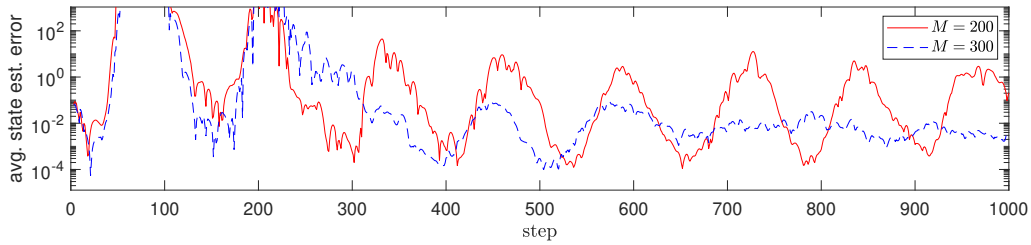

Fig. 4.14: A comparison of the state estimation errors with $M = 200$ and $M = 300$, where the average values of the first states of all the nodes are shown, respectively.

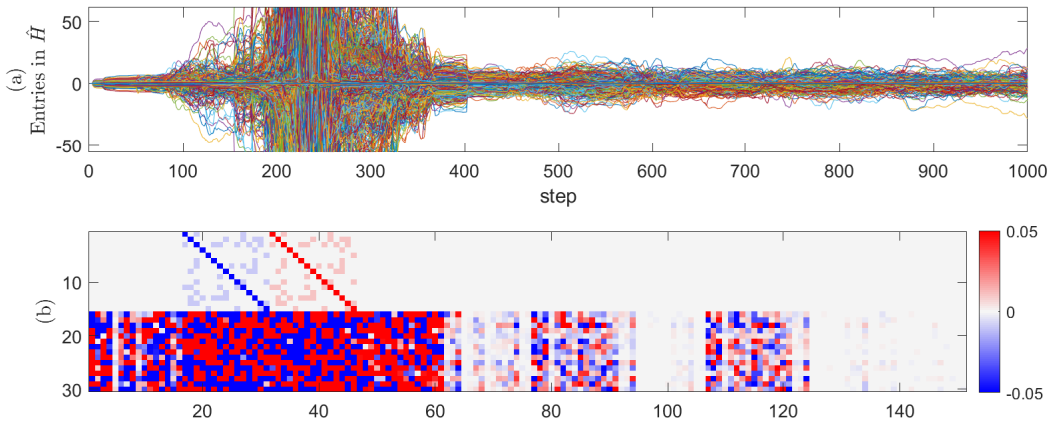

Fig. 4.15: (a) Time-evolution of the entries in $\hat{H}$ in the case where the span of the observables does not contain the coupling function; (b) the $\hat{H}^\top[1000]$ matrix shown in color.

where the trigonometric functions are removed from (4.20). Let $M = 200$ and other conditions and parameters remain the same. Fig.4.13 shows the result of state estimation, and as the figures show, estimation errors exist. Time-evolution of entries in $\hat{H}$ is shown in Fig.4.15(a), and the entries fail to converge to constant values. Fig.4.15(b) shows the obtained $\hat{H}$ matrix, whose bottom part fails to show a direct relationship with the network topology. In this case, there does not exist an H with which $\|H\Psi(\xi, y) - \mathrm{col}_{i=1}^{N}\mathrm{col}_{\ell=1}^{m}(b_\ell(\xi_i, y_i, u_i))\| = 0$, and $\hat{H}$ is obtained as a practical minimizer. As a result, the estimation errors depend greatly on the amount of data, i.e., M. Fig.4.14 shows a comparison of the identification errors of the average values of the first states $y_{i,11}$ with $M = 200$ and $M = 300$, respectively, and the latter obtains smaller error. On the other hand, since the estimations of the states of the original network system, i.e., entries in θ, are obtained by iterating the dynamics of the derive-response system two times, small errors between $(\theta_1, \cdots, \theta_{15})^\top$ and $(y_{1,11}, \cdots, y_{15,11})^\top$ indicate that v_i approximates $\mathrm{col}_{\ell=1}^{m}(b_\ell(\xi_i, y_i, u_i))$ decently. Also, since all the states are estimated, the method described in Chapter 2 can be employed to obtain the nonlinear coupling function.

4.4 Conclusions and discussions

In this chapter, the identification problem of network structures using measured output data is considered, where the dynamics of nodes in the network are assumed to be known. Under the assumptions that the nodes can be input-output decoupled [99] and that the internal dynamics of the nodes are convergent [100], a drive-response system is designed to estimate delayed past data of the original network system as well as the unknown network dynamics. The states of the network in real-time are also estimated by iterating the dynamics of the drive-response system. Numerical identification examples showed the usefulness and validity of the obtained results.

In this chapter, three assumptions are posed which ensure that the input-output model can be constructed, that the reconstructed system is equivalent to the original and that the internal dynamics is convergent. If Assumption 4.1 or Assumption 4.3 fails to hold, then the proposed method would fail and it is encouraged to employ the method proposed in Chapter 5 for such networks. If Assumption 4.2 fails to hold, then $\boldsymbol{b}(y, \xi)$ can be obtained but it may not be able to recover $x^{+,id}$ and therefore $\boldsymbol{g}(x)$ any longer. In such case, the network structure may be recovered in terms of y and ξ as the information sent from others, as in the case in Chapter 3 where the assumptions do not hold.

5 Identification of Networks Structures for Networks with Partially-measurable States and Unknown Dynamical Models

5.1 Introduction

In the previous chapter, a drive-response-system-based method is proposed to identify the structures of networks, the dynamical models of whose nodes are considered known. In this chapter, the requirement of knowledge about the dynamical models of the nodes is released, and an identification method is proposed for networks of nodes with partially known or unknown dynamics using measured output data.

Compared to many other topics in the field of network structure identification, the identification of networks having hidden variables with unknown dynamics is a less-considered topic due to lacking available information. The hidden variables are usually modeled as functions of time acting as an external input ([32, 89, 90, 52, 98, 36]), and the network is reconstructed in the subspace spanned by the measurable states. In [32, 89], data-correlation-based methods are employed, where the hidden variables are considered noises and the adjacency matrix of the subnetwork consisting of measurable nodes is derived using data correlation. [98] describes the effect of hidden variables on the result of such correlation-based methods. On the other hand, [90, 52] use a covariance-based method under the principle that hidden inputs would enlarge the covariance of the identified adjacency matrix of the measurable sub-network. In [36], a similar method combined with data entropy detects hidden sources of propagation networks. Besides, [101] studies the identifiabililty of networks modeled by unknown transfer functions, assuming the topology of the network to be known.

This chapter considers the identification problem of network structures, the dynamics of whose nodes are partially known or unknown. It is supposed that the outputs of all the signals are measurable. Under the assumption that a subspace model of the nodes in the space spanned by the measurable states is available, the network is reconsidered as a network of fully known nodes coupled dynamically, where the measurable states are considered as the full states of the new nodes, and the hidden states are considered as the unknown dynamical couplings. Under the assumption that the dimension of the hidden

variables is smaller than that of the measurable ones, new variables with to-be-determined dynamical models are defined which approximates the hidden dynamical inputs, in the sense that they have the same influence on the dynamics of the known variables. Here, it may be impossible to identify the original coupling function accurately, so the structure is defined as the function describing the data flow in the network in terms of the new variables.

This chapter is organized as follows. Section 5.2 describes the details of the identification method of networks consisting of nodes with partially known dynamical models. Section 5.3 shows an identification example of a network of Lorenz systems to show the usefulness of the proposed method. Section 5.4 concludes this chapter and gives some remarks.

5.2 Identification by considering hidden variables as new states

In practical situations, it is common that some knowledge of the dynamical models of the nodes in networks is available a priori. However, such knowledge may only be a linearized subspace model or is inaccurate due to modeling errors or other limitations. This chapter considers the case that the dynamical models of the nodes are partially known, and tries to extract the data flow in the network.

Consider the network system of N nodes described by

$$\begin{aligned} x_i^+ =& f(x_i) + Bu_i(x), \\ u_i(x) =& \sum_{j=1}^{N} a_{ij} g(x_i, x_j), \quad w_i = Cx_i \end{aligned} \tag{5.1}$$

where $x_i \in \mathbb{R}^n$, $x = \mathrm{col}_{i=1}^N(x_i) \in \mathbb{R}^{Nn}$ denotes the states, $f : \mathbb{R}^n \to \mathbb{R}^n$ is locally Lipschitz continuous, $w_i \in \mathbb{R}^m$ is the output of node i, and $u_i(x) : \mathbb{R}^{Nn} \to \mathbb{R}^m$ denotes the transmission sent to node i via the network where a_{ij} is the (i, j) entry of the adjacency matrix associated with the network topology. Define $w = \mathrm{col}_{i=1}^N(w_i)$ and rewrite the dynamics of the network into

$$\begin{aligned} x^+ =& \boldsymbol{f}(x) + \boldsymbol{B}\boldsymbol{g}(x), \\ w =& \boldsymbol{C}x, \end{aligned} \tag{5.2}$$

where $\boldsymbol{f}(x) = \mathrm{col}_{i=1}^N(f(x_i))$, $\boldsymbol{g}(x) = \mathrm{col}_{i=1}^N(u_i)$, $\boldsymbol{B} = I_N \otimes B$, $\boldsymbol{C} = I_N \otimes C$ and $\otimes$ denotes the Kronecker product. Here, information about the network structure is fully contained in $\boldsymbol{g}(x)$, so the network structure identification problem is reduced to identifying $\boldsymbol{g}(x)$. Specifically, this chapter considers the case where a linear approximation of the dynamical model is known and attempts to identify the network structure from measured output data.

First, the dynamical models of the nodes are reformulated such that the outputs w_i correspond to the full states, and the unmeasurable states are considered some unknown dynamical inputs to the outputs. Let Fx be a linear approximation of $f(x)$ where $F \in \mathbb{R}^{n\times n}$, $f(x) \equiv Fx + \tau(x)$ and $\tau(x)$ denotes the modeling error. Let $T \in \mathbb{R}^{(n-m)\times n}$ be such that $\mathrm{col}(C, T)$ has full rank, and rewrite (5.1) into

$$w_i^+ = Cx_i^+ = CFx_i + C\tau(x_i) + CBu_i(x), \tag{5.3a}$$

$$Tx_i^+ = TFx_i + T\tau(x_i) + TBu_i(x). \tag{5.3b}$$

Since only data of the outputs w_i of the nodes can be measured, rewrite CFx_i into $CFx_i \equiv F_1 w_i + F_2 x_i$, where $F_1 \in \mathbb{R}^{m\times m}$ consists of the first m columns of $CF\begin{bmatrix} C \\ T \end{bmatrix}^{-1}$ and $F_2 \in \mathbb{R}^{m\times n}$. Define $y_i = F_2 x_i + C\tau(x_i) + CBu_i(x)$ for $i = 1, \cdots, N$. Substituting y_i into (5.3a), y_i is considered a dynamical input to w_i, i.e., $w_i^+ = F_1 w_i + y_i$, where the dynamics of y_i is unknown. The merits of defining the variables y_i are twofold: the dynamics of w_i becomes fully known and $y_i[k]$ can be obtained as $w_i[k+1] - F_1 w_i[k]$. This chapter considers two cases where the dimension of $\mathrm{col}(w_i, y_i)$ is smaller than the dimensional of x_i or not, respectively. Note that although y_i is unknown, data for y_i can be calculated from w_i and the dimension of y_i can be inferred by checking the linear dependency of the data series.

First, consider the case where $\dim(y_i) + m \geq n$. In this case, no additional variables are required to span the dynamics of x_i, so let the dynamics of y_i be described by $y_i^+ = h_i(w, y)$, where $y = \mathrm{col}_{i=1}^N(y_i) \in \mathbb{R}^{Nm}$ and $h_i : \mathbb{R}^{Nm} \times \mathbb{R}^{Nm} \to \mathbb{R}^m$. Reformulate the dynamical models of the nodes as

$$w_i^+ = F_1 w_i + y_i, \tag{5.4a}$$

$$y_i^+ = h_i(w, y), \tag{5.4b}$$

for $i = 1, \cdots, N$, and rewrite the dynamics of the network into

$$w^+ = \boldsymbol{F}_1 w + y, \tag{5.5a}$$

$$y^+ = \boldsymbol{h}(w, y), \tag{5.5b}$$

where $\boldsymbol{h}(w, y) = \mathrm{col}_{i=1}^N(h_i(w, y))$, $\boldsymbol{F}_1 = I_N \otimes F_1$ and $\otimes$ denotes the Kronecker product.

Next, the dynamics of y, i.e., $\boldsymbol{h}(w, y)$, is extracted from measured data $w[k]$ and $y[k]$ using the Koopman operator theory. Define $\psi_i(w, y) \in \mathcal{F}$ to be an observable for $i = 1, \cdots, q$ where $\mathcal{F}$ is the space of all the complex-valued scalar functions, i.e., $\mathcal{F} = \{f \mid f : \mathbb{R}^{Nm} \times \mathbb{R}^{Nm} \to \mathbb{C}\}$. Define $\Psi(w, y) = \mathrm{col}(\psi_1, \cdots, \psi_q) : \mathbb{R}^{Nm} \times \mathbb{R}^{Nm} \to \mathbb{C}^q$ to be the observable set. Let K denote the Koopman operator that governs the evolution of the observables associated with dynamics (5.5), i.e.,

$$K\psi_i(w, y) = \psi_i(\boldsymbol{F}_1 w + y, \boldsymbol{h}(w, y)), \tag{5.6}$$

for $i = 1, \cdots, q$. Then, a q-dimensional approximation of $K\varphi$ can be obtained as

$$K\varphi \approx c_\varphi A\Psi,$$

for any $\varphi \in \mathcal{F}$ where $c_\varphi = \text{argmin}_c \|f - c\Psi\|_{L_2}$ and $A = \text{argmin}_H \|\Psi(\boldsymbol{F}_1 w + y, \boldsymbol{h}(w, y)) - H\Psi\|_{L_2}$. As a result, the right-hand side of (5.5b) can be approximated as

$$\boldsymbol{h}(w, y) = Ky \approx C_y A\Psi(w, y),$$

where C_y is such that $y \equiv C_y\Psi(w, y)$. Note that the existence of the expansion matrix C_y can always be ensured by including the states w and y as observables in $\Psi(w, y)$.

To obtain A from data, suppose that $M + 2$ steps of data, indexed by $w[0], w[1], \cdots, w[M], w[M + 1]$, are measured. It is required that $M > q$ and M can be designed considering the dynamical characteristics of the nodes, e.g., enlarging M for nodes that oscillate slowly. Then data for $y[k]$ can be obtained as $y[k] = w[k + 1] - \boldsymbol{F}_1 w[k]$ for $k = 0, \cdots, M$. Define data matrices $X, Y \in \mathbb{C}^{q\times M}$ as

$$X = \begin{bmatrix} \Psi(w[0], y[0]) & \cdots & \Psi(w[M-1], y[M-1]) \end{bmatrix}, \tag{5.7a}$$

$$Y = \begin{bmatrix} \Psi(w[1], y[1]) & \cdots & \Psi(w[M], y[M]) \end{bmatrix}. \tag{5.7b}$$

According to the definition of K, $KX = Y$ holds, and a matrix approximation of K can be obtained as the transition matrix A that maps X to Y, i.e.,

$$A = \underset{H}{\text{argmin}} \ \|HX - Y\|_F^2, \tag{5.8}$$

where $\|\cdot\|_F$ denotes the Frobenius norm. Denote the optimality of optimization problem (5.8) by A^{opt}, and an approximation of dynamics (5.5b) is obtained as

$$y^{+,id} = \boldsymbol{h}^{id}(w, y) = C_y A^{opt}\Psi(w, y). \tag{5.9}$$

Next, information about the network structure is obtained from the identified dynamics of y, i.e., $\boldsymbol{h}^{id}(w, y)$. Specifically, data transmission sent to the nodes from other nodes via the network is extracted. If all the connections in the network were cut, then $\boldsymbol{g}(x) = 0$ and y_i^+ should depend solely on y_i and w_i. This fact indicates that the transmission from node j to node i can be identified as the terms in the dynamical model of node i that depend on w_j or y_j. It follows (5.9) that

$$y_i^+ = C_i C_y A^{opt}\Psi(w, y), \tag{5.10}$$

where $C_i \in \mathbb{R}^{m\times Nm}$ is such that $y_i \equiv C_i y$. Define $\Psi_i(w_i, y_i) \in \mathbb{R}^q$ to be the observable vector such that all the entries, which are *dependent* on w_j or y_j for any $j \neq i$, in $\Psi(w, y)$

are set to 0, and define $\Psi_i'(w,y) = \Psi(w,y) - \Psi_i(w_i,y_i)$. Note that $\Psi_i(w_i,y_i)$ now contains observables that only depend on the states of node i. Then (5.10) can be rewritten as

$$y_i^+ = C_i C_y A^{opt} \Psi_i(w_i,y_i) + C_i C_y A^{opt} \Psi_i'(w,y). \tag{5.11}$$

Here, $C_i C_y A^{opt} \Psi_i'(w,y)$ corresponds to the information sent from other nodes to node i via the network and is considered as the network structure to be identified. As a result, the dynamics of the network is identified as

$$w^+ = \boldsymbol{F}_1 w + y \tag{5.12a}$$
$$y_i^+ = C_i C_y A^{opt} \Psi_i(w_i,y_i) + \boldsymbol{g}^{id}(w,y). \tag{5.12b}$$

where

$$\boldsymbol{g}^{id}(w,y) = \mathrm{col}_{i=1}^N (C_i C_y A^{opt} \Psi_i'(w,y)) \tag{5.13}$$

is the identified coupling function.

Remark 5.1. Since Tx_i in (5.3b) is $n-m$ dimensional, theoretically only $n-m$ linearly independent variables are required to fully describe the dynamics. Without loss of generality, define $\tilde{y}_i$ to be the vector consisting of the first $n-m$ linearly independent entries in y_i and define $\tilde{y} = \mathrm{col}_{i=1}^N(\tilde{y}_i) \in \mathbb{R}^{N(n-m)}$. Then, dynamics (5.5b) can be rewritten into

$$y^+ = \boldsymbol{h}'(w,\tilde{y}), \tag{5.14}$$

where $\boldsymbol{h}' : \mathbb{R}^{Nm} \times \mathbb{R}^{N(n-m)} \to \mathbb{R}^{Nm}$.

Next, consider the case where $\dim(y_i) + m < n$. In such case, with y_i defined by $y_i = CF_2 x_i + C\tau(x_i) + CBg(x)$ as in (5.4), $\dim(\mathrm{col}(w_i,y_i)) < \dim(x_i)$, which means that additional variables are required for the dynamics of x_i to be fully embedded into the space spanned by the new variables. Here, delay coordinates are employed to complement the dimension. Let r be the smallest integer such that $r \cdot \dim(y_i) + m \geq n$, and rewrite the dynamics of the network (5.5) into

$$w^+ = \boldsymbol{F}_1 w + y, \tag{5.15a}$$
$$y^{r+} = \boldsymbol{h}(w, y, \cdots, y^{(r-1)+}), \tag{5.15b}$$

where $\boldsymbol{F}_1$ is defined the same as in (5.5). Further, define $z_i = y^{i+} \in \mathbb{R}^{Nm}$ for $i = 1, \cdots, r-1$ and define $z = \mathrm{col}(z_1, \cdots, z_{r-1})$. Then, $\dim(\mathrm{col}(w,y,z)) = r \cdot \dim(y_i) + m \geq n$ holds and the dynamics of x can be embedded into the space spanned by w, y and z. The identification is then performed by finding an approximation A^{opt} of the Koopman operator defined by

$$K\psi_i(w,y,z_1,\cdots,z_{r-1}) = \psi_i(\boldsymbol{F}_1 w + y, z_1, z_2, \cdots, \boldsymbol{h}(w,y,z)), \tag{5.16}$$

using data matrices defined by

$$X = \begin{bmatrix} \Psi(w[0], y[0], z[0]) & \cdots & \Psi(w[M-1], y[M-1], z[M-1]) \end{bmatrix}, \tag{5.17a}$$

$$Y = \begin{bmatrix} \Psi(w[1], y[1], z[1]) & \cdots & \Psi(w[M], y[M], z[M]) \end{bmatrix}. \tag{5.17b}$$

The dynamics of the network is then identified as

$$\begin{aligned} w^+ =& \boldsymbol{F}_1 w + y, \\ y^+ =& z_1, \\ z_1^+ =& z_2, \\ &\vdots \\ z_{r-1}^+ =& \operatorname{col}_{i=1}^N (C_i C_z A^{opt} \Psi_i(w, y, z)) + \boldsymbol{g}^{id}(w, y, z), \end{aligned}$$

where $C_z \in \mathbb{R}^{Nm \times q}$ is such that $z_{r-1} \equiv C_z \Psi(w, y, z_1, \cdots, z_{r-1})$, Ψ_i contains observables that solely depend on the states of node i, and

$$\boldsymbol{g}^{id}(w, y, z) = \operatorname{col}_{i=1}^N (C_i C_z A^{opt} \Psi_i'(w, y, z)) \tag{5.18}$$

is the identified coupling function, where $\Psi_i' = \Psi - \Psi_i$ as in (5.11). Note that the case where $\dim(y_i) + m \geq n$ can be considered as a special case where $r = 1$ and z does not exist.

The proposed identification algorithm is summarized in Algorithm 5.1.

Next, consider the relationship between the identified coupling function $\boldsymbol{g}^{id}(w, y, z)$ and the original $\boldsymbol{g}(x)$, and discuss the identification error in terms of the difference between the original and the identified dynamics of the measured output w.

Proposition 5.1. If data are sufficient ($M \to \infty$) and are sampled uniformly randomly, then for $i = 1, \cdots, N$ and $j = 1, \cdots, m$, the jth component of the identified coupling function for the ith node, i.e., $\boldsymbol{e}_j^\top C_i \boldsymbol{g}^{id}(w, y, z)$, is a projection of $\boldsymbol{e}_j (w_i^+ - F_1 w_i)^{r+}$ onto $\operatorname{span}\{\Psi_i\}$:

$$\boldsymbol{e}_j^\top C_i \boldsymbol{g}^{id}(w, y, z) = \mathbb{P}_{\operatorname{span}\{\Psi_i'(w,y,z)\}} (\boldsymbol{e}_j^\top (w_i^+ - F_1 w_i)^{r+}) \tag{5.19}$$

with respective to dynamics (5.15).

Proof. First, the relationship between the theoretical and the identified dynamics of y is considered, and then the validity of equation (5.19) is verified.

As shown in [94] the solution of optimization problem (5.8), i.e., A^{opt}, minimizes $\|A\Psi(w, y, z) - K\Psi(w, y, z)\|_{L_2}$ over the manifold where data are measured, so A^{opt} is an approximation of the Koopman operator defined in (5.6), in the sense that for any complex-value scalar function $\varphi(w, y, z)$ ([94]),

$$\mathbb{P}_{\operatorname{span}\{\Psi\}} \big(K (\mathbb{P}_{\operatorname{span}\{\Psi\}} \varphi) \big) = c_\varphi A^{opt} \Psi(w, y, z),$$

Algorithm 5.1 Proposed identification algorithm

Input: measured time series of the outputs of the nodes, Fx_i as an approximation of $f(x_i)$, C, and n

Output: $\boldsymbol{g}^{id}(w,y)$ or $\boldsymbol{g}^{id}(w,y,z)$

1. Initialization: find r as the minimum integer with which $r\cdot\dim(y_i)+m\geq n$

2. Matrices construction:

if $r=1$ **then**

design an observable set $\Psi(w,y)$ and construct data matrices X,Y with (5.7)

else

design an observable set $\Psi(w,y,z)$ and construct data matrices X,Y with (5.17)

end if

3. Approximate the Koopman operator: calculate A^{opt} with (5.8)

4. Obtain the coupling function:

if $r=1$ **then**

obtain $\boldsymbol{g}^{id}(w,y)$ with (5.13)

else

obtain $\boldsymbol{g}^{id}(w,y,z)$ with (5.18)

end if

5. Output: $\boldsymbol{g}^{id}(w,y)$ or $\boldsymbol{g}^{id}(w,y,z)$

where $c_\varphi=\mathrm{argmin}_c\|\varphi-c\Psi(w,y,z)\|$. Since one can design Ψ to contain w,y and z as observables, the evolution of the jth entry of y_i is obtained as

$$\begin{aligned}\boldsymbol{e}_j^\top C_i y^{r+,id}=\boldsymbol{e}_j^\top C_i z_{r-1}^{+,id}=&\boldsymbol{e}_j^\top C_i C_z A^{opt}\Psi(w,y,z)\\ =&\mathbb{P}_{\mathrm{span}\{\Psi\}}(\boldsymbol{e}_j^\top C_i z_{r-1}^{+})=\mathbb{P}_{\mathrm{span}\{\Psi\}}(\boldsymbol{e}_j^\top C_i y^{r+}),\end{aligned}$$

i.e., the identified evolution $\boldsymbol{e}_j^\top C_i y^{r+,id}$ is a projection of the true evolution $\boldsymbol{e}_j^\top C_i y^{r+}$ onto the space spanned by the observables in $\Psi(w,y,z)$.

On the other hand, by the construction of $\boldsymbol{g}^{id}(w,y,z)$ in (5.18), the coupling function of node i is obtained as a linear combination of the observables in $\Psi_i'(w,y,z)$, i.e.,

$$\begin{aligned}\boldsymbol{e}_j^\top C_i\boldsymbol{g}^{id}(w,y,z)=&\mathbb{P}_{\mathrm{span}\{\Psi_i'(w,y,z)\}}(\boldsymbol{e}_j^\top C_i z_{r-1}^{+,id})\\ =&\mathbb{P}_{\mathrm{span}\{\Psi_i'(w,y,z)\}}\mathbb{P}_{\mathrm{span}\{\Psi\}}(\boldsymbol{e}_j^\top C_i y^{r+}).\end{aligned}$$

Making use of dynamics (5.15a) that $w^+-\boldsymbol{F}_1 w=y$ and the fact that $\mathrm{span}\{\Psi_i'(w,y,z)\}\subset\mathrm{span}\{\Psi(w,y,z)\}$, the following equations hold

$$\begin{aligned}\boldsymbol{e}_j^\top C_i\boldsymbol{g}^{id}(w,y,z)=&\mathbb{P}_{\mathrm{span}\{\Psi_i'(w,y,z)\}}(\boldsymbol{e}_j^\top C_i y^{r+})\\ =&\mathbb{P}_{\mathrm{span}\{\Psi_i'(w,y,z)\}}(\boldsymbol{e}_j^\top (w_i^+-F_1 w_i)^{r+}).\end{aligned}$$

where $C_i y=y_i=w_i^+-F_1 w_i$ is substituted. □

Proposition 5.1 means that the coupling function is obtained in terms of the r-step-future and the $(r+1)$-step-future values of w, which is estimated using the dynamics identified from measured data.

Remark 5.2. The identification error of the proposed method depends on two factors, namely the design of the observable set $\Psi(w,y,z)$ and the amount of measured data. Define

$$\begin{aligned}\varepsilon(w,y,z) =& y^{r+}(w,y,z) - y^{r+,id}(w,y,z)\\ =& \boldsymbol{h}(w,y,z) - C_z A^{opt}\Psi(w,y,z)\end{aligned}$$

to be the identification error, then ε can be estimated as

$$\begin{aligned}\|\varepsilon\| =& \|\boldsymbol{h}(w,y,z) - \mathbb{P}_{\mathrm{span}\{\Psi\}}\boldsymbol{h}(w,y,z) + \mathbb{P}_{\mathrm{span}\{\Psi\}}\boldsymbol{h}(w,y,z) - C_z A^{opt}\Psi(w,y,z)\|\\ \leq& \|\boldsymbol{h}(w,y,z) - \mathbb{P}_{\mathrm{span}\{\Psi\}}\boldsymbol{h}(w,y,z)\| + \|\mathbb{P}_{\mathrm{span}\{\Psi\}}\big((K-K^{approx})C_z\Psi(w,y,z)\big)\|.\end{aligned}$$

Here, the first term corresponds to the identification error caused by the design of the observable set, and the second term corresponds to the error between the approximated and the original Koopman operator. If $\boldsymbol{h} \in \mathrm{span}\{\Psi\}^{Nm}$, then $\|\boldsymbol{h} - \mathbb{P}_{\mathrm{span}\{\Psi\}}\boldsymbol{h}\| = 0$. Also, if $C_{r-1}(Y - A^{opt}X) = 0$ holds for all the trajectories of the system, then $K^{approx}\Psi(w,y,z) = \Psi(w^+,y^+,z^+)$ always holds (at least on $\mathcal{M}$), which leads to $(K-K^{approx})C_y\Psi(w,y,z) = 0$.

Remark 5.3. By using streaming data sets, i.e., defining data matrices X and Y over a horizon of length M and updating the recorded data at every step k, the proposed can be implemented in real-time for networks with topology changes, as stated in Chapter 3.

Remark 5.2 indicates that to reduce the identification error, the observable set should be designed sufficiently rich to cover $\boldsymbol{h}(w,y,z)$ as much as possible. Also, more samples should be measured independently from various points in the state space.

5.3 Numerical Examples

5.3.1 Identification without dimension complement

Consider a network of 8 interconnected systems described by

$$x_{i1}^+ = x_{i1} + 0.1(x_{i2}), \tag{5.20a}$$

$$x_{i2}^+ = x_{i2} + 0.1(-x_{i1} + x_{i2} - x_{i1}^2 x_{i2} + x_{i3}), \tag{5.20b}$$

$$x_{i3}^+ = x_{i3} + 0.1(-x_{i3} + u_i), \tag{5.20c}$$

$$u_i = \sum_{j=1}^{8} a_{ij}(x_{2j} - x_{2i}), \qquad w_i = \begin{pmatrix} x_{i1} & x_{i2}\end{pmatrix}^\top,$$

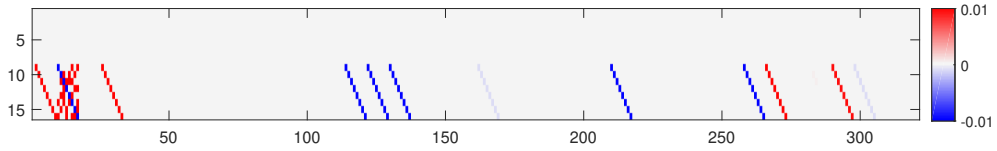

Fig. 5.1: Entries of the obtained matrix $C_yA \in \mathbb{R}^{16\times 321}$, where the value of $[C_yA]_{ij}$ entry is represented by the color at coordinate (i, j). The network topology can be inferred by the non-diagonal entries in the 8×8 sub-block of rows 9 to 16 and columns 10 to 17.

for $i = 1, \cdots, 8$, which are Van der Pol oscillators with damped inputs and discretized using the 1st order Euler method with 0.1-long time steps. Suppose that only a linearized model of the oscillators is known:

$$\begin{aligned} w_{i1}^+ =& w_{i1} + 0.1w_{i2} + \tau_{i1}(x), \\ w_{i2}^+ =& -0.1w_{i1} + 1.1w_{i2} + \tau_{i2}(x), \\ x_{i3}^+ =& 0.9x_{i3} + \tau_{i3}(x). \end{aligned}$$

Define $y_{i1} = \tau_{i1}(x), y_{i2} = \tau_{i2}(x)$ and consider the nodes described by (w_i, y_i):

$$\begin{aligned} w_{i1}^+ =& w_{i1} + 0.1w_{i2} + y_{i1}, \\ w_{i2}^+ =& -0.1w_{i1} + 1.1w_{i2} + y_{i2}, \\ y_{i1}^+ =& h_{i1}(w, y), \\ y_{i2}^+ =& h_{i2}(w, y), \end{aligned}$$

where $w = \mathrm{col}_{i=1}^8(w_i)$ and $y = \mathrm{col}_{i=1}^8(y_i)$. Rewrite the dynamics of the network into

$$\begin{aligned} w^+ =& \boldsymbol{F}w + y, \\ y^+ =& \boldsymbol{h}(w, y), \end{aligned}$$

where $\boldsymbol{F} = I_8 \otimes \begin{bmatrix} 1 & 0.1 \\ -0.1 & 1.1 \end{bmatrix}$.

Suppose that 5000 trajectories of 3 steps of the outputs, denoted by ${}^jw, {}^jw^+, {}^jw^{2+}$, are measured from random initial points distributed uniformly in $[-2, 2]^{16}$. Then, data for y and y^+ can be calculated as

$$\begin{aligned} {}^jy_{i1} =& {}^jw_{i1}^+ - {}^jw_{i1} - 0.1({}^jw_{i2}), \\ {}^jy_{i2} =& {}^jw_{i2}^+ + 0.1({}^jw_{i1}) - 1.1({}^jw_{i2}), \\ {}^jy_{i1}^+ =& {}^jw_{i1}^{2+} - {}^jw_{i1}^+ - 0.1({}^jw_{i2}^+), \\ {}^jy_{i2}^+ =& {}^jw_{i2}^{2+} + 0.1({}^jw_{i1}^+) - 1.1({}^jw_{i2}^+), \end{aligned}$$

for $j = 1, \cdots, 5000$. Define Koopman operator K by

$$K\psi(w, y) = \psi(\boldsymbol{F}w + y, \boldsymbol{h}(w, y)), \tag{5.21}$$

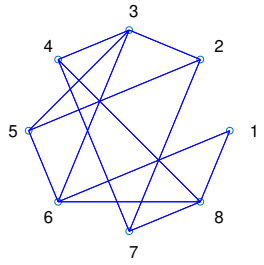

Fig. 5.2: The identified network topology.

where $\psi : \mathbb{R}^{16} \times \mathbb{R}^{16} \to \mathbb{C}$. To obtain an approximation of K, define $\Psi(w, y) : \mathbb{R}^{16} \times \mathbb{R}^{16} \to \mathbb{R}^{321}$ as

$$\begin{aligned}\Psi(w,y) =& \mathrm{col}\big(1, w, y, w_{i1}w_{i2}, w_{i1}y_{i1}, w_{i1}y_{i2}, w_{i2}y_{i1}, w_{i2}y_{i2}, y_{i1}y_{i2}, w_{i1}^2, w_{i2}^2, y_{i1}^2, y_{i2}^2,\\ & w_{i1}^2w_{i2}, w_{i1}w_{i2}^2, w_{i1}^2y_{i1}, w_{i1}y_{i1}^2, w_{i1}^2y_{i2}, w_{i1}y_{i2}^2, w_{i2}^2y_{i1}, w_{i2}y_{i1}^2, w_{i2}^2y_{i2},\\ & w_{i2}y_{i2}^2, y_{i1}^2y_{i2}, y_{i1}y_{i2}^2, w_{i1}w_{i2}y_{i1}, w_{i1}w_{i2}y_{i2},\\ & \cos w_{i1}, \cos w_{i2}, \cos y_{i1}, \cos y_{i2}, \sin w_{i1}, \sin w_{i2}, \sin y_{i1}, \sin y_{i2},\\ & \cos w_{i1}\sin w_{i1}, \cos w_{i2}\sin w_{i2}, \cos y_{i1}\sin y_{i1}, \cos y_{i2}\sin y_{i2}\big),\end{aligned} \tag{5.22}$$

where the variables with subscript i denote abbreviations of the corresponding states of all the nodes, i.e., $y_{i1}w_{i1}$ is an abbreviation of $\mathrm{col}_{i=1}^{N}(y_{i1}w_{i1})$. Define data matrices X, Y by

$$\begin{aligned}X &= \begin{bmatrix}\Psi({}^1w, {}^1y) & \cdots & \Psi({}^{5000}w, {}^{5000}y)\end{bmatrix},\\ Y &= \begin{bmatrix}\Psi({}^1w^+, {}^1y^+) & \cdots & \Psi({}^{5000}w^+, {}^{5000}y^+)\end{bmatrix}.\end{aligned}$$

Then, a matrix approximation of K can be obtained as $A = \mathrm{argmin}_H \|HX - Y\|_F$, and $\boldsymbol{h}(w, y)$ can be obtained as

$$\boldsymbol{h}^{id}(w, y) = C_y A \Psi(w, y),$$

where $C_y = \begin{bmatrix}\mathbf{0}_{16\times 17} & I_{16} & \mathbf{0}_{16\times 288}\end{bmatrix}$ is such that $C_y\Psi(w, y) = y$. Entries of the obtained C_yA are plotted in Fig.5.1, where the color at coordinates (i, j) represents the value of entry $[C_yA]_{ij}$.

Next, the first node is taken as an illustrative example to show the process of obtaining

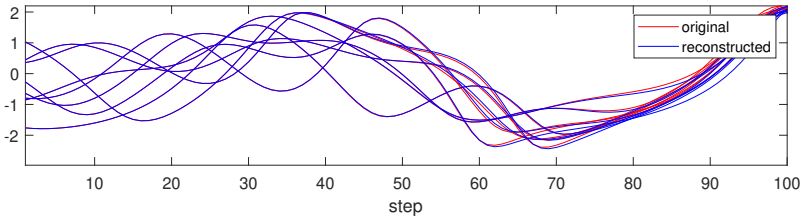

Fig. 5.3: A comparison of the first components of the 12 nodes in the original network and the reconstructed network starting from the same initial positions.

the coupling function. The dynamics of y_{11} and y_{12} is identified as

$$\begin{aligned}
y_{11}^{+,id} =& \boldsymbol{e}_1^\top \boldsymbol{h}^{id} = 0,\\
y_{12}^{+,id} =& \boldsymbol{e}_9^\top \boldsymbol{h}^{id} = -0.084\psi_2 - 0.029\psi_{10} + 0.010\psi_{15} + 0.010\psi_{17} + 0.899\psi_{26} - 0.180\psi_{114}\\
&- 0.022\psi_{122} - 0.100\psi_{130} - 0.001\psi_{162} - 0.020\psi_{210} - 0.093\psi_{258} + 0.010\psi_{266}\\
&+ 0.009\psi_{290} - 0.001\psi_{298}\\
=& - 0.084w_{11} - 0.029w_{12} + \underline{0.010w_{62} + 0.010w_{82}} + 0.899y_{12} - 0.180w_{11}^2 w_{21}\\
&- 0.022w_{11}w_{21}^2 - 0.100w_{11}^2 y_{12} - 0.001w_{12}^2 y_{12} - 0.020w_{i1}w_{i2}y_{i1}\\
&- 0.093\sin w_{11} + 0.0102\sin w_{12} + 0.009\cos w_{11}\cos w_{11} - 0.001\cos w_{12}\sin w_{12},
\end{aligned}$$

where entries smaller than $\mathcal{O}(5\times 10^{-4})$ are omitted. Here only the terms $0.010\psi_{15} + 0.010\psi_{17}$ contain states sent from other nodes and are hence considered the coupling function. As a result, the dynamics of the first node is identified as

$$\begin{aligned}
w_{11}^+ =& w_{11} + 0.1w_{12} + y_{11},\\
w_{12}^+ =& - 0.1w_{11} + 1.1w_{12} + y_{12},\\
y_{11}^+ =& 0,\\
y_{12}^+ =& \sum_{i\in N_1} [C_y A]_{(9,i)}\psi_i + 0.01w_{62} + 0.01w_{82},
\end{aligned}$$

where $N_1 = \{2, 10, 26, 114, 122, 130, 162, 210, 258, 266, 290, 298\}$. By performing the same procedures to all the nodes, the topology of the network is then identified as shown in Fig.5.2. A comparison between a reconstructed system using the identified result and the original is also shown in Fig.5.3. As the figure shows, starting from the same initial position, the reconstructed system tracks the original for about the first 50 steps and deviates due to identification errors.

5.3.2 Identification with dimension complement

In this subsection, consider the case where the dimension of the output is too low that the dynamics of the nodes cannot be embedded into the space spanned by w and y, i.e.,

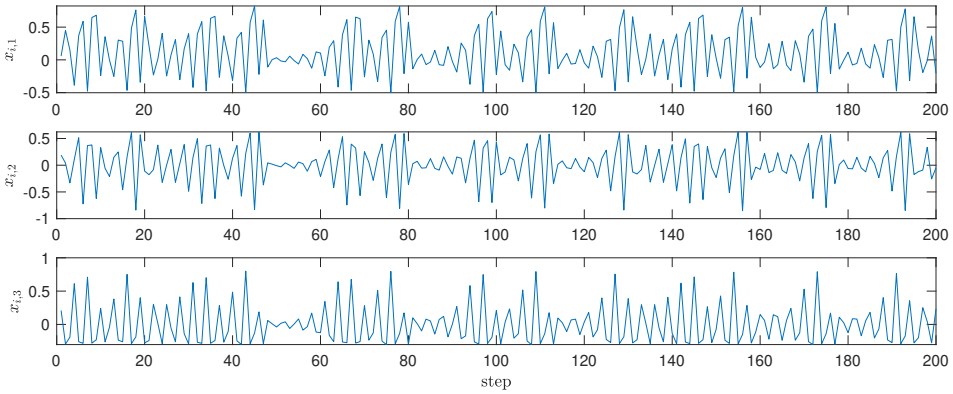

Fig. 5.4: Trajectory of system i described by (5.23) with $u_i = 0$.

the case where $r \geq 1$. Consider the network of 12 nodes described by

$$x_{i,1}^+ = 0.9x_{i,1} + x_{i,2} + x_{i,3}, \tag{5.23a}$$
$$x_{i,2}^+ = -0.9x_{i,2} + x_{i,3} + u_i, \tag{5.23b}$$
$$x_{i,3}^+ = 0.01x_{i,3} + 1.2(x_{i,1} + x_{i,2} + x_{i,3})(x_{i,1} + x_{i,2} + x_{i,3} - 1), \tag{5.23c}$$
$$u_i = 0.1\sum_{j=1}^{12} a_{ij}(x_{i,2} - x_{j,2}), \qquad w_i = x_{i,1},$$

for $i = 1, \cdots, 12$. The trajectory of node i described by (5.23) when $u_i = 0$ is shown in Fig.5.4.

Suppose that only a linearized model in the space spanned by the output, which is also inaccurate, is known, i.e., $w_i^+ = 1.0w_i + \tau_i(x)$ where $1.0w_i$ is the inaccurate known part and $\tau_i(x)$ denotes the unknown dynamics. Reformulate the dynamics of the nodes into the following form

$$\begin{aligned} w_i^+ &= w_i + y_i, \\ y_i^+ &= z_i, \\ z_i^+ &= h_i(w, y, z), \end{aligned}$$

and rewrite the dynamics of the network into

$$w^+ = w + y, \tag{5.24a}$$
$$y^+ = z, \tag{5.24b}$$
$$z^+ = \boldsymbol{h}(w, y, z), \tag{5.24c}$$

where $w = \mathrm{col}_{i=1}^{12}(w_i) \in \mathbb{R}^{12}$, $y \in \mathbb{R}^{12}$ and $z \in \mathbb{R}^{12}$. Let $\psi(w, y, z) : \mathbb{R}^{36} \to \mathbb{C}$ denote an observable and defined Koopman operator K by

$$K\psi(w, y, z) = \psi(w + y, z, \boldsymbol{h}(w, y, z)).$$

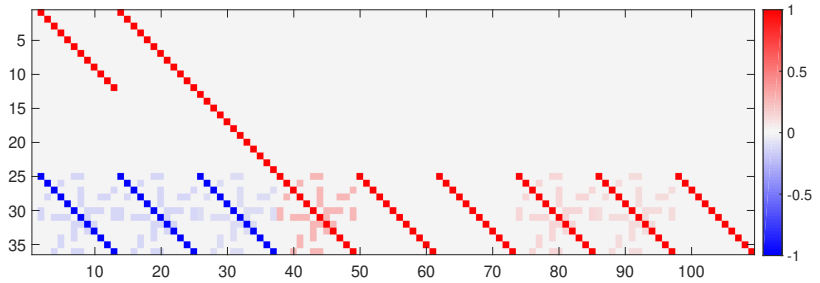

Fig. 5.5: The obtained $CA \in \mathbb{R}^{36\times 109}$ matrix shown in color.

Next, consider the problem of obtaining an approximation of K. Define a set of observable functions $\Psi(w,y,z) : \mathbb{R}^{36} \to \mathbb{R}^{109}$ by

$$\begin{aligned}\Psi(w,y,z) =& \mathrm{col}_{i=1}^{12}\big(1, w, y, z, \mathrm{col}_{i=1}^{12}(w_i y_i), \mathrm{col}_{i=1}^{12}(w_i z_i), \mathrm{col}_{i=1}^{12}(y_i z_i),\\ & \mathrm{col}_{i=1}^{12}(w_i^2), \mathrm{col}_{i=1}^{12}(y_i^2), \mathrm{col}_{i=1}^{12}(z_i^2)\big),\end{aligned} \tag{5.25}$$

and suppose that a 203-step-long trajectory of the outputs of the coupled nodes in the network is measured, which is denoted by $w[k] \in \mathbb{R}^{12}$ for $k = 1, \cdots, 203$. Then, data series of y and z are obtained as

$$\begin{aligned} y[k] =& w[k+1] - w[k], \quad k = 1, \cdots, 202,\\ z[k] =& y[k+1], \quad k = 1, \cdots, 201,\end{aligned}$$

and $\mathrm{col}(w[k], y[k], z[k])$ for $k = 1, \cdots, 201$ is a 201-step-long trajectory of system (5.24). Define data matrices $X, Y \in \mathbb{R}^{109\times 200}$ by

$$X = \begin{bmatrix}\Psi(w[1], y[1], z[1]) & \cdots & \Psi(w[200], y[200], z[200])\end{bmatrix}, \tag{5.26a}$$

$$Y = \begin{bmatrix}\Psi(w[2], y[2], z[2]) & \cdots & \Psi(w[201], y[201], z[201])\end{bmatrix}, \tag{5.26b}$$

and a matrix approximation A of Koopman K can be obtained as

$$A = \underset{H}{\mathrm{argmin}} \|HX - Y\|_F.$$

As the result of the identification, the obtained CA matrix, where C is such that $C\Psi(w,y,z) = \mathrm{col}(w,y,z)$, is shown in Fig.5.5, which corresponds to the identified dynamics of w, y and z. The $\boldsymbol{h}(w,y,z)$ function can be identified obtained as

$$\boldsymbol{h}^{id}(w,y,z) = C_z A \Psi(w,y,z),$$

where $C_z \in \mathbb{R}^{12\times 109}$ is such that $z \equiv C_z \Psi(w,y,z)$. As an illustrative example, the 26th row of A, which corresponds to the unknown dynamics of the second node, i.e., $h_2(w,y,z)$,

reads

$$\begin{aligned}\boldsymbol{e}_{26}^{\top} A\Psi(w,y,z) =& -3.8742\psi_3 - 0.1419\psi_5 - 3.6510\psi_{15} - 0.1290\psi_{17} - 2.0900\psi_{27} \\ & - 0.1000\psi_{29} + 7.6560\psi_{39} + 0.2640\psi_{41} + 2.6400\psi_{51} + 2.6400\psi_{63} \\ & + 4.0656\psi_{75} + 0.1452\psi_{77} + 3.6120\psi_{87} + 0.1200\psi_{89} + 1.2000\psi_{99} \\ =& -3.8742w_2 - 0.1419w_4 - 3.6510y_2 - 0.1290y_4 - 2.0900z_2 \\ & - 0.1000z_4 + 7.6560w_2y_2 + 0.2640w_4y_4 + 2.6400w_2z_2 + 2.6400y_2z_2 \\ & + 4.0656w_2^2 + 0.1452w_4^2 + 3.6120y_2^2 + 0.1200y_4^2 + 1.2000z_2^2,\end{aligned}$$

where readings smaller than $\mathcal{O}(10^{-4})$ were omitted. It can be seen that node 2 only receives transmissions from node 4, which is explicitly identified as the terms in $\boldsymbol{e}_{26}^{\top} A\Psi(w,y,z)$, i.e.,

$$g_2^{id} = -0.1419w_4 - 0.1290y_4 - 0.1000z_4 + 0.2640w_4y_4 + 0.1452w_4^2 + 0.1200y_4^2.$$

Fig.5.6 shows comparisons of trajectories of system (5.24) with the identified $\boldsymbol{h}^{id}(w,y,z)$ function and the original system starting from the same initial values. Specifically, the new states w, y, z and the corresponding true values w^t, y^t, z^t, calculated by

$$\begin{aligned}w_i^t =& x_{i,1}, \\ y_i^t =& x_{i,2} + x_{i,3} - 0.1x_{i,1}, \\ z_i^t =& -0.09x_{i,1} - 1.0x_{i,2} + 0.91x_{i,3} + 1.2(x_{i,1} + x_{i,2} + x_{i,3})(x_{i,1} + x_{i,2} + x_{i,3} - 1.0) + u_i(x),\end{aligned}$$

respectively, are compared. As the figures show, the errors between the trajectories stay low for around 250 steps, and deviate due to small identification errors. The identified network topology is shown in Fig.5.7, and the coupling function is obtained from $\boldsymbol{h}^{id}$ using (5.18). This example also indicates that the incorrectness of the a priori linear model in the space of the output would not disable the proposed identification method.

5.4 Conclusions

In this chapter, the identification problem of network structures using measured output data was considered. The structures of networks were modeled as coupling functions that describe the data transmission in the networks and proposed identification methods to identify the coupling functions from measured data. The identification was performed in a three-step manner, where the unmeasurable states of the nodes were considered dynamical inputs. Then, the dynamical input signals were considered new variables, and the dynamics of the network was identified using the Koopman operator theory. Finally, the coupling function was obtained as the information that was sent to the nodes from

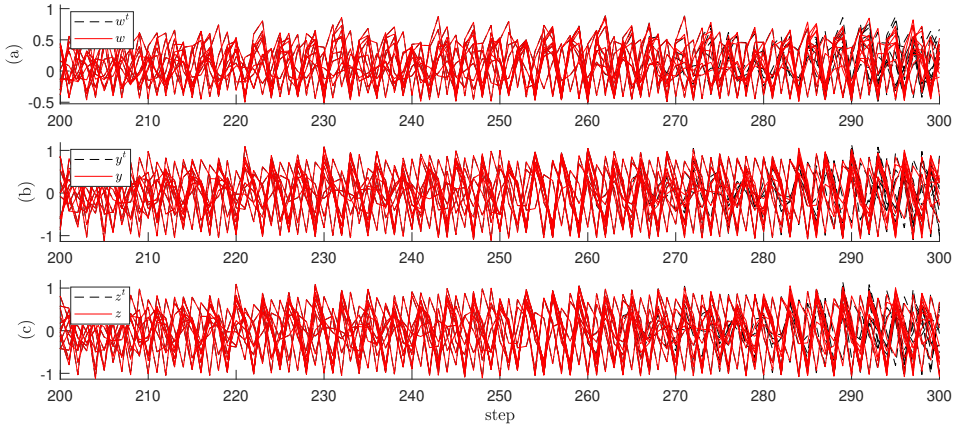

Fig. 5.6: Comparisons between the trajectories of the reconstructed system using the identification results and the original system. Note that the time interval of $k \in [200, 300]$ is shown.

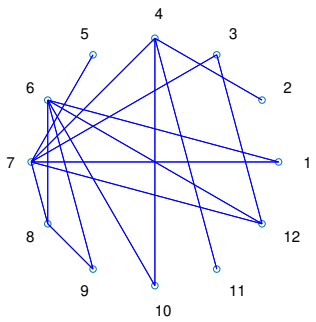

Fig. 5.7: The identified network topology.

other nodes via the network. Numerical identification examples showed the usefulness and validity of the obtained results.

A significant drawback of the proposed methods is that the computational cost would blow up as the number of nodes or the complexity of the coupling function increase. Since there is no a priori knowledge about the coupling functions, one can only design the observable set to be as rich as possible to hope the span contains the coupling function, i.e., by using trigonometric basis and power series. Such a fact reveals a trade-off between computation costs and identification accuracy of nonlinearity.

6 Conclusions and Discussions

6.1 Summary and conclusions

This dissertation addressed the problem of network identification. Methods were developed which recover the structures of networks using measured data, and the developed methods are based on the Koopman operator theory. In the cases where the full states of the nodes in the networks are measurable, the key idea was to note that the difference between the two Koopman operators K_1 and K_2, associated with the original network dynamics and the unconnected network dynamics, respectively, is related to the structure of the network, which is represented by the coupling functions. Approximations of Koopman operators acting on the states, i.e., $K_1 x$ and $K_2 x$ were obtained from measured data and the coupling function is extracted as $\boldsymbol{g}^{id}(x) = K_1 x - K_2 x$. For networks where only the outputs of the nodes are measurable, two cases are considered where the dynamical models of the nodes are known or not, respectively. In the case where the dynamical models of the nodes are known and the full states can be recovered from measured data, a response system was designed to identify the coupling function and recover the hidden states simultaneously. In the cases where the hidden states cannot be recovered, new variables were designed based on measured data to span the manifold of the dynamics, and identification was performed based on the newly defined variables.

Chapter 2 and Chapter 3 considered identifications assuming that the full states of the nodes were measurable. In Chapter 2, it was assumed that both Koopman operators K_1 and K_2 can be directly obtained from data. Data of an isolated node was employed to approximate Koopman operator K_2 associated with the network with isolated nodes. Approximations of Koopman operators K_1 and K_2 are obtained as the transition matrices relating two different data matrices, respectively, and the coupling function is extracted as the difference between the images of two Koopman operators acting on the states as observables. Theoretically, it was shown that the identified coupling function is an L_2-projection of the (infinite-dimensional) space of observable to the q-dimensional subspace spanned by the pre-designed observables. The proposed method obtains an approximation of the coupling function, also in terms of a linear combination of the observables, such that the obtained coupling function minimizes the L_2-norm of the identification error as a (vector of) function(s) over the subspace where the data are measured. Two numerical examples verified the usefulness of the proposed method: the first example served as a

detailed example of imitating an unconnected network and performing identification, and the second example addressed the case where the span of observables does not contain the coupling function.

Chapter 3 extends the method proposed in Chapter 2 for detecting network topology changes. The assumption of data for an isolated node posed in Chapter 2 is released by posing some restrictions on the network structure, i.e., to assume that the graph associated with the topology is undirected and that the coupling functions between any two nodes are skew-symmetric. The new assumptions mean that the data exchange pattern between any two nodes is symmetric, so they would cancel out if numerically added up. This relationship bridges the dynamics of nodes in the network (K_1x) and the dynamics of isolated nodes (K_2x) and enables K_2x to be recovered from K_1x. On the other hand, the method proposed in Chapter 2 is a post-processing method, i.e., the method collects all the data and obtains a result with one optimization. If the network topology changes with time, then data taken after the topology change would contradict those taken before the topology change, and the method would fail. To account for networks with topology changes, the method proposed in Chapter 3 employs a streaming data set that is updated at every time step with newly measured data. It is also shown theoretically that the obtained result is a projection of the coupling function onto the space spanned by the observables, and the design of the observables greatly influences the identification performance. Numerical examples including one with data from a SPICE model showed the usefulness of the proposed method.

On the other hand, Chapter 4 and Chapter 5 considered identifications using only output data. In Chapter 4, it was assumed that the dynamical models of the nodes without inputs are known. The strategy was to first define a response system that tracks past data of the original. Under assumptions, the dynamical models of the nodes are decoupled into the input-output dynamics and the internal dynamics. The coupling function was formulated as a linear combination of the observables, and the coefficient matrix of the linear combination was considered a variable in the response system. The coefficient matrix as a variable was then updated in such a manner that the errors between the variable and the true expansion matrix of the coupling function converge to 0 asymptotically, and the convergence was theoretically ensured. The states of the original network system at the current step were also obtained by iterating the dynamical model reconstructed out of the identification results. Two numerical examples concerning SISO and MIMO cases, respectively, were presented to show the validity of the proposed method.

In Chapter 5, the identification problem of networks consisting of nodes with unknown dynamics was considered. It was assumed that some a priori knowledge on the dynamics of the nodes, e.g., a linearized model in the spanned space of the measurable outputs, is available. The strategy was to consider the dynamics of the output signals as the full dynamic of the nodes, and consider the hidden variables as dynamical couplings

with unknown dynamics which connect these nodes. Two cases were considered where the dimension of the output signal is sufficiently high or not, and the low dimension is complemented using past data. The dynamics of the network was then obtained in terms of the measurable outputs and the newly defined variables. The reconstructed system is equivalent to the original in the sense that its outputs have the same dynamical behaviors. Numerical examples addressing the cases where dimension complement is applied or not, respectively, showed the validity of the proposed method.

6.2 Discussions and future works

This section summarizes some drawbacks and problems that remain to be solved and discusses the tasks that should be done in the future. Possible extensions and applications of the results are also addressed.

From the perspective of technical improvements, the following problems exist and may be improved.

Requirements on the measured signals

Conceptually, the methods proposed in this dissertation minimize $\sum_{i=1}^{M} \|\boldsymbol{g}(x_i) - \boldsymbol{g}^{id}(x_i)\|$ by finding a proper $\boldsymbol{g}^{id}$, where x_i are the measured data. The obtained results are approximations of certain coupling functions and are only valid over the field where data are measured. Therefore, it is desired that the output signals are exciting and ergodic, i.e., the outputs cover the domain where one concerns about the coupling function. If the outputs and the coupling functions converge to constant values including 0, then the proposed methods fail. If the outputs converge to some manifold which is a subset of the state space, then the identified coupling function would be some function which has the same projection over the manifold as the true coupling function.

Robustness of the identification result

In Chapter 2, it is supposed that data are measured with measurement noises, which are modeled as random variables uniformly distributed over a small interval ($[-0.005, 0.005]$). While in other chapters, no measurement noise is involved. The proposed method may remain valid if noises are present, and it remains an important problem to derive the allowable upper bound of the noise signals with which the proposed method stays valid.

For the methods proposed in Chapter 2 and 3, the validity of the proposed methods is equivalent to the recoverability of the sparse vectors by solving the ℓ_1-minimization

problems, i.e.,

$$\begin{aligned} \underset{a_{1i},a_{2i}}{\text{minimize}} \quad & \|a_{1i} - a_{2i}\|_1, \\ \text{subject to} \quad & a_{1i}X_1 = y_{i1}, \\ & a_{2i}X_2 = y_{i2}, \end{aligned}$$

taking the identification method proposed in Chapter 2 as an example. When measurement noises are present, the constraints no longer hold strictly, and the ℓ_1-minimization problem can be transformed into

$$\begin{aligned} \underset{a_{1i},a_{2i}}{\text{minimize}} \quad & \|a_{1i} - a_{2i}\|_1, \\ \text{subject to} \quad & \|a_{1i}X_1 - y_{i1}\|_2^2 \leq \eta, \\ & \|a_{2i}X_2 - y_{i2}\|_2^2 \leq \eta, \end{aligned}$$

for some $\eta > 0$. If the measurement noise is so large that there exists some $a_{1i}^\star$ such that $\|a_{1i}^\star\|_1 \leq \|a_{1i}^{true}\|_1$ and $\|a_{1i}^\star X_1 - y_{i1}\|_2 \leq \|a_{1i}^{true} X_1 - y_{i1}\|_2$, then the true vector is unrecoverable and the identification fails. It lacks quantitative analysis of the influences of optimization parameters and noise size on the accuracy of the identifications. Towards such problems, the robust basis pursuit analysis (see, e.g., chapters 4-6 [82]) addressed with the null space property, the covariance and the restricted isometry property of the data matrices may help establish the robustness analysis of the proposed identification method.

For the method considered in Chapter 4, it can be verified that if noise presents, then the origin of the tracking error dynamics of the response system would no longer be asymptotically stable. However, the error would stay bounded in a region containing the origin. In Chapter 5, if data are sufficient, then the identification error would be related to the statistical characteristics of the measurement noise.

Evaluation of obtained results

Throughout this dissertation, the obtained results are evaluated by comparing them to the theoretical results. However, knowledge of such theoretical results is not available, and it becomes an important problem to verify if the obtained results are correct. Verification in such cases can be achieved by comparing the data for the reconstructed network to those for the original, using spectral analysis, Fourier analysis or comparing their trajectories from the same initial states. This problem becomes even more obvious when the true coupling function is not in the spanned space of the observables, like in the example in Chapter 3 where square wave functions are employed as the basis to approximate the hidden dynamics. As the number of the radial basis functions increases, more accurate reconstruction of the behavior of the dynamics may be achieved, but the identification

results become more difficult to be comprehended. It remains a future work to develop an evaluating algorithm that estimates the accuracy of the obtained result.

Optimal design of observables

Throughout this dissertation, the coupling functions are identified in terms of linear combinations of observables. The design of observable vector $\Psi(x)$ influences the performance of the proposed method greatly since the observables span the functional space onto which the coupling function is projected. Numerically in the case where sufficient data are measured over a certain set, the proposed method obtains an approximation that minimizes the L_2 norm over the set where data are measured. Also, when sparse identification is applied, different choices of observable sets lead to different sparsity of the coefficient vectors, which is related to the amount of required data. For nodes with unknown dynamical models, the optimal design of observables remains an important problem.

From the viewpoint of Koopman theory, to obtain an approximation of the Koopman operator, the space spanned by the observables should be (at least almost) invariant under the action of the Koopman operator. Making use of the Koopman mode decomposition, there should exist an invertible linear transformation between the first q dominant eigenfunctions and the observables. Also, the propositions in this dissertation showed that the spanned space of the observables should contain the coupling function to obtain high accuracy. Practically, since the coupling functions are unknown, the observables could be designed as power series, radial basis functions, Fourier series or polynomial basis of the variables, with which an approximation is ensured to exist by the Weierstrass theorem. Also, since data are available, the basis functions can be designed as the eigenfunctions of the Koopman operator calculated theoretically using the GLA method.

Designing the observables simply as a group of basis functions also has some drawbacks. The major one is that the calculation cost may become unaffordably large if the observables are designed as polynomials. It remains an open problem to design the observables optimally making use of known information, such as the measured data series of the nodes or the physical characteristics of the systems from which data are measured.

From the perspective of applying the proposed methods to a wider range of network systems, the following problems exist.

Networks with nonidentical nodes

Throughout this dissertation, networks consisting of identical dynamical systems are considered. While in reality, it is usually the case that there exist differences between parameters of dynamical systems due to practical reasons.

In Chapter 2, it is assumed that data series can be measured from at least one isolated node, and these data were used to imitate data for a network without connections. If the assumption is strengthened such that all the connections in the network can be manually cut off, and data can be taken from all the isolated nodes, then the method becomes applicable to networks with nonidentical nodes. In such case, data matrices X_2, Y_2 in (2.9) are constructed with the data from the isolated nodes, and the imitating procedure, as shown in Chapter 2.3, can be omitted.

In Chapter 3, the assumption of data from isolated nodes was replaced by the assumption that data transmission between any pair of nodes is symmetric. If the nodes are not identical, the proposed method may fail, because the unforced models of the nodes, i.e., $K_2 x_i$, can no longer be extracted from the summation $\sum_{i=1}^{N} K_2 x_i$. In such case for node i, the best to do is to formulate the coupling function as the information sent from other nodes, i.e., node j, to node i by checking the observables having x_j as variables for $j \neq i$.

Chapters 4 and 5 allow the nodes to be nonidentical, because the nodes are assumed known, or the coupling function is already reformulated as the information sent from other nodes, respectively.

To extend the proposed method to networks with nonidentical nodes, two cases should be considered separately. The first case is that the nodes are slightly different, such as in the situation where the nodes possess parameter uncertainty. Robust identification methods may be employed in such cases. The second case is that the nodes are largely different, such as networks consisting of different physical systems. In such cases, identification methods can be developed based on the method described in Chapter 5.

Identifiability of networks using the proposed methods

This dissertation proposed several methods for identifying network structures formulated as a coupling function $\boldsymbol{g}(x)$. The identifiability problem concerns whether the obtained results are ensured to be unique, and the problem can be considered from two perspectives considering whether the obtained $\boldsymbol{g}(x)$ is unique and whether the identified network structure is unique, respectively. In Chapters 2, 3 and 4, the network structure is formulated as the inputs originating from the network transmissions, and assumptions are posed, respectively, to ensure that $\boldsymbol{g}(x)$ can be recovered from measured data. It is considered that the obtained results under the assumptions are unique, however, the necessity and the sufficiency of these conditions are not addressed. On the other hand, in Chapter 5, the network structure is formulated as the terms in the dynamical model of the output signals originating from other nodes in the network. In this case, the obtained results are also considered unique. However, the necessity and the sufficiency of the conditions are not theoretically discussed. Future works should focus on determining the optimized formulation and verifying the necessity and the sufficiency of the proposed conditions.

Other problems

There are other problems such as dealing with synchronized or non-exciting signals, analyzing the convergence of the methods with streaming data sets, deriving the amount of required data, visualizing the obtained results and optimizing the parameters of ADMM, which are left as future tasks.

Next, besides applying to network identification-related problems, discussions about two possible extensions of this work are presented.

Network Structure design

Given some desired behaviors of dynamical systems, the proposed method can be used to design connections among these systems to realize such behaviors. This is achieved by considering these desired behaviors as those of existing nodes of an unknown virtual network, and 'identifying' the structure of the virtual network. An example of such a problem is the design of central pattern generators ([102, 103]).

Network reduction

The proposed methods can be applied to obtain a reduced model of networks with partially synchronized nodes. When p partial synchronization clusters exist, the set $\{1, 2, \cdots, N\}$ can be partitioned into p sets $\mathcal{M}_1, \cdots, \mathcal{M}_p$ such that

$$\begin{aligned} \cup_{i=1}^{p} \mathcal{M}_i =& \{1, 2, \cdots, N\}, \\ \mathcal{M}_i \cap \mathcal{M}_j =& \varnothing, \quad i \neq j, \\ x_j[k] =& x_l[k], \quad \forall j, l \in \mathcal{M}_i. \end{aligned}$$

Define $z = \text{col}(z_1, \cdots, z_p) \in \mathbb{R}^{pn}$ such that $z_i = x_j$ where j is the smallest integer in $\mathcal{M}_i$, then z_i accounts for the dynamical behaviors of the nodes in the i-th cluster. In this case, the data matrices X and Y defined as described in this dissertation no longer have full ranks, and the matrices consisting of the linearly independent rows can be considered instead.

For the matrix approximation A of a Koopman operator such that

$$\Psi(x^+) = A\Psi(x),$$

Let $\Psi(z)$ denote the sub-vector which contains all the linearly independent entries in $\Psi(z)$. Then

$$\Psi(z^+) = T_x^\dagger A T_x \Psi(z)$$

holds and $\bar{A} := T_x^{\dagger} A T_x$ can be considered an approximation of the Koopman operator associated with the reduced network represented with z. Then the coupling function can be obtained in terms of z, which corresponds to the dynamics of the reduced network.

Reference

[1] S. Saidi, L. Kattan, P. Jayasinghe, P. Hettiaratchi, and J. Taron. Integrated infrastructure systems-a review. *Sustainable Cities and Society*, Vol. 36, pp. 1–11, 2018.

[2] A. Roebroeck, E. Formisano, and R. Goebel. The identification of interacting networks in the brain using fMRI: Model selection, causality and deconvolution. *NeuroImage*, Vol. 58, No. 2, pp. 296–302, 2011.

[3] M. P. van den Heuvel and H. E. Hulshoff Pol. Exploring the brain network: A review on resting-state fmri functional connectivity. *European Neuropsychopharmacology*, Vol. 20, No. 8, pp. 519 – 534, 2010.

[4] V. N. Smelyanskiy, D. G. Luchinsky, A. Stefanovska, and P. V. E. McClintock. Inference of a nonlinear stochastic model of the cardiorespiratory interaction. *Physical Review Letters*, Vol. 94, No. 9, 2005.

[5] R.N. Mantegna. Hierarchical structure in financial markets. *The European Physical Journal B*, Vol. 11, No. 1, p. 193–197, 1999.

[6] J. K. Lee, J. Choi, C. Kim, and Y. Kim. Social media, network heterogeneity, and opinion polarization. *Journal of communication*, Vol. 64, No. 4, pp. 702–722, 2014.

[7] S. Shelke and V. Attar. Source detection of rumor in social network - a review. *Online Social Networks and Media*, Vol. 9, pp. 30–42, 2019.

[8] J. Chan, A. Holmes, and R. Rabadan. Network analysis of global influenza spread. *PLOS Computational Biology*, Vol. 6, No. 11, pp. 1–10, 2010.

[9] F. Emmert-Streib, G. Glazko, A. Gökmen, and R. de Matos Simoes. Statistical inference and reverse engineering of gene regulatory networks from observational expression data. *Frontiers in Genetics*, Vol. 3, p. 8, 2012.

[10] J. F. Donges, Y. Zou, N. Marwan, and J. Kurths. The backbone of the climate network. *Europhysics Letters*, Vol. 87, No. 4, p. 48007, 2009.

[11] J. Kleinberg, M. Sandler, and A. Slivkins. Network failure detection and graph connectivity. In *SODA*, Vol. 4, pp. 76–85, 2004.

[12] D. Witthaut and M. Timme. Braess's paradox in oscillator networks, desynchronization and power outage. *New journal of physics*, Vol. 14, No. 8, p. 083036, 2012.

[13] M. Pajic, I. Lee, and G. J. Pappas. Attack-resilient state estimation for noisy dynamical systems. *IEEE Transactions on Control of Network Systems*, Vol. 4, No. 1, pp. 82–92, 2016.

[14] R. R. Kompella, S. Singh, and G. Varghese. On scalable attack detection in the network. In *Proceedings of the 4th ACM SIGCOMM conference on Internet measurement*, pp. 187–200, 2004.

[15] S. Huang, J. Li, J. Ye, A. Fleisher, K. Chen, T. Wu, E. Reiman, and Alzheimer's Disease Neuroimaging Initiative. A sparse structure learning algorithm for gaussian bayesian network identification from high-dimensional data. *IEEE Transactions on Pattern Analysis and Machine Intelligence*, Vol. 35, No. 6, pp. 1328–1342, 2013.

[16] T. Schreiber. Measuring information transfer. *Physical Review Letters*, Vol. 85, pp. 461–464, 2000.

[17] M. G. Rosenblum, A. S. Pikovsky, and J. Kurths. Phase synchronization of chaotic oscillators. *Physical review letters*, Vol. 76, No. 11, p. 1804, 1996.

[18] M. Le Van Quyen, C. Adam, M. Baulac, J. Martinerie, and F. J. Varela. Nonlinear interdependencies of eeg signals in human intracranially recorded temporal lobe seizures. *Brain Research*, Vol. 792, No. 1, pp. 24–40, 1998.

[19] P. Bereziński, B. Jasiul, and M. Szpyrka. An entropy-based network anomaly detection method. *Entropy*, Vol. 17, No. 4, pp. 2367–2408, 2015.

[20] A. Chiuso and G. Pillonetto. A bayesian approach to sparse dynamic network identification. *Automatica*, Vol. 48, No. 8, pp. 1553–1565, aug 2012.

[21] R. Goebel, A. Roebroeck, D. Kim, and E. Formisano. Investigating directed cortical interactions in time-resolved fmri data using vector autoregressive modeling and granger causality mapping. *Magnetic resonance imaging*, Vol. 21, No. 10, pp. 1251–1261, 2003.

[22] A non-parametric approach to non-linear causality testing. *Economics Letters*, Vol. 51, No. 1, pp. 7–18, 1996.

[23] D. Materassi and G. Innocenti. Topological identification in networks of dynamical systems. *IEEE Transactions on Automatic Control*, Vol. 55, No. 8, pp. 1860–1871, 2008.

[24] D. Yu, M. Righero, and L. Kocarev. Estimating topology of networks. *Physical Review Letters*, Vol. 97, No. 18, 2006.

[25] L. Chen, J. Lu, and C. K. Tse. Synchronization: An obstacle to identification of network topology. *IEEE Transactions on Circuits and Systems II: Express Briefs*, Vol. 56, No. 4, pp. 310–314, 2009.

[26] M. Timme. Revealing network connectivity from response dynamics. *Physical Review Letters*, Vol. 98, p. 224101, 2007.

[27] Z. Levnajić and A. Pikovsky. Network reconstruction from random phase resetting. *Physical Review Letters*, Vol. 107, p. 034101, 2011.

[28] R. Shi, C. Deng, and S. Wang. Detecting directed interactions of networks by random variable resetting. *Europhysics Letters*, Vol. 124, No. 1, p. 18002, 2018.

[29] J. Ren, W. Wang, B. Li, and Y. Lai. Noise bridges dynamical correlation and topology in coupled oscillator networks. *Physical Review Letters*, Vol. 104, No. 5, 2010.

[30] L. M. Pecora, L. Moniz, J. Nichols, and T. L. Carroll. A unified approach to attractor reconstruction. *Chaos: An Interdisciplinary Journal of Nonlinear Science*, Vol. 17, No. 1, p. 013110, 2007.

[31] W. Wang, J. Ren, Y. Lai, and B. Li. Reverse engineering of complex dynamical networks in the presence of time-delayed interactions based on noisy time series. *Chaos: An Interdisciplinary Journal of Nonlinear Science*, Vol. 22, No. 3, p. 033131, 2012.

[32] R. Shi, W. Jiang, and S. Wang. Detecting network structures from measurable data produced by dynamics with hidden variables. *Chaos: An Interdisciplinary Journal of Nonlinear Science*, Vol. 30, No. 1, p. 013138, 2020.

[33] S. Boyd and L. Vandenberghe. *Convex Optimization*. Cambridge University Press, USA, 2004.

[34] D. Napoletani and T. D. Sauer. Reconstructing the topology of sparsely connected dynamical networks. *Physical Review E*, Vol. 77, No. 2, 2008.

[35] B. M. Sanandaji, T. L. Vincent, and M. B. Wakin. Exact topology identification of large-scale interconnected dynamicalsystems from compressive observations. No. nodes., 2011.

[36] Z. Shen, W. Wang, Y. Fan, Z. Di, and Y. Lai. Reconstructing propagation networks with natural diversity and identifying hidden sources. *Nature Communications*, Vol. 5, No. 1, 2014.

[37] G. Li, X. Wu, J. Liu, J. Lu, and C. Guo. Recovering network topologies via taylor expansion and compressive sensing. *Chaos: An Interdisciplinary Journal of Nonlinear Science*, Vol. 25, No. 4, p. 043102, 2015.

[38] Y. Shen, B. Baingana, and G. B. Giannakis. Kernel-based structural equation models for topology identification of directed networks. *IEEE Transactions on Signal Processing*, Vol. 65, No. 10, pp. 2503–2516, 2017.

[39] G. Mei, X. Wu, Y. Wang, M. Hu, J. Lu, and G. Chen. Compressive-sensing-based structure identification for multilayer networks. *IEEE Transactions on Cybernetics*, Vol. 48, No. 2, pp. 754–764, 2018.

[40] S. G. Shandilya and M. Timme. Inferring network topology from complex dynamics. *New Journal of Physics*, Vol. 13, No. 1, p. 013004, 2011.

[41] A. Pikovsky. Reconstruction of a scalar voltage-based neural field network from observed time series. *Europhysics Letters*, Vol. 119, No. 3, p. 30004, 2017.

[42] C. W. J. Granger. Investigating causal relations by econometric models and cross-spectral methods. *Econometrics*, Vol. 37, pp. 424–438, 1969.

[43] 近原鷹一, 藤野昭典. 教師あり学習に基づく granger causality の推定. 情報処理学会論文誌数理モデル化と応用, Vol. 11, No. 3, 2018.

[44] 北野勝則. Transfer entropy を用いた神経回路の解析. Annual Review 神経, Vol. 2017, pp. 1–5, 2017.

[45] R. Kobayashi K. Ryota and K. Kitano. Impact of network topology on inference of synaptic connectivity from multi-neuronal spike data simulated by a large-scale cortical network model. *Journal of computational neuroscience*, Vol. 35, No. 1, pp. 109–124, 2013.

[46] H. K. Khalil. *Nonlinear systems; 3rd ed.* Prentice-Hall, Upper Saddle River, NJ, 2002.

[47] S. Zhu, J. Zhou, G. Chen, and J. Lu. A new method for topology identification of complex dynamical networks. *IEEE Transactions on Cybernetics*, Vol. 51, No. 4, pp. 2224–2231, 2021.

[48] Z. Levnajić and A. Pikovsky. Untangling complex dynamical systems via derivative-variable correlations. *Scientific Reports*, Vol. 4, No. 1, 2014.

[49] Z. Zhang, Z. Zheng, H. Niu, Y. Mi, S. Wu, and G. Hu. Solving the inverse problem of noise-driven dynamic networks. *Physical Review E*, Vol. 91, No. 1, 2015.

[50] P. Lai. Reconstructing network topology and coupling strengths in directed networks of discrete-time dynamics. *Physical Review E*, Vol. 95, No. 2, 2017.

[51] Y. Chen, Z. Zhang, T. Chen, S. Wang, and G. Hu. Reconstruction of noise-driven nonlinear networks from node outputs by using high-order correlations. *Scientific Reports*, Vol. 7, No. 1, 2017.

[52] R. Su, W. Wang, X. Wang, and Y. Lai. Data-based reconstruction of complex geospatial networks, nodal positioning and detection of hidden nodes. *Royal Society Open Science*, Vol. 3, No. 1, p. 150577, 2016.

[53] D. L. Donoho. Compressed sensing. *IEEE Transactions on Information Theory*, Vol. 52, No. 4, pp. 1289–1306, 2006.

[54] F. Dörfler and F. Bullo. Synchronization in complex networks of phase oscillators: A survey. *Automatica*, Vol. 50, No. 6, pp. 1539–1564, 2014.

[55] W. Rudin. *Functional Analysis 2nd edt.* New York: McGraw-Hilll, New York, 1991.

[56] R. A. Horn and C. R. Johnson. *Matrix analysis*. Cambridge university press, 2012.

[57] H. Brezis. *Functional analysis, Sobolev spaces and partial differential equations*. Springer, New York, USA, 2011.

[58] B. O. Koopman. Hamiltonian systems and transformation in hilbert space. *Proceedings of the national academy of sciences of the united states of america*, Vol. 17, No. 5, p. 315, 1931.

[59] M. Budisic, R. Mohr, and I. Mezić. Applied koopmanism. *Chaos: An Interdisciplinary Journal of Nonlinear Science*, Vol. 22, No. 4, p. 047510, 2012.

[60] A. Mauroy, I. Mezić, and Y. Susuki. *The Koopman Operator in Systems and Control: Concepts, Methodologies, and Applications*, Vol. 484. Springer Nature, 2020.

[61] S. Klus, P. Koltai, and C. Schütte. On the numerical approximation of the perron-frobenius and koopman operator. *arXiv preprint arXiv:1512.05997*, 2015.

[62] A. Mauroy and I. Mezić. On the use of fourier averages to compute the global isochrons of (quasi) periodic dynamics. *Chaos: An Interdisciplinary Journal of Nonlinear Science*, Vol. 22, No. 3, p. 033112, 2012.

[63] P. Holmes, J. L. Lumley, G. Berkooz, and C. W. Rowley. *Turbulence, coherent structures, dynamical systems and symmetry*. Cambridge university press, 2012.

[64] P. J. Schmid. Dynamic mode decomposition of numerical and experimental data. *Journal of fluid mechanics*, Vol. 656, pp. 5–28, 2010.

[65] M. O. Williams, I. G. Kevrekidis, and C. W. Rowley. A data–driven approximation of the koopman operator: Extending dynamic mode decomposition. *Journal of Nonlinear Science*, Vol. 25, No. 6, pp. 1307–1346, 2015.

[66] I. Mezić. Spectral properties of dynamical systems, model reduction and decompositions. *Nonlinear Dynamics*, Vol. 41, No. 1, pp. 309–325, 2005.

[67] I. Mezić. Analysis of fluid flows via spectral properties of the koopman operator. *Annual Review of Fluid Mechanics*, Vol. 45, pp. 357–378, 2013.

[68] A. S. Sharma, I. Mezić, and B. J. McKeon. Correspondence between koopman mode decomposition, resolvent mode decomposition, and invariant solutions of the navier-stokes equations. *Physical Review Fluids*, Vol. 1, No. 3, p. 032402, 2016.

[69] A. Mauroy and I. Mezić. Global stability analysis using the eigenfunctions of the koopman operator. *IEEE Transactions on Automatic Control*, Vol. 61, No. 11, pp. 3356–3369, 2016.

[70] C. W. Rowley, I. Mezić, S. Bagheri, P. Schlatter, and Dan S. Henningson. Reduced-order models for flow control: balanced models and koopman modes. In *Seventh IUTAM Symposium on Laminar-Turbulent Transition*, pp. 43–50. Springer Netherlands, 2010.

[71] H. Arbabi, M. Korda, and I. Mezić. A data-driven koopman model predictive control framework for nonlinear flows, 2018.

[72] E. Kaiser, J. N. Kutz, and S. L. Brunton. Data-driven discovery of koopman eigenfunctions for control. *arXiv preprint arXiv:1707.01146*, 2017.

[73] N. Hiramatsu, Y. Susuki, and A. Ishigame. Koopman mode decomposition of oscillatory temperature field inside a room. *Physical Review E*, Vol. 102, No. 2, p. 022210, 2020.

[74] Y. Susuki and I. Mezić. Nonlinear koopman modes and coherency identification of coupled swing dynamics. *IEEE Transactions on Power Systems*, Vol. 26, No. 4, pp. 1894–1904, 2011.

[75] I. Mezić. Spectrum of the koopman operator, spectral expansions in functional spaces, and state-space geometry. *Journal of Nonlinear Science*, Vol. 30, No. 5, pp. 2091–2145, 2020.

[76] M. S. Hemati, C. W. Rowley, E. A. Deem, and L. N. Cattafesta. De-biasing the dynamic mode decomposition for applied koopman spectral analysis of noisy datasets. *Theoretical and Computational Fluid Dynamics*, Vol. 31, No. 4, pp. 349–368, 2017.

[77] M. S. Hemati, M. O. Williams, and C. W. Rowley. Dynamic mode decomposition for large and streaming datasets. Vol. 26, No. 11, p. 111701, nov 2014.

[78] Z. Bai, E. Kaiser, J. L. Proctor, J. N. Kutz, and S. L. Brunton. Dynamic mode decomposition for compressive system identification. *AIAA Journal*, Vol. 58, No. 2, pp. 561–574, 2020.

[79] J. Proctor, S. L. Brunton, and J. N. Kutz. Dynamic mode decomposition with control. *SIAM Journal on Applied Dynamical Systems*, Vol. 15, No. 1, pp. 142–161, 2016.

[80] M. O. Williams, M. S. Hemati, S. T. M. Dawson, I. G. Kevrekidis, and C. W. Rowley. Extending data-driven koopman analysis to actuated systems. *IFAC-PapersOnLine*, Vol. 49, No. 18, pp. 704–709, 2016.

[81] E. Berger, M. Sastuba, D. Vogt, B. Jung, and H. Ben Amor. Estimation of perturbations in robotic behavior using dynamic mode decomposition. *Advanced Robotics*, Vol. 29, No. 5, pp. 331–343, 2015.

[82] S. Foucart and H. Rauhut. *A Mathematical Introduction to Compressive Sensing*. Birkhäuser Basel, 2013.

[83] E. J. Candès, J. Romberg, and T. Tao. Robust uncertainty principles: Exact signal reconstruction from highly incomplete frequency information. *IEEE Transactions on information theory*, Vol. 52, No. 2, pp. 489–509, 2006.

[84] M. Nagahara. *Sparsity Methods for Systems and Control*. Boston-Delft: now publishers.

[85] R. Tibshirani. Regression shrinkage and selection via the lasso. *Journal of the Royal Statistical Society. Series B (Methodological)*, Vol. 58, No. 1, pp. 267–288, 1996.

[86] S. Boyd. Distributed optimization and statistical learning via the alternating direction method of multipliers. *Foundations and Trends® in Machine Learning*, Vol. 3, No. 1, pp. 1–122, 2010.

[87] Y. Wang, W. Yin, and J. Zeng. Global convergence of ADMM in nonconvex nonsmooth optimization. *Journal of Scientific Computing*, Vol. 78, No. 1, pp. 29–63, 2018.

[88] M. G. Leguia, R. G. Andrzejak, and Z. Levnajić. Evolutionary optimization of network reconstruction from derivative-variable correlations. *Journal of Physics A: Mathematical and Theoretical*, Vol. 50, No. 33, p. 334001, 2017.

[89] C. Zhang, Y. Chen, and G. Hu. Network reconstructions with partially available data. *Frontiers of Physics*, Vol. 12, No. 3, 2017.

[90] R. Su, W. Wang, and Y. Lai. Detecting hidden nodes in complex networks from time series. *Physical Review E*, Vol. 85, No. 6, 2012.

[91] P. M. J. Van den Hof, A. Dankers, P. S. C. Heuberger, and X. Bombois. Identification of dynamic models in complex networks with prediction error methods—basic methods for consistent module estimates. *Automatica*, Vol. 49, No. 10, pp. 2994 – 3006, 2013.

[92] T. Stankovski, A. Duggento, P. V. E. McClintock, and A. Stefanovska. Inference of time-evolving coupled dynamical systems in the presence of noise. *Physical Review Letters*, Vol. 109, No. 2, 2012.

[93] R. Dubey, S. R. Samantaray, B. K. Panigrahi, and V. G. Venkoparao. Koopman analysis based wide-area back-up protection and faulted line identification for series-compensated power network. *IEEE Systems Journal*, Vol. 12, No. 3, pp. 2634–2644, 2018.

[94] M. Korda and I. Mezić. On convergence of extended dynamic mode decomposition to the koopman operator. *Journal of Nonlinear Science*, Vol. 28, No. 2, pp. 687–710, 2018.

[95] Z. Mei and T. Oguchi. Network structure identification via koopman analysis and sparse identification. *Nonlinear Theory and Its Applications*, Vol. 13, No. 2, pp. 477–492, 2022.

[96] L. M. Pecora, F. Sorrentino, A. M. Hagerstrom, T. E. Murphy, and R. Roy. Cluster synchronization and isolated desynchronization in complex networks with symmetries. *Nature Communications*, Vol. 5, No. 1, 2014.

[97] L. A. B. Tôrres and L. A. Aguirre. Inductorless chua's circuit. *Electronics Letters*, Vol. 36, No. 23, p. 1, 2000.

[98] E. S. C. Ching and P. H. Tam. Effects of hidden nodes on the reconstruction of bidirectional networks. *Physical Review E*, Vol. 98, No. 6, 2018.

[99] H. Nijmeijer and A. Van der Schaft. *Nonlinear dynamical control systems*, Vol. 175. Springer, 1990.

[100] A. Pavlov, A. Pogromsky, N. van de Wouw, and H. Nijmeijer. Convergent dynamics, a tribute to boris pavlovich demidovich. *Systems & Control Letters*, Vol. 52, No. 3-4, pp. 257–261, 2004.

[101] J. M. Hendrickx, M. Gevers, and A. S. Bazanella. Identifiability of dynamical networks with partial node measurements. *IEEE Transactions on Automatic Control*, Vol. 64, No. 6, pp. 2240–2253, 2019.

[102] A. J. Ijspeert and A. Crespi. Online trajectory generation in an amphibious snake robot using a lamprey-like central pattern generator model. In *Proceedings of the 2007 IEEE international conference on robotics and automation (ICRA 2007)*, No. CONF, pp. 262–268. IEEE, 2007.

[103] A. J. Ijspeert. Central pattern generators for locomotion control in animals and robots: A review. *Neural Networks*, Vol. 21, No. 4, pp. 642–653, may 2008.

謝辞

四年前の三月、入学式に向かうバスに乗っていた私は、吊革をつかみ揺れながら学業をおさめるときの気持ちを想像していました。そして今その時が来て、結果として大きな成果を残せなかったことを少々悔しく思いながらも、「確かに頑張ってきた」と胸を張って言えることを嬉しく思っています。学位を取得するのは自分自身の努力だけでなく、親戚、教師、友人からの助けも重要な役割を果たしたことをよく知っています。ここに、心より御礼申し上げます。

まずは経済的、精神的等多くのサポートをくれた母に感謝を申し上げます。あなたの強さと不屈の精神は、私の人生における最高の模範です。あなたのおかげで、私は遠慮なく自分の選んだ道を歩めます。

指導教官の東京都立大学の小口俊樹先生に感謝の意を申し上げます。修士の二年間を含め、小口先生との付き合いはこれで六年目です。この六年間、小口先生は私の研究の方向性を示し、学問的な問題について私と議論し、本論文の完成にかけがえのない重要な役割を果たしてくださいました。私の中では、小口先生はいつも神秘的で、近いけど遠い人でした。博士の友人と彼らの指導教官方々との仲を見てうらやむように感じ、自分はどこで何を間違えたのかを自分に問い続けたこともありましたが、この数年間に経験したことはきっと今後社会に出てからのかけがえのない貴重な経験になるとも深く認識しました。心より小口先生のご指導とご指摘に感謝を申し上げます。併せて、博士論文審査会審査員の吉村先生、増田先生、薄先生、及び研究活動にサポートしてくださいました真鍋先生と片山先生に心より感謝いたします。

この数年にわたって私を支えてくれた友人たちに感謝します。先輩と同期の林田さんと長谷研の王さんに感謝を申し上げます。博士課程で、ともに研究し毎日を過ごす仲間がいてほんとに幸せことでした。町田くん、劉くん、青山くん等の後輩に、一緒に充実な学生生活を過ごしてくれたことに感謝の気持ちを申し上げます。友人の Xv さん、Ran さん、Li さん、Wang さんからの多くの面での応援に感謝いたします。

最後に、「光之天流」の友人 Wang「tg」、Jiang「Feiyun」、Xu「Dage」、Li「Kangkang」の友人に感謝の気持ちを申し上げます。私の心を支えてくれてほんとにありがとうございます。私たちの友情が永遠に続きますように。

致谢

四年前的三月，在去往入学式的公车上，随着扶手摇晃的我曾试着想象自己完成学业那一刻的心情。而现在，虽然也会遗憾自己终究没有做出什么意义重大的成果，不过也还是暗自欣喜可以问心无愧的说一句“努力过了”。我深知，能够取得学位绝不仅是靠自己的努力，来自亲人、老师和朋友们的帮助也起到了至关重要的作用。在此，请容我致以最诚挚的感谢。

感谢我的母亲，为我提供了经济、精神等多方面的帮助与支持。您的坚强与不屈是我人生路上最好的榜样。感谢您让我没有任何后顾之忧，可以尽情在自己选择的道路上拼搏。

感谢我的指导教授，东京都立大学的小口俊树老师。算上修士的两年，我与小口老师已经共同度过了六年的时光了。这六年间，小口老师为我指明了研究道路的方向，与我共同探讨了学术方面的难题，为我完成这份学位论文起到了无可替代的重要作用，请允许我敬以最深的谢意。在我心中，小口老师对我来说是神秘的，是遥不可及的。我曾羡慕其他博士朋友与他们的指导教授的朋友般的感情，但我也相信这几年的经历的风雨一定会成为进入社会后不可或缺的宝贵经历。同时，也请允许我向博士论文审查委员会的吉村老师，增田老师，薄老师以及曾予以我宝贵帮助的真锅老师，片山老师致以衷心的感谢。

其次，感谢支持我度过了这些年的朋友们。感谢我的前辈与同期的林田以及长谷研的王。在博士生期间能有共同研究、共同欢笑的同期，实在是不可多得的幸事。感谢我的后辈町田、刘、青山等，感谢你们陪我度过的时光。感谢徐，冉，李，王等朋友在各种方面对我予以的陪伴和帮助。

最后，感谢“光之天流”的小伙伴们王“tg”、姜“飞云”、徐“大哥”和李“康康”，感谢你们构成了我茶余饭后的时光。愿我们的友谊地久天长。

Acknowledgement

Four years ago in March, riding on the bus to the entrance ceremony of my Ph.D. course, I tried to imagine the feeling when I would finally finish my studies and get the degree, and now, the time comes. Although there are still some regrets remain that nothing I made had a significant impact, I still feel some relief and happiness that I can look back and say "I worked hard" confidently. I know very well that it is not only my own efforts to finish the work, but the help from my relatives, teachers and friends also played a vital role. Here, please allow me to express my most sincere thanks.

Thanks to my mother for providing me with financial, mental and other helps and supports. Your strength and unyielding is the best example in my life. Thank you for letting me have no worries, so I can work hard on the path of my choice.

I would like to appreciate my supervisor, Prof. Oguchi, Toshiki from Tokyo Metropolitan University. Counting the two years for my Master's degree, I have spent six years together with Prof. Oguchi. Prof. Oguchi pointed out the direction of my research path, discussed academic problems with me, and played irreplaceable and important roles in my completing this dissertation. Please allow me to express my deepest appreciation. In my heart, Prof. Oguchi is always mysterious, and right there but kind of far away. When I saw the friend-like relationships between my other doctoral friends and their supervisors I sometimes became emotional and cannot stop asking what I did was wrong, but I realized and believe that the ups and downs experienced in the past few years will definitely become an indispensable and precious experience after me entering society. At the same time, please allow me to express my heartfelt thanks to Prof. Yoshimura, Prof. Masuda and Prof. Susuki on the doctoral dissertation review committee, and Prof. Manabe and Prof. Katayama for their valuable help and support.

Appreciations to my friends who provided me with great support during these years. Appreciations to Dr. Hayashida and Dr. Wang. It is really a great blessing to have someone do the work together and share the feelings. Appreciations to Machida, Liu, Aoyama and other friends in the lab, thank you for the time we spent together. I also want to thank Xv, Ran, Li, Wang and other friends for their company and help in various aspects.

Finally, I would like to appreciate the friends from "GuangZhiTianLiu": Wang "tg", Jiang "Feiyun", Xu "Big Brother" and Li "Kangkang". May our friendship last forever.